NASA-CR-123587

# RESEARCH REPORT

Battelle
Columbus Laboratories

requested 11/17

FIRST INTERIM REPORT

on

# DEGRADATION AND REUSE OF RADIATIVE-THERMAL-PROTECTION-SYSTEM MATERIALS FOR THE SPACE SHUTTLE

to

NATIONAL AERONAUTICS AND
SPACE ADMINISTRATION
GEORGE C. MARSHALL
SPACE FLIGHT CENTER

For the Period
June 26, 1970 - July 26, 1971

Contract No. NAS 8-26705
Control No. DCN 1-0-50-09638 (1F)

by

E. S. Bartlett, D. J. Maykuth, I. M. Grinberg,
and R. G. Luce

BATTELLE
Columbus Laboratories
505 King Avenue
Columbus, Ohio 43201

Battelle

November 10, 1971

National Aeronautics and Space Administration
George C. Marshall Space Flight Center
Marshall Space Flight Center, Alabama 35812

Attention A & TS-PR-M

Gentlemen:

Enclosed is an approved copy of the First Interim Report on Contract No. NAS 8-26205, DCN 1-0-50-09638 (1F), entitled "Degradation and Reuse of Radiative Thermal Protection System Materials for the Space Shuttle".

In addition to the required distribution shown below, 18 copies of this report have also been sent to the organizations on the attached list with the approval of the NASA Project Monitor.

Very truly yours,

Edwin S. Bartlett

Edwin S. Bartlett
Technical Advisor
Nonferrous Metallurgy Division

ESB:nn

cc: A & TS-MS-IL (1)
A & TS-MS-IP (2)
A & TS-TU (1)
S & E-ASTN-RRI (11) + 1 reproducible master

cc: letter only:
Defense Contract Administration Services Office
Building 1, Section 1
Defense Construction Supply Center
Columbus, Ohio 43215
Attention Billy E. Conley, DCRO-GCC
Contracting Officer

NOTICE

This report was prepared by the Columbus Laboratories of Battelle Memorial Institute under Contract NAS 8-26205, "Degradation and Reuse of Radiative-Thermal-Protection-System Materials for the Space Shuttle", for the George C. Marshall Space Flight Center of the National Aeronautics and Space Administration. The work was administered under the technical direction of the Astronautics Laboratory of the George C. Marshall Space Flight Center, with Mr. R. Rowe as the technical monitor.

TABLE OF CONTENTS

TABLE OF CONTENTS
(Continued)

# DEGRADATION AND REUSE OF RADIATIVE-THERMAL-PROTECTION-SYSTEM MATERIALS FOR THE SPACE SHUTTLE

by

E. S. Bartlett, D. J. Maykuth, I. M. Grinberg, and R. G. Luce

## SUMMARY

Three silicide-coated columbium alloys and two cobalt alloys were subjected to identical simulated reentry profiling exposures in both "static" (controlled vacuum leak) and "dynamic" (hypersonic plasma shear) environments.

Primary emphasis in the columbium-alloy evaluation was on the Cb752 and C129Y alloys with a lesser amount on FS85. Commercial silicide coatings of the R512E and VH109 formulations were used. The coated specimens were intentionally defected to provide the types of coating flaws that are expected in service. Tempe atures were profiled up to peak temperatures of either 2350 F or 2500 F for 15 minutes in each cycle.

In the dynamic cycling, pressure at the specimen surface was on the order of 10 to 25 torr, free-stream velocity was Mach 4 to 5, and aerodynamic shear levels were of the order of 2 psf. It was observed that, under these dynamic conditions, a critical temperature appears to exist below which flaw gro th is slow (less than 0.1 mil/minute for 3 to 5 cycles) and well behaved. Above this critical temperature, flaws grow rapidly such that holes as large as 1/4 inch in diameter might be expected in as few as one reentry. Neither flaw type (within the limits studied) nor coating system appeared to have an influence on the flaw growth behavior observed, and 2490 F was indicated as the most probable value of the critical temperature for the coating systems evaluated.

In static cycling, similar pressures, times, and temperatures were used. However, in contrast to the dynamic exposures, no measurable flaw growth occurred and the principal result of the static exposures was slow substrate contamination hardening at the defect site.

For the R512E/Cb752 system, the contamination introduced at small coating-defect sites after up to five dynamic subcritical exposures was not degrading to this system's room-temperature ultimate tensile or yield strength, but tensile elongation values were decreased on the order of 40 percent. Identical specimens exposed in the static environment did not show this ductility degradation, which suggests that the extent or level of contamination introduced in this environment was appreciably less than that in the dynamic environment. The effects of dynamic cycling on the room-temperature tensile properties of intentionally defected VH109/C129Y and R512E/FS85 specimens were similar to those observed for R512E/Cb752.

Both unwelded and TIG-welded specimens of the cobalt alloys, L605 and HS188, were exposed to a total of 12 simulated reentry cycles, each of which included 5 minutes' exposure at 1900 F. Neither the room-temperature or 1900 F tensile properties nor the

1900 F creep-deformation properties of either material were significantly affected as a result of these exposures.

## INTRODUCTION, OBJECTIVES, AND PROGRAM APPROACH

Oxidation-resistant metallic skins to disperse the heat of reentry by reradiation contend strongly as a thermal-protection-system (TPS) scheme for use on the NASA space shuttle. The selection of metallic skin materials depends largely on the temperature profiles predicted for the various areas of the shuttle vehicles. Selected areas of the lower planform and control surfaces are predicted to attain temperatures up to about 2400 F for normal reentry profiles, and may spike to higher temperatures under selected conditions (e.g., abort or unusual reentry maneuvering). At this highest end of the temperature spectrum (neglecting nose and leading-edge sections where nonmetallic TPS materials are planned), coated columbium TPS is most attractive. At somewhat lower temperatures, oxidation-resistant cobalt-base alloys are predominant in current thinking.

Economic argument upon which the space shuttle is founded requires that at least the major portion of the TPS system possess reusability with minimal refurbishment or repair for the life of the vehicle – 100 flight and reentry missions. This requirement, coupled with the largely unknown specific-materials response to the hypersonic shear rarified air environment, demands the conduct of studies to establish the degradation kinetics and, hence, reuse capabilities of selected TPS materials. The aforementioned coated columbium and cobalt alloys, because of the aggressively high temperatures involved in their use, pose the major areas of uncertainty.

In June, 1970, the NASA Marshall Space Flight Center authorized Battelle-Columbus to conduct a laboratory study of the degradation and reuse capability of selected state-of-the-art coated columbium and cobalt-base materials with the following objectives:

(1) To develop data to assess the functional reliability of, the reuse capability of, and degradation effects on materials for the radiative thermal protection system of the space shuttle as affected by expected flight environmental conditions

(2) To establish defect tolerances, susceptibility, failure modes, and methods of assurance of the integrity of radiative-thermal-protection-system materials of the space shuttle as affected by expected flight environmental conditions.

At the outset, it was recognized that past and anticipated concurrent studies at other laboratories, on high-temperature TPS materials were expected to contribute to the degradation and reuse analysis. However, a major area of uncertainty involved the influence of a dynamic, hypersonic shear environment upon material performance, thermal stability, and reuse capability. Indeed, there was reason to expect gross differences in the response of materials to dynamic as opposed to static (subsonic flow) environments.

The early results of Stein at NASA-Langley Research Center regarding degradation of oxidation resistance of TD-NiCr in dynamic versus static environments dictated that the possibility of a similar response in cobalt alloys be explored. These alloys

(HS188 and L605 in this program) rely upon protective $Cr_2O_3$ formation for resistance to oxidation in static, ambient air. The possibility of loss of protection via $CrO_3$ volatilization in dynamic, low-pressure air was considered real.

For coated columbium, available data on failure statistics suggested that the life-limiting aspect of coated columbium performance in TPS panel use would be the occurrence of premature coating failure and loss of protection at local sites. While prior work at McDonnell Douglas Astronautics Co.-East* and Sylvania** had shown good tolerance for coating defects under static conditions, anticipated shuttle temperatures were sufficiently close to those reportedly required for dynamic autoignition of columbium that realistic dynamic reentry simulation of defected coated columbium was considered a most critical area for investigation.

With the foregoing considerations in mind, the approach selected for this program was to expose specimens of the selected cobalt alloys and coated columbium materials under dynamic, hypersonic shear, reduced-air-pressure environments that would simulate as closely as possible, on a relatively small scale, the airstream environment expected for the respective planform surfaces of the shuttle vehicle. These exposures were conducted in the Battelle-Columbus 1.5-megawatt plasma-arc facility using a wedge model specially designed for this program. Because of greater complexities of possible material-environment interaction, major emphasis was directed towards coated columbium alloys. Further, because premature coating failure is indicated to be life-limiting in these systems, specimens with intentionally introduced coating flaws received the major attention. To allow direct assessment of the effects of environment dynamics and, further, to provide check-point correlation with results of contract studies at other laboratories, parallel exposures of the same material conditions under the same temperature-pressure profiles but in a static environment were planned.

Following limited exposure cycling under several environmental conditions, specimens were examined visually and metallographically, and selected mechanical properties were evaluated.

This interim report summarizes the results obtained during the first year's effort, and covers work from June 26, 1970, through July 30, 1971. Results to date provide an initial assessment of material response to environmental exposures as necessary to define areas that are most critical to an evaluation of degradation kinetics and reuse capability. These results provide a basis for preliminary assessment of reuse capability for limited cyclic exposures. This program is planned for continuation for an additional year during which more extensive data for coated columbium will be generated as required to fully meet the stated program objectives.

Because of the interim nature of this report, the reader is cautioned that present analyses of results, discussion, and conclusions presented are tentative and subject to change pending assimilation and analysis of more complete data.

---

* Fitzgerald, B. G., and Reisert, E. L., "Evaluation of the Fused Slurry Silicide Coating Considering Component Design and Reuse", AFML-TR-70-154 (December, 1970).

** Priceman, S., and Sama, L. "Development of Fused Slurry Silicide Coatings for the Elevated-Temperature Oxidation Protection of Columbium and Tantalum Alloys", AFML-TR-68-210 (December, 1968).

# EXPERIMENTAL PROCEDURES

## Materials and Conditions

### Cobalt Alloys

Approximately 6 square feet each of the L605 and HS188 alloys was ordered as 0.015-inch-thick sheet and received from the Stellite Division of the Cabot Corporation. The certified analyses of these materials were reported as follows:

| | Analysis (Balance Cobalt, weight percent | | | | | | | | | |
|---|---|---|---|---|---|---|---|---|---|---|
| Alloy | Cr | W | Ni | Fe | C | Si | Mn | P | S | La |
| L605 | 19.45 | 15.30 | 9.95 | 2.57 | 0.11 | <0.01 | 1.46 | 0.012 | 0.001 | - |
| HS188 | 21.94 | 14.11 | 22.15 | 1.38 | 0.10 | 0.22 | 0.59 | 0.005 | 0.001 | 0.05 |

Duplicate specimens of both alloys, as received, were subjected to room-temperature tensile tests, and the properties obtained were in good agreement with the certified property values as shown in Table 1.

Both alloy sheets appeared free of any edge or surface defects in the as-received condition which was as solution treated at 2150 F followed by descaling and pickling. These cleanup treatments imparted a light, frosty-gray color to both alloy sheets which was regarded as undesirable from emissivity considerations. Accordingly, duplicate test specimens of both alloys were subjected to 10-minute exposures at 1900 F and 2150 F in dry air and terminated by water quenching. While both treatments were effective in imparting a dark, charcoal-gray oxide to both alloys, the 2150 F treatment resulted in a significant decrease in the room-temperature tensile properties of the L605 sheet, as shown in Table 1.

Metallographic examination of these specimens indicated that the decrease in strength and ductility of the 2150 F solution-treated L605 sheet resulted from excessive grain growth associated with this heat treatment. No significant structural or property changes were observed in the L605 material heated to 1900 F or in any of the heat-treated HS188 specimens. Accordingly, a preoxidation exposure of 10 minutes at 1900 F in dry air was selected for both alloys. Since termination of this treatment by water quenching might be expected to introduce warpage, air cooling was elected for all of the specimens on this test program.

Several welded specimens of both cobalt alloys were prepared to verify the joining parameters selected for these materials. All welds were prepared using automatic gas-tungsten-arc welding equipment to produce a square, butt joint configuration in the 0.015-inch sheet materials.

Individual sheet specimens of each alloy in a 1-7/8 by 11-inch size were prepared by grinding the 11-inch edges and butting these together. The specimen orientation was such that the weld direction was perpendicular to the longitudinal grain direction (i.e., final rolling direction) of each alloy sheet. The welding fixture comprised copper clamping bars and a copper backing plate having a 1/8-inch slot, 1/16 inch deep, directly under the weld joint. Holes were drilled in the slot to permit an argon-gas backup shield. The welding torch provided argon-gas shielding for the weld face. All welds

TABLE 1. ROOM-TEMPERATURE TENSILE PROPERTIES OF BASE MATERIALS[a]

| Condition | Ultimate Tensile Strength, ksi | 0.2% Offset Yield Strength, ksi | Elongation, percent |
|---|---|---|---|
| | L605 Alloy | | |
| Certified values | 137 | 65 | 55 |
| As received | 143 | 67 | 56 |
| 10 min/2150 F, water quenched | 130 | 58 | 44 |
| 10 min/1900 F, water quenched | 136 | 67 | 51 |
| | HS188 Alloy | | |
| Certified values | 136 | 61 | 54 |
| As received | 139 | 64 | 53 |
| 10 min/2150 F, water quenched | 136 | 60 | 54 |
| 10 min/1900 F, water quenched | 137 | 58 | 54 |
| | Cb752 Alloy, Heat 770022[b] | | |
| Certified values | 82.6 | 64.0 | 26 |
| As received: | | | |
| 0.015-inch gage | 82.5 | 65.3 | 28 |
| 0.025-inch gage | 83.0 | 65.2 | 2? 5 |
| | C129Y Alloy, Heat 572038[b] | | |
| Certified values | 91.7 | 74.4 | 25 |
| As received: | | | |
| 0.015-inch gage | 86.2 | 68.1 | 27.5 |
| 0.025-inch gage | 85.7 | 67.5 | 30 |

(a) All results represent the average of duplicate test specimens.

(b) Based on test specimens with 1/4 x 1-inch gage sections. Later results on 1/8 x 1/2-inch specimens showed some differences, as described in section on Results.

were made using an 0.040-inch-diameter W-1$ThO_2$ electrode and direct current with straight polarity, electrode negative.

Table 2 lists the range of welding parameters explored for both alloys along with the indicated optimum parameters for each.

TABLE 2. WELDING PARAMETERS FOR COBALT ALLOYS

| Parameter | Range of Values Explored | Indicated Optimum Values | |
|---|---|---|---|
| | | L605 | HS188 |
| Current, amperes | 12.5 to 24 | 13.5 | 16 |
| Voltage | 7 to 12 | 10.5 | 9 |
| Travel Speed, inches/min | 15, 20 | 15 | 15 |
| Torch Gas Flow, $ft^3/hr$ | 15, 20 | 15 | 15 |
| Backup Gas Flow, $ft^3/hr$ | 5 to 8 | 5 | 5 |
| Shielding Cup Diameter, inch | 1/4, 5/16 | 5/16 | 5/16 |
| Cup-to-Work Distance, inch | 1/8 to 1/4 | 3/16 | 3/16 |
| Electrode-to-Work Distance, inch | 0.020 | 0.020 | 0.020 |
| Clamping Bar Spacing, inch | 1/4, 3/8 | 3/8 | 3/8 |

No difficulty was encountered in welding the L605 sheet and welds of good quality, as determined by dye-penetrant inspection as well as visual and X-ray examination, were obtained. In some HS188 welds, a weld-root defect was occasionally observed which was characterized by a shiny, depressed region along the weld centerline. This was believed to be caused by incomplete weld-metal flow and was overcome by increasing the weld energy input and by cleaning the specimens by polishing with 400X metallographic paper and wiping with acetone and Kimwipes before welding. For the L605 alloy, a cleaning procedure of acetone degreasing followed by acid etching (30 percent $HNO_3$, 5 percent HF, balance water; heated to 160 F), water rinsing, and air dying was found to be adequate.

Twenty-two plasma-arc test specimens were fabricated from both alloys to the design configuration shown in Figure 1. This configuration permitted mounting of the specimens on the model holder by the insertion of pins through the corner end tabs into a supporting block. After plasma-arc exposure, the end tabs were removed and each specimen was sheared lengthwise to yield two 3/8 by 3-inch coupons from which duplicate tensile or creep test specimens were prepared.

Eight (four each of each alloy) of the arc-test specimens were prepared from butt-fusion-welded sheet stock with the weld orientation transverse to the rolling direction and to the longitudinal dimension of the test specimen. The remaining 14 specimens (seven each of each alloy) were also prepared with the rolling direction parallel to the longitudinal dimension of the plasma-arc-test specimens. After shearing to size, and

| Sheet Material | t | R | D | A |
|---|---|---|---|---|
| Cobalt alloys | 0.015 | 0.015 | 0.0625 | 0.043 |
| Columbium | 0.015 | 0.015 | 0.067 | 0.043 |
| Columbium | 0.025 | 0.025 | 0.067 | 0.048 |

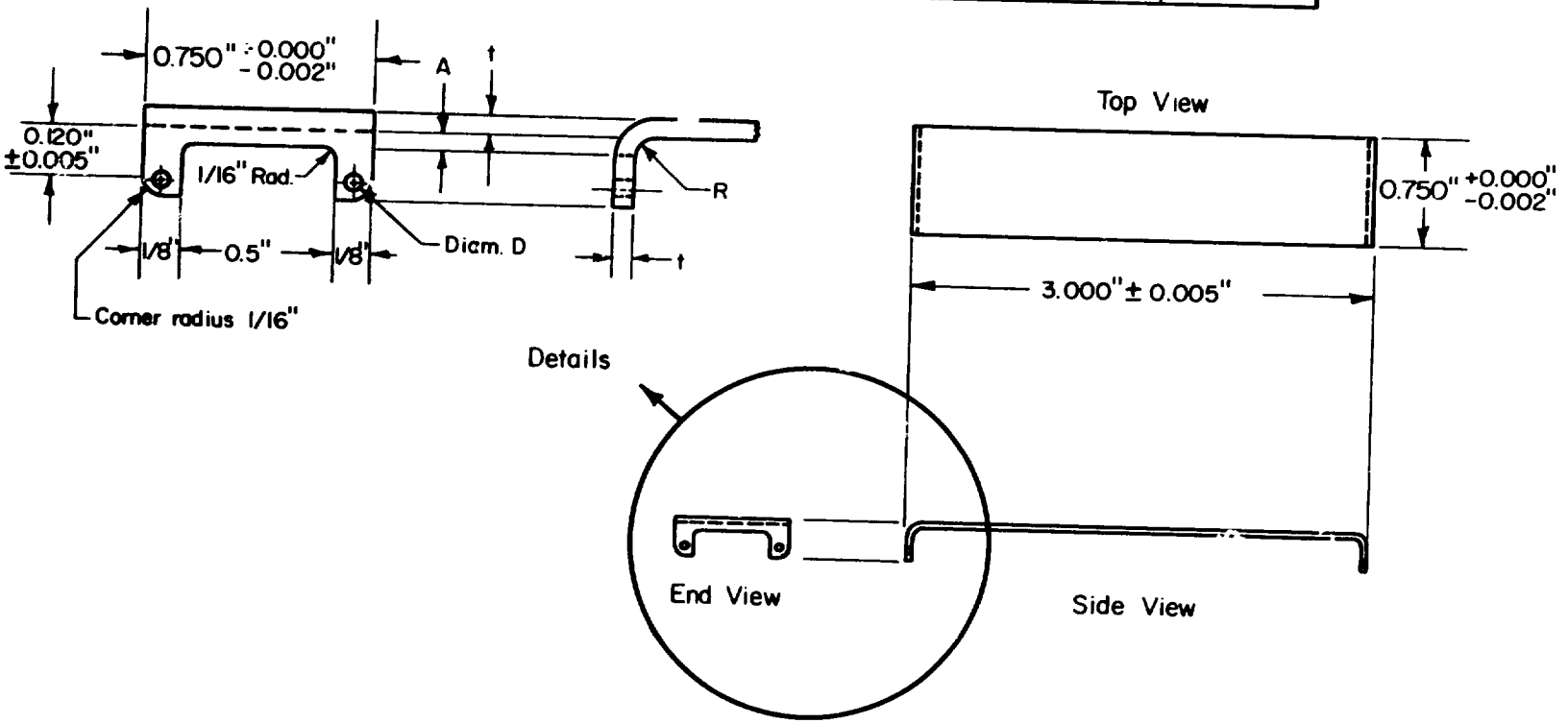


FIGURE 1. DESIGN DETAILS OF PLASMA-ARC TEST SPECIMENS

cleaning (by acid etching, water and alcohol rinsing and drying), all of the flat blanks were preoxidized for 10 minutes in dry air at 1900 F and air cooled.

No distortion of the blanks was apparent as a result of this treatment. All specimens were oxidized to a uniformly dark-gray matte finish, with the HS188 material exhibiting a slightly darker gray color than the HS25 material. The average thickness and weight increases of these specimens as a result of this preoxidation treatment were determined as follows:

| Alloy | Total Thickness Increase, mil | Weight Increase, $mg/cm^2$ |
|---|---|---|
| L605 | 0.25 to 0.30 | 0.5 to 0.6 |
| HS188 | 0.10 to 0.15 | 0.3 to 0.4 |

The 22 preoxidized blanks were then fabricated to test specimens. Both the forming and all machining operations were effected without damaging the preoxidized plasma-arc exposure surface of these specimens. Each specimen was then degreased in readiness for attachment to the plasma-arc model holder.

A similar series of 22 specimens was prepared for exposure in a static environment. These specimens were simply rectangular in shape, having a width of 3/4 inch and a length of 3-1/2 inches. A 1/8-inch-diameter hole was provided at a distance of 3/16 inch from one end to permit suspension of the specimens for the static exposure cycling. After exposure, each specimen was sheared to yield two duplicate 3/8 by 3-inch coupons for mechanical-property evaluations. As with the plasma-arc-test specimens, the rectangular static-environment test specimens were also preoxidized prior to exposure.

## Columbium Alloys

Approximately 3 pounds each of 0.015 and 0.025-inch-thick sheet of both the Cb752 and C129Y alloys was purchased from the Wah Chang Albany Corporation for this program. All of the material for each alloy was from the same heat, and the certified analyses on these are given in Table 3. In addition, certified analyses for the interstitial impurities in both alloy sheet products at the 0.015-inch-thich gage were reported as follows:

| | Impurity Content, ppm | | |
|---|---|---|---|
| Alloy | C | O | N |
| Cb752 | 40 | 70 | 40 |
| C129Y | 40 | 90 | 35 |

In compliance with the Battelle purchase specification, all of the alloy sheet materials were also certified to have a 100 percent fully recrystallized structure and to be capable of sustaining bends around a 1T radius at room temperature without signs of cracking.

Visual inspection of each of the columbium-alloy sheets showed all were free of oxide, cracks, laps, seams, and other visible defects. Room-temperature tensile tests were performed, in duplicate, on samples of each of the as-received alloy sheets. The

TABLE 3. CERTIFIED CHEMICAL ANALYSES AND HARDNESS OF AS-RECEIVED COLUMBIUM ALLOYS

| Element | Cb752 Alloy Ingot Analysis on Heat 770022 Composition, weight percent Top | Cb752 Alloy Ingot Analysis on Heat 770022 Composition, weight percent Bottom | C129Y Alloy Ingot Analysis on Heat 572038 Composition, weight percent Top | C129Y Alloy Ingot Analysis on Heat 572038 Composition, weight percent Bottom |
|---|---|---|---|---|
| W | 9.7 | 10.5 | 9.2 | 9.6 |
| Hf | -- See below -- | | 10.9 | 9.2 |
| Zr | 2.8 | 2.6 | -- See below -- | |
| Cb | Balance | | Balance | |
| | Impurities, ppm | | Impurities, ppm | |
| Al | <20 | <20 | <20 | <20 |
| B | <1 | <1 | <1 | <1 |
| C | 70 | <40 | 40 | 60 |
| Cd | <5 | <5 | -- | -- |
| Co | <10 | <10 | <10 | <10 |
| Cu | -- | -- | <40 | <40 |
| Cr | <20 | <20 | -- | -- |
| Fe | <50 | <50 | <50 | 50 |
| H | 5 | 9 | 2.9 | 2.6 |
| Hf | 480 | 390 | -- See above -- | |
| Mg | <20 | <20 | <20 | <25 |
| Mn | <20 | <20 | <20 | <20 |
| Mo | 100 | 150 | 150 | 100 |
| N | 50 | 50 | 45 | 29 |
| Ni | <20 | <20 | <20 | <20 |
| O | 110 | 160 | 60 | 120 |
| Pb | <20 | <20 | <20 | <20 |
| Si | <50 | <50 | <50 | <50 |
| Sn | 15 | 10 | 10 | 25 |
| Ta | 3800 | 4300 | 3700 | 3700 |
| Ti | <40 | <40 | <40 | <40 |
| V | <20 | <20 | <20 | <20 |
| Zr | -- See above -- | | 4000 | 3700 |
| Y | -- | -- | 600 | 180 |
| | Hardness, Bhn | | Hardness, Bhn | |
| | Range 185 to 192 | | Range 197 to 212 | |
| | Average 188 | | Average 202 | |

results of these tests, given in Table 1, show good agreement with the certified test values as well as good reproducibility in the properties of both alloys for both of the gages selected.

Later in the program, approximately 3 square feet of 0.030-inch-thick FS85 alloy sheet was also received from the U. S. Naval Air Development Center. This material was prepared for the Navy by the Fansteel Metallurgical Corporation* and was identified as Sheet No. 1 of Heat 85D-1560. According to the reference cited, the average analyses on four other sheets from the same heat of material were as follows:

| Element | Content, wt % | Element | Content, wt % |
|---|---|---|---|
| Ta | 27.58 | C | 0.0015 |
| W | 10.77 | O | 0.0020 |
| Zr | 0.95 | N | 0.0050 |
| Fe | <0.007 | H | 0.0001 |
| Si | <0.005 | | |

Similarly, the reported average room-temperature tensile properties for this material in the longitudinal test direction were cited as:

| | |
|---|---|
| Ultimate tensile strength | 86,700 psi |
| Yield strength | 69,300 psi |
| Elongation | 23 percent in 1 inch |

Specimen Preparation. Specimens of the as-received columbium sheet alloys were fabricated to the same configurations for plasma-arc and static-exposure testing as those described previously for the cobalt alloys. After forming and/or shearing to size, the columbium specimens were prepared for coating by:

(1) Abrasive tumbling in a $Al_2O_3$-water slurry for 2 hours to provide edge radii on the specimens

(2) Acid pickling in a 20 percent $HNO_3$, 5 percent HF, 75 percent water solution

(3) Water rinsing

(4) Alcohol rinsing and air drying.

Coatings. All of the specimens intended for either dynamic or static test exposure were submitted to commercial vendors for the application of a 3-mil-thick, slurry-silicide coating. The coatings selected were R512E and VH109.

The R512E coating was applied by Sylvania Electric Products of Hicksville, New York, and has a nominal composition of Si-20Cr-20Fe. The VH109 coating was applied

* Davis, J. W., and Curcio, R. M., "Fabrication of Fansteel 85 Metal Sheet", Fansteel Metallurgical Corporation Final Report under Contract NOW-65-0498 f, North Chicago, Illinois (March, 1966).

by the Vac Hyd Processing Corporation of Torrance, California, and consists basically of silicon with hafnium and tantalum as important auxiliary additions.

In addition to the larger specimens, 17 coated 3/4 by 1-1/2-inch tab specimens were also prepared to characterize the thickness and structure of the four major coating systems of interest. These included standards of the Cb752 and C129Y alloy substrates to which both coatings were applied in thicknesses of 1, 3, and 5 mils.

Electrodischarge machining (EDM) techniques were used to introduce either of three types of intentional coating defects into the coated specimens according to the following specifications:

Type A – through flaw, a 40-mil-diameter hole entirely through the coated sheet to represent micrometeorite damage

Type B – large flaw, a 40-mil-diameter hole through the coating, terminating in the substrate to represent major areal damage from extrinsic sources

Type C – small flaw, a 4-mil-diameter hole through the coating, terminating in the substrate to represent the type of flaw occurring randomly in service.

Figure 2 illustrates these intentionally introduced flaws.

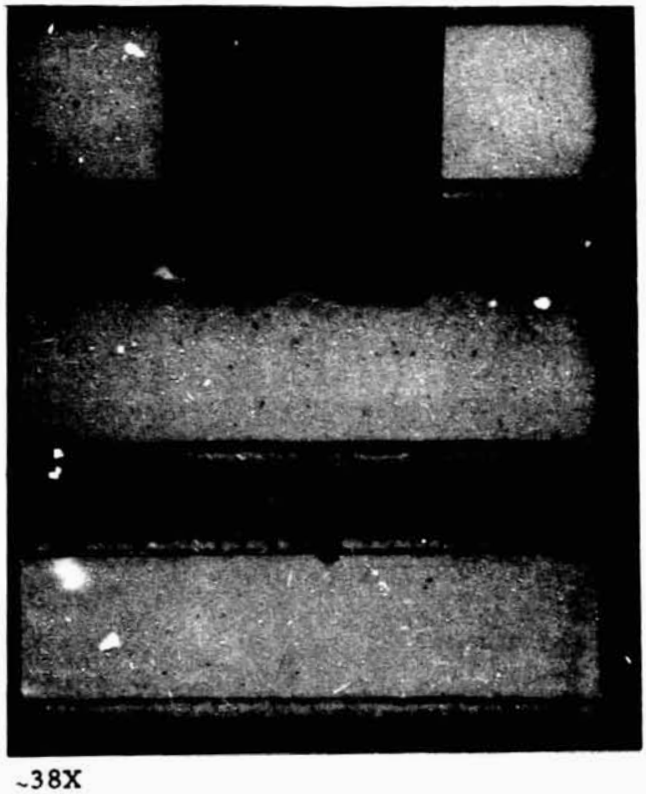

~38X

FIGURE 2. "THROUGH", "LARGE", AND "SMALL" FLAWS INTRODUCED IN COATED COLUMBIUM BY EDM

## Static Environment Exposures

### Equipment

The major pieces of equipment comprising the static low-pressure environment (LPE) facility are illustrated schematically in Figure 3. The heart of this equipment is a 2-inch-ID by 12-inch-long quartz chamber in which the specimens are suspended vertically and induction heated for thermal exposure. The top of this chamber is provided with a valved, air-inleakage line and chamber pressure is controlled manually by preprogrammed adjustments of a 1/4-inch-diameter valve located in the vacuum line between the bottom of the furnace chamber and a mechanical vacuum pump (Edward's High Speed Rotary Pump, Model ED-100, maximum pumping speed of 3.54 $ft^3$/min).

The specimens are heated by radiation from a 1.2-inch-ID by 2-inch-long CS Grade graphite susceptor. The furnace can accommodate up to seven each of the rectangular, 3/4 by 3-1/2-inch specimens at peak temperatures through 2500 F. The specimens are suspended vertically on a high-purity alumina support rod using alumina spacers between specimens. In order to prevent overheating of the quartz walls as well as to improve temperature uniformity of the specimens, the graphite susceptor and specimen support rods were contained within a 1-3/4-inch-diameter by 6-inch-long high-purity alumina tube (not shown in Figure 3).

For monitoring and controlling temperature, two Pt/Pt-10Rh thermocouples were suspended centrally among the given samples constituting a run. Calibration runs showed the following degree of specimen temperature control could be achieved over the distances indicated:

| Specimen Material | Control Temperature, F | Temperature Variation Over Vertical Distance Indicated |
|---|---|---|
| Cobalt | 1900 | ±10 F over 1 inch |
| Columbium | 2500 | ±20 F over 1-1/2 inch |

### Temperature and Pressure Profiling

Cobalt Alloys. The simulated static reentry profiling conditions selected for the cobalt-alloy specimens consisted of a continuous sequence of twelve, 9-minute cycles each of which included 5 minutes' exposure at a peak temperature of 1900 F. The target profiling conditions for each cycle were as follow:

(1) Ramp type of heatup to 1900 F in 2 minutes

(2) Hold at 1900 F for 5 minutes

(3) Cool down to below 1300 F in 2 minutes.

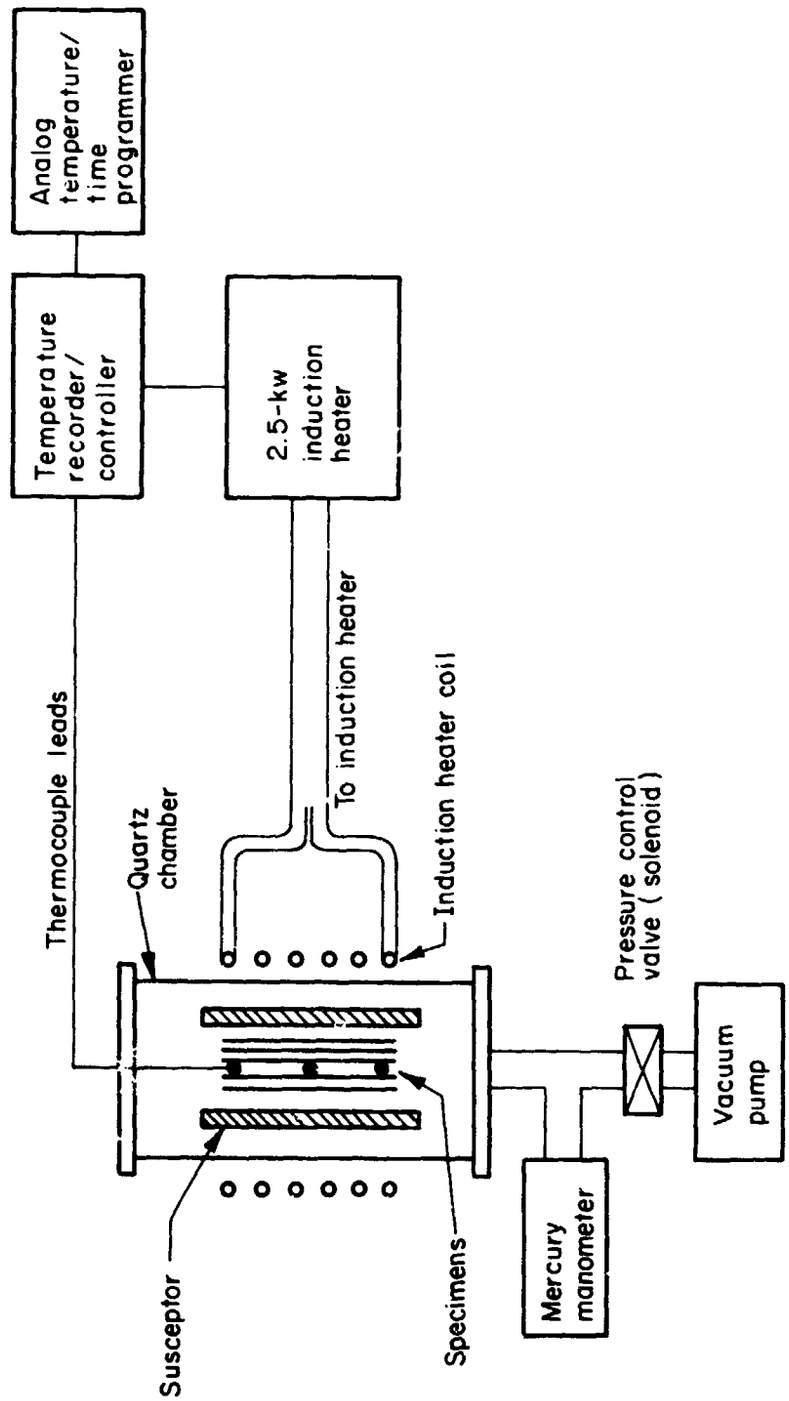


FIGURE 3. SCHEMATIC OF EQUIPMENT SETUP FOR LOW-PRESSURE THERMAL CYCLING OF COBALT AND COATED COLUMBIUM SPECIMENS

Pressure was increased linearly with time from 1 to 30 torr over the first 7 minutes, and then decreased linearly with time over the last 2 minutes of each cycle.

Twenty 3/4 by 3-1/2-inch alloy blanks were exposed in four runs, each of which consisted of nominally 12 cycles. Table 4 identifies the alloy blanks which were contained in the individual runs and also identifies the individual mechanical-test specimens which were later prepared from these.

TABLE 4. IDENTIFICATION OF COBALT-ALLOY TEST SPECIMENS EXPOSED TO STATIC CYCLIC PROFILING AT 1900 F

| Run | Blank | Alloy | Welded? | Mechanical Test Specimens |
|---|---|---|---|---|
| Co-1 | C1 | HS188 | Y | 73, 74 |
| | C2 | L605 | Y | 75, 76 |
| | C3 | L605 | Y | 77, 78 |
| | C4 | L605 | Y | 79, 80 |
| | C5 | L605 | Y | 81, 82 |
| Co-2 | C6 | L605 | N | 83, 84 |
| | C7 | L605 | N | -- |
| | C8 | L605 | N | 85, 86 |
| | C9 | L605 | N | 87, 88 |
| | C10 | L605 | N | 89, 90 |
| | C11 | HS188 | Y | 91, 92 |
| Co-3 | C12 | HS188 | Y | 93, 94 |
| | C13 | HS188 | Y | 95, 96 |
| | C14 | HS188 | N | -- |
| | C15 | HS188 | N | 97, 98 |
| | C16 | HS188 | N | 99, 100 |
| | C17 | HS188 | N | 101, 102 |
| | C18 | HS188 | N | 103, 104 |
| Co-4 | C19 | L605 | N | 105, 106 |
| | C20 | HS188 | N | 107, 108 |

Figure 4 illustrates a typical time-temperature-pressure profile for one of these 12-cycle runs and incorporates a reduced-size copy of the actual time-temperature recorded data trace obtained during Run Co-3. Details on the actual times and temperatures achieved in each of the cycles in all four runs are given in Tables A-1 through A-5 in the appendix. The nominal versus actual time-temperature data for all four runs are summarized in Table 5. Agreement in the total exposure times and temperatures among the four runs is reasonably good, although some effects of the number of specimens included in the individual runs are apparent. Thus, longer average heatup times were required for the seven specimens in Run Co-3, and these specimens received about 10 percent less exposure time at 1900 F than the other groups of specimens. Conversely, the two specimens in Run Co-4 reached peak temperatures more rapidly than the others (compare Tables A-1 through A-4 in the appendix). As a consequence, even though this

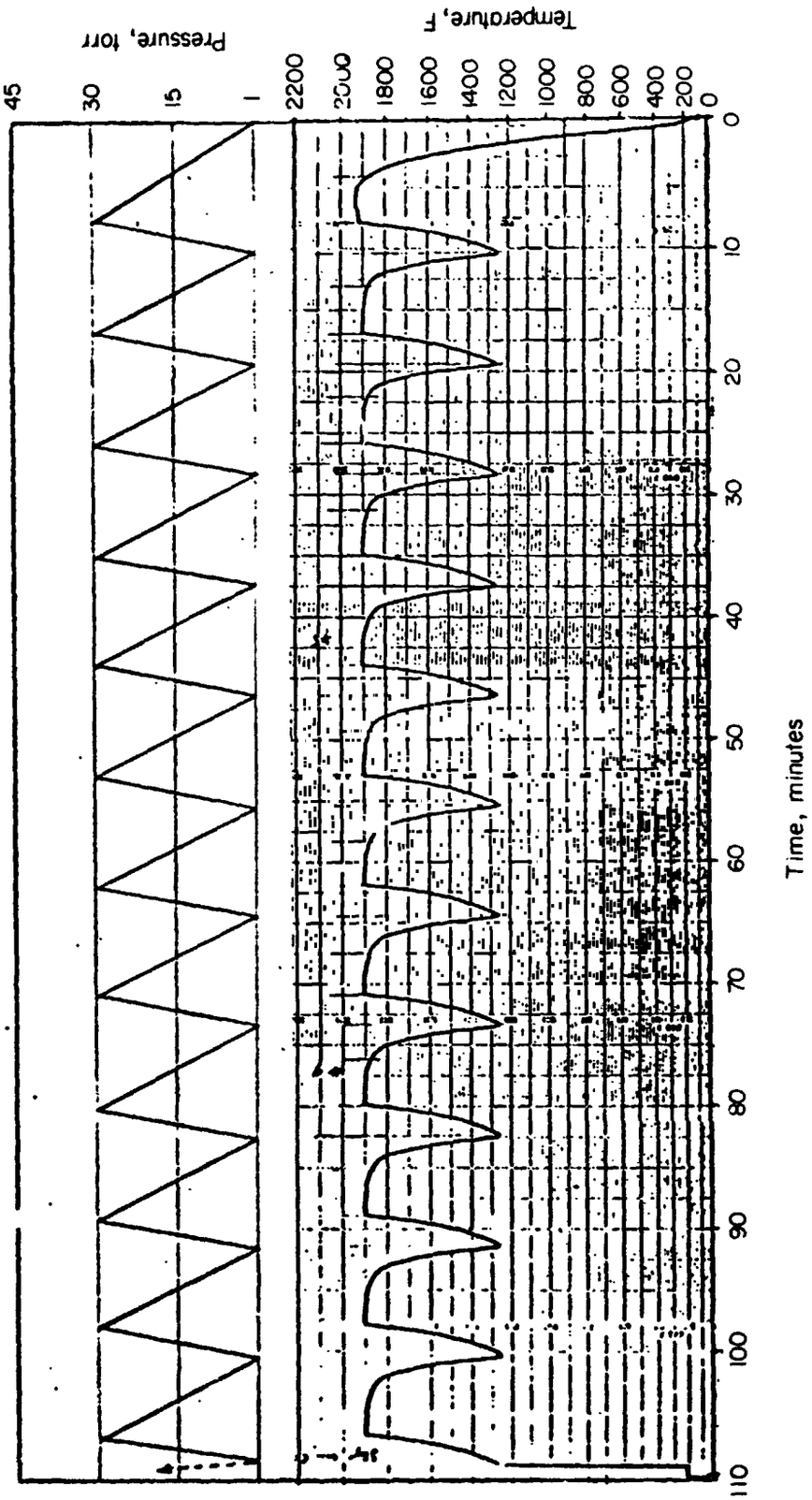


FIGURE 4. TIME-TEMPERATURE-PRESSURE PROFILES USED IN STATIC CYCLING OF COBALT ALLOY SPECIMENS

run was inadvertently terminated after only 11 cycles, the total exposure time for this run at 1900 F was about the same as for Runs Co-1 and Co-2.

TABLE 5. SUMMARIZED TIME-TEMPERATURE DATA FOR STATIC PROFILING RUNS ON COBALT-ALLOY SPECIMENS

| Item | Target Values | Achieved Values in Runs | | | |
|---|---|---|---|---|---|
| | | Co-1 | Co-2 | Co-3 | Co-4 |
| Number of Cycles | 12 | 12 | 12 | 12 | 11 |
| Number of Specimens | 20 | 5 | 6 | 7 | 2 |
| Average Time/Cycle, minutes | | | | | |
| Heatup to 1900 F | 2 | 2.2 | 2.4 | 3.0 | 2.3 |
| Hold at 1900 F | 5 | 4.3 | 4.2 | 3.8 | 4.5 |
| Cool to <1300 F | 2 | 2.5 | 2.4 | 2.5 | 2.4 |
| Totals | 9 | 9.0 | 9.0 | 9.3 | 9.2 |
| Total Exposure Times, minutes | | | | | |
| Heatup and Cooldown | 48 | 56.0 | 57.7 | 66.5 | 51.9 |
| Hold at 1900 F | 60 | 51.4 | 50.9 | 44.9 | 49.4 |
| Time for 12 Cycles | 108 | 107.4 | 108. | 111.4 | 101.3 |
| Temperature Control (12 Cycles) | | | | | |
| Peak Temperature, F | | | | | |
| Minimum Value | -- | 1900 | 1900 | 1900 | 1900 |
| Maximum Value | -- | 1940 | 1935 | 1935 | 1915 |
| Average Value | 1900 | 1913 | 1911 | 1905 | 1907 |
| Cooldown Temperature, F | | | | | |
| Minimum Value | -- | 1260 | 1245 | 1250 | 1180 |
| Maximum Value | <1300 | 1285 | 1260 | 1265 | 1260 |

Columbium Alloys. Two simulated, static, reentry profiling conditions were used for the coated columbium specimens. These differed essentially in the peak exposure temperature and in the time-pressure conditions. Thus, the initial target profile conditions which were used in the first two runs were as follows:

(1) Ramp type of heatup to 1450 F in 2 minutes

(2) Hold at 1450 F for 5 minutes

(3) Ramp type of heatup to 2500 F in 2 minutes

(4) Hold at 2500 F for 15 minutes

(5) Cool down to below 1300 F in 6 minutes.

Pressure was increased linearly with time from 1 to 30 torr over the 30-minute exposure period.

However, after the first two dynamic cyclic exposures were completed, the subsequent static profiling conditions were modified by

(1) Decreasing the peak exposure temperature from 2500 F to 2350 F

(2) Changing the pressure profile to vary with time as follows:

(a) Maintaining an isobaric pressure of 15 torr over the first 7 minutes' exposure

(b) Linearly increasing pressure from 15 to 25 torr over the next 2 minutes' exposure

(c) Maintaining an isobaric pressure of 25 torr over the next 15 minutes' exposure

(d) Linearly decreasing pressure from 25 to 15 torr over the final 6 minutes' exposure.

These changes, particularly in the pressure profile, were made to correspond more closely to the actual measured pressures, which were found to maintain at the 1450 F and 2350 F to 2500 F temperature plateaus during the dynamic cycling.

Twenty-two, 3/4 by 3-inch coated columbium blanks were exposed in five runs which consisted of one to five cycles at peak exposure temperatures of 2350 F or 2500 F. Table 6 identifies the individual coated specimens which were contained in these runs.

TABLE 6. IDENTIFICATION OF COATED COLUMBIUM SPECIMENS EXPOSED TO STATIC CYCLIC PROFILING

| Run | No. of Cycles | Peak Exposure Temp, F | Sample | Coating System | Substrate Thickness, mils | Defect Types Represented |
|---|---|---|---|---|---|---|
| Cb-1 | 1 | 2500 | S1 | R512E/Cb752 | 15 | A, B, C |
| | | | S2 | R512E/Cb752 | 25 | A, B, C |
| | | | S3 | R512E/C129Y | 15 | A, B, C |
| | | | S4 | R512E/C129Y | 25 | A, B, C |
| Cb-2 | 1 | 2500 | S5 | VH109/Cb752 | 15 | A, B, C |
| | | | S6 | VH109/Cb752 | 25 | A, B, C |
| | | | S7 | VH109/C129Y | 15 | A, B, C |
| | | | S8 | VH109/C129Y | 25 | A, B, C |
| Cb-3 | 1 | 2350 | S9 | R512E/Cb752 | 25 | C |
| | | | S10 | R512E/Cb752 | 25 | C |
| | | | S11 | R512E/Cb752 | 25 | C |
| | | | S12 | R512E/Cb752 | 25 | C |
| | | | S13 | R512E/Cb752 | 25 | C |
| | | | S14 | R512E/Cb752 | 25 | C |
| Cb-4 | 3 | 2350 | S15 | R512E/Cb752 | 25 | C |
| | | | S16 | R512E/Cb752 | 25 | C |
| | | | S17 | R512E/Cb752 | 25 | C |
| | | | S18 | R512E/Cb752 | 25 | C |
| Cb-5 | 5 | 2350 | S19 | R512E/Cb752 | 25 | C |
| | | | S20 | R512E/Cb752 | 25 | C |
| | | | S21 | R512E/Cb752 | 25 | C |
| | | | S22 | R512E/Cb752 | 25 | C |

The first two of these five runs were intended to compare the oxidation and contamination behavior of three types of intentional coating defects in the four coating systems of primary interest in static cycling at 2500 F. Accordingly, as indicated in Table 6, each of these coated specimens contained one each of the three coating-defect types (described earlier) which were spaced 3/4-inch-apart along the specimen's length. On the basis of the results obtained from these two runs as well as those obtained from an identical series of specimens cycled under the same time-temperature conditions in the dynamic encironment, the small Type C defect was selected as a standard to evaluate the extent of mechanical-property change as a function of thermal exposure. Accordingly, the balance of three static runs employed specimens containing only one Type C defect at the center surface on one side.* Also, as shown in Table 6, these statically cycled specimens for subsequent mechanical-property determinations were restricted in this first-year effort (more or less arbitrarily) to the R512E/Cb752 system.

Figures 5 and 6 illustrate the typical time-temperature-pressure profiling conditions achieved in the two profile types accorded the coated columbium specimens. Details on the actual times and temperatures achieved in each of the cycles of all five runs are given in Tables A-6 and A-7 in the appendix. The nominal versus actual time-temperature data for all five runs are summarized in Table 7.

TABLE 7. SUMMARIZED TIME-TEMPERATURE DATA FOR STATIC PROFILING RUNS ON INTENTIONALLY DEFECTED COATED COLUMBIUM SPECIMENS

| Item | Target Values | Achieved Values in Runs Indicated | | | | |
|---|---|---|---|---|---|---|
| | | Cb-1 | Cb-2 | Cb-3 | Cb-4 | Cb-5 |
| Number of Cycles | -- | 1 | 1 | 1 | 3 | 5 |
| Average Time/Cycle, minutes | | | | | | |
| Rise to 1450 F | 2 | 1.7 | 2.1 | 2.4 | 0.5 | 1.0 |
| Hold at 1450 F | 5 | 5.3 | 5.1 | 4.0 | 5.4 | 4.9 |
| Rise to $T_{max}$ | 2 | 2.0 | 2.2 | 2.9 | 3.0 | 2.9 |
| Hold at $T_{max}$ | 15 | 14.8 | 15.3 | 15.1 | 15.0 | 15.2 |
| Decay to <1300, F | 6 | 8.3 | 7.9 | 4.0 | 7.0 | 7.7 |
| Totals | 30 | 32.1 | 32.6 | 28.4 | 29.9 | 31.7 |
| Temperature Control[a] (All Cycles) | | | | | | |
| 1450 F Plateau | | | | | | |
| Minimum Value, F | -- | 1400 | 1400 | 1400 | 1395 | 1400 |
| Maximum Value, F | -- | 1480 | 1485 | 1450 | 1460 | 1460 |
| Average Value, F | 1450 | 1440 | 1443 | 1437 | 1440 | 1437 |
| $T_{max}$ Plateau | | | | | | |
| Minimum Value, F | -- | 2500 | 2470 | 2340 | 2330 | 2340 |
| Maximum Value, F | -- | 2540 | 2510 | 2355 | 2362 | 2360 |
| Average Value, F | -- | 2500 | 2490 | 2340 | 2358 | 2356 |

(a) Temperature at center of specimen.

* Each of these blanks was later machined into a tensile-test specimen which incorporated the defected coating region at the center of its reduced section.

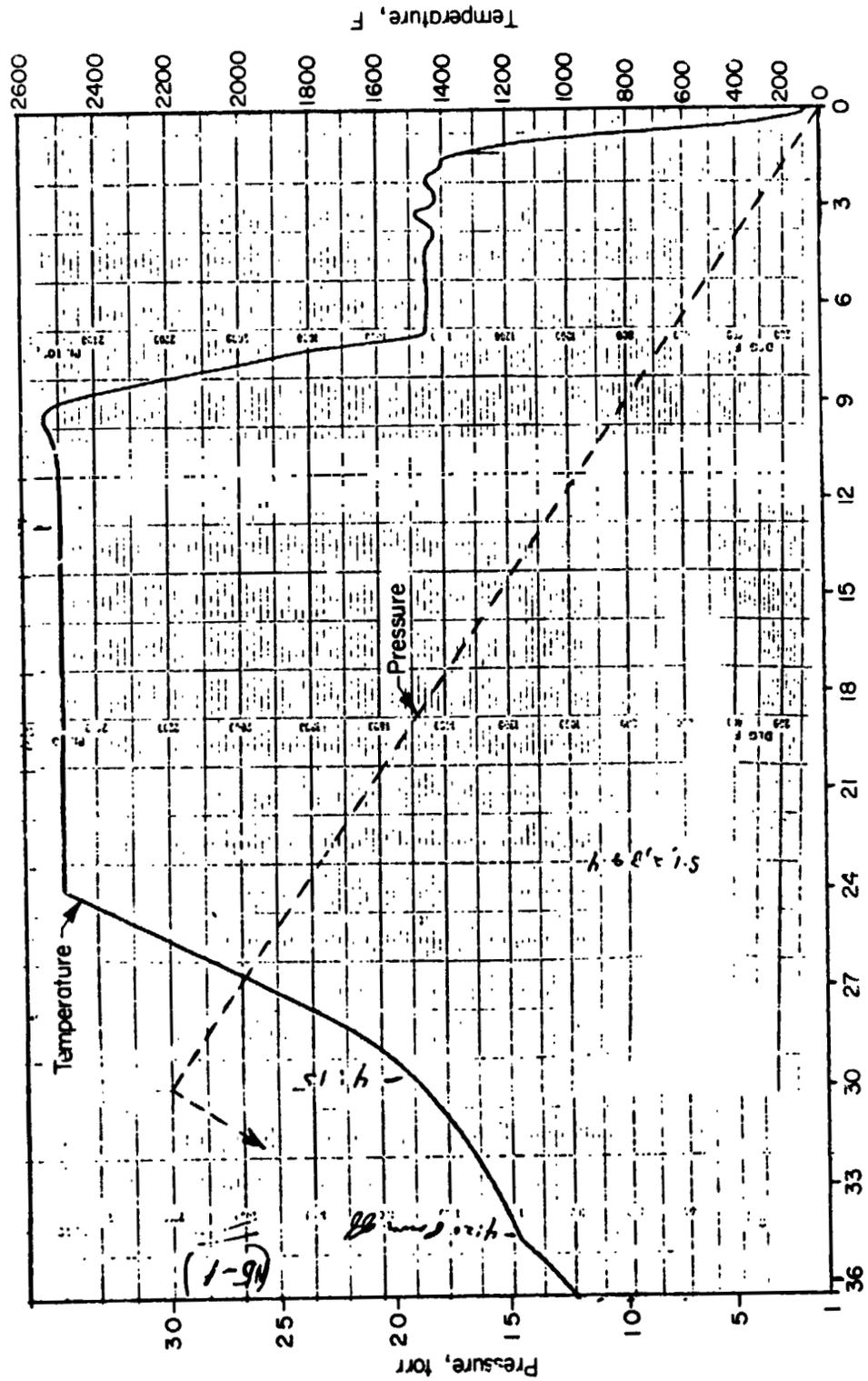


FIGURE 5. TIME-TEMPERATURE-PRESSURE PROFILES USED IN STATIC CYCLING OF COATED COLUMBIUM SPECIMENS FOR RUNS Cb-1 AND Cb-2

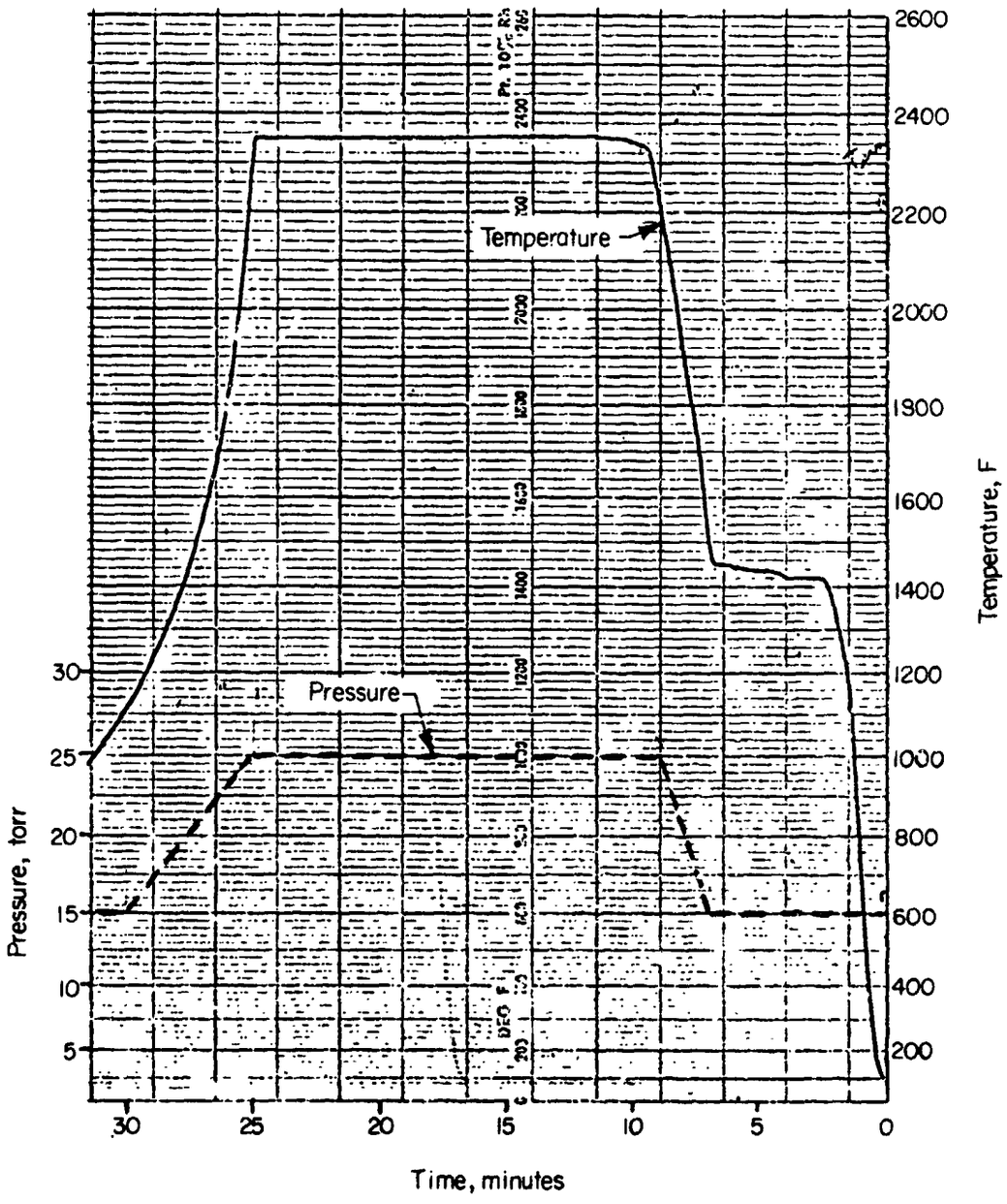


FIGURE 6. TIME-TEMPERATURE-PRESSURE PROFILES USED IN STATIC CYCLING OF COATED COLUMBIUM SPECIMENS FOR RUNS Cb-3, Cb-4, AND Cb-5

## Dynamic Environment Exposures

### Equipment

Aerothermal Research Facility. The plasma-arc exposures were conducted in the Battelle-Columbus Aerothermal Research Facility. The facility consists of two separate in-tunnel legs each of which includes a continuous-flow arc heater, a conical convergent-divergent nozzle, a free-jet test cabin, and a conical convergent-divergent diffuser. Each leg exhausts to the pressure recovery system which consists of a five-stage steam ejector. Electrical power for both legs is supplied by a 1.5-megawatt rectifier substation controlled by a saturable reactor. A schematic layout of the facility is shown in Figure 7.

For these exposures, the nontoxic, nonradioactive leg was used with the high-enthalpy arc heater. This arc heater is of a modular design with a segmented column and gas stabilization of the arc column. Nitrogen gas is injected tangentially just downstream of the cathode and oxygen is injected into the plenum which is downstream of the anode and upstream of the expansion nozzle. The plenum damps spatial and temporal variations in gas properties and provides for a uniform test stream. A pressure tap is provided on the plenum to continuously monitor reservoir pressure during a test. A nozzle with a 1-inch-diameter throat and 5-inch-diameter exit was used for these tests.

The envelope of reservoir conditions which can be obtained with the high-enthalpy heater is shown in Figure 8. Nominal reservoir conditions at peak temperature conditions for the coated-columbium-alloy specimens and cobalt-alloy specimens are indicated in Figure 8. Enthalpy and pressure can be varied independently as a function of time during a test, either manually or by analog control of arc current and/or heater gas flow rate. During these tests, the specimen temperatures were varied as a function of test time by analog control of the arc current.

Specimen Housing. As shown in Figure 1, the arc test-specimen configuration permits mounting of the specimens on the model holder by the insertion of pins through the corner end tabs into a supporting block. Stainless steel blocks were used as the holder material for the cobalt-alloy specimens, while silicide-coated molybdenum blocks were used as the holder material for the columbium-alloy specimens. In each case, three specimens were mounted on each of two blocks. After plasma-arc exposure the end tabs were removed and the remaining rectangular blank was prepared for mechanical-property evaluations. Figure 9 shows the molybdenum blocks mounted in the water-cooled copper housing. The pins on the leading edge of the rear block can be seen along the leading edge of the rear molybdenum block in the photograph. The specimens are free to expand along the pins which extend slightly beyond the end tabs. The pins at the trailing edges are inserted through the holes in the specimens and into the blocks after the specimens are mounted on the blocks using the front pins. The compartments in the supporting blocks were filled with fibrous zirconia thermal insulation (Zircar™ Type ZYF-Union Carbide). Thermocouples protruding through holes in the bottom of each support block can be seen in Figure 9.

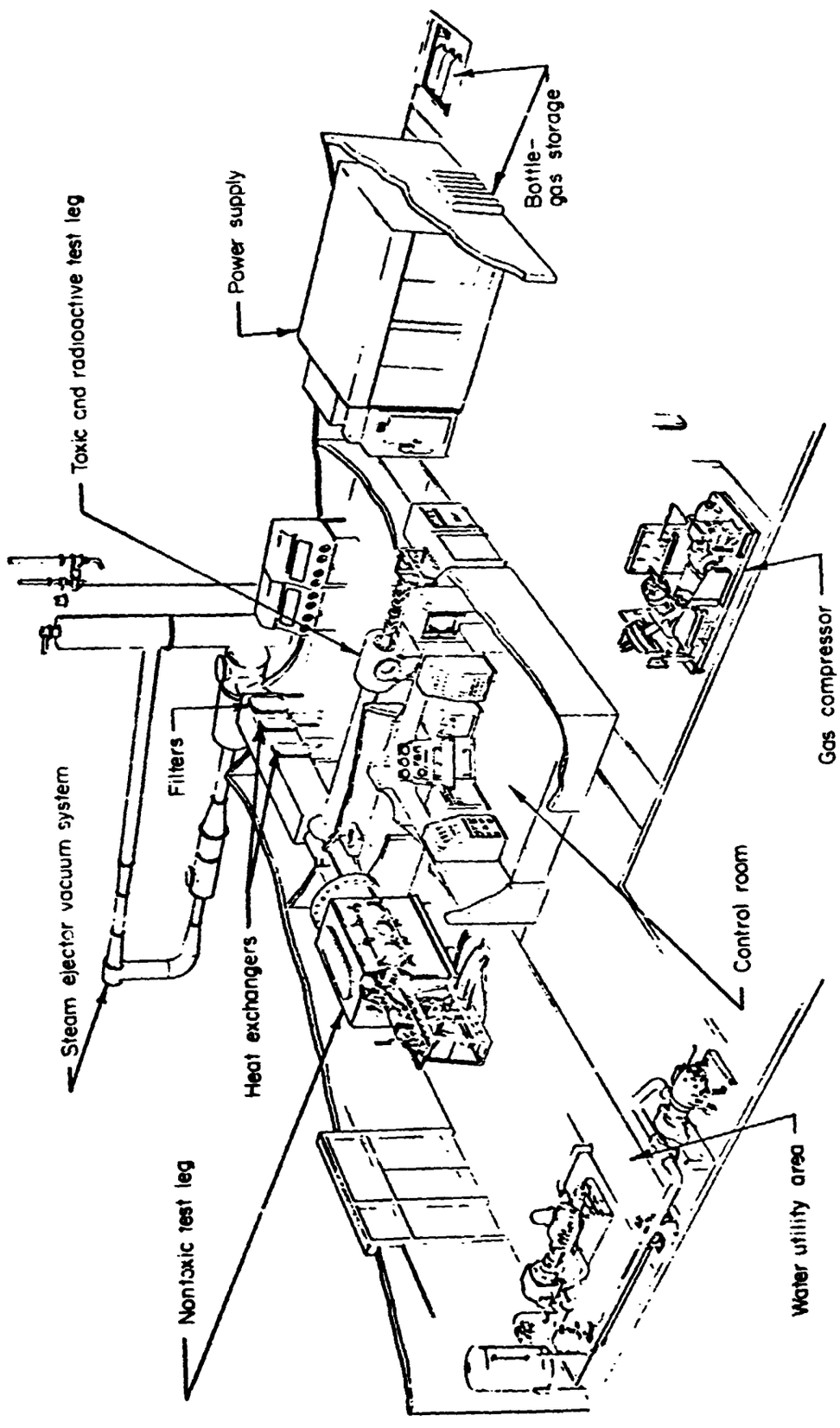


FIGURE 7. AEROTHERMAL RESEARCH FACILITY - BATTELLE'S COLUMBUS LABORATORIES

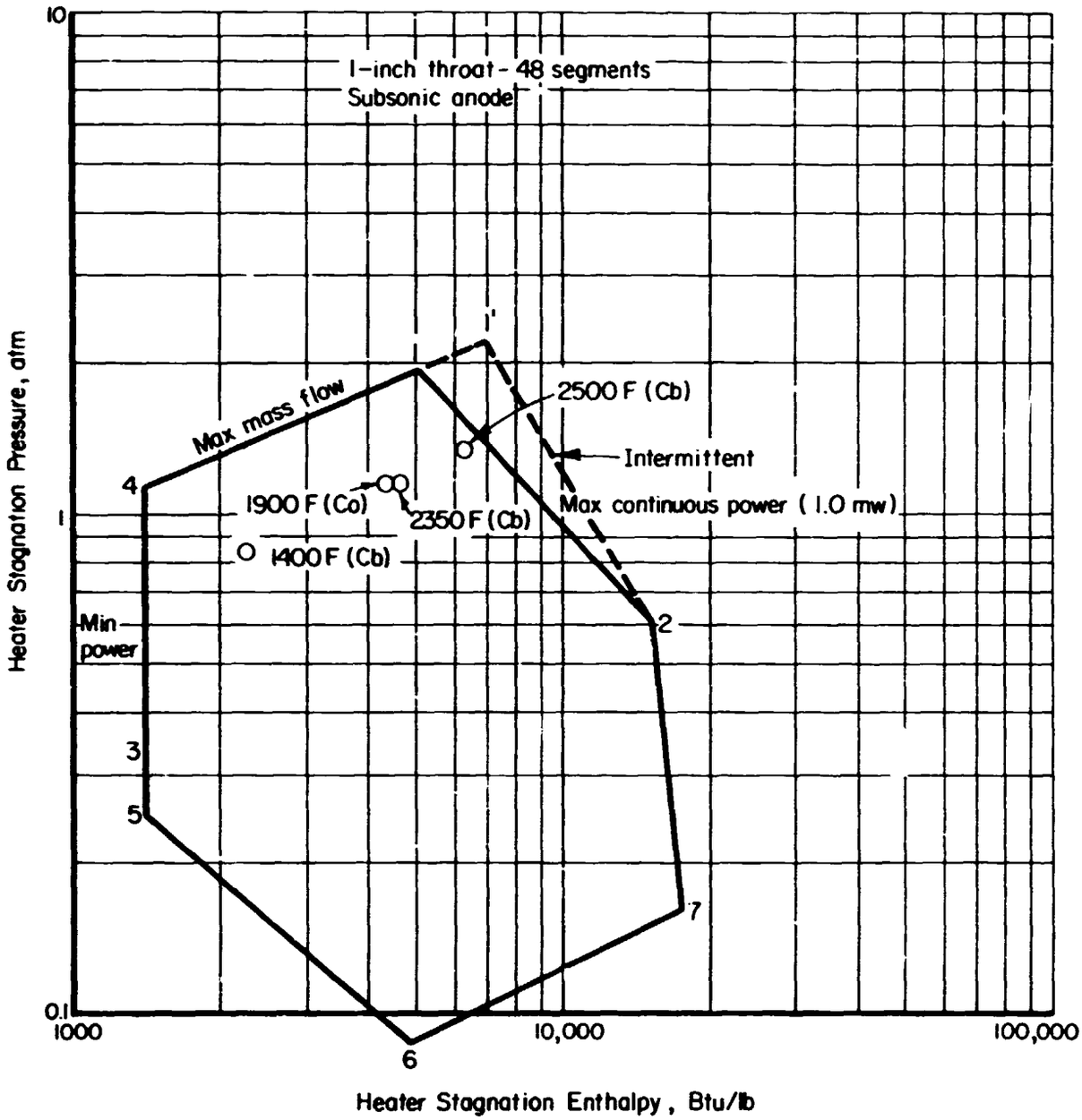


FIGURE 8. ENVELOPE OF HIGH-ENTHALPY ARC-HEATER-RESERVOIR CONDITIONS

~1X

FIGURE 9. TOP VIEW OF FORWARD AND REAR (ABOVE LEFT AND RIGHT, RESPECTIVELY), SILICIDE-COATED MOLYBDENUM SPECIMEN HOLDER BLOCKS IN MODEL HOLDER ASSEMBLY

The front support block is held and positioned in the water-cooled copper plate by a combination of eight machine screws in a push-pull arrangement which allows for varying the specimen height and orientation relative to the copper plate. A bottom rear view of the assembly is shown in Figure 10. The rear block is mounted on a pair of scissor jacks for positioning. The jacks can be actuated independently by direct-current motor-driven screws during a test for fine adjustment of specimen elevation and inclination, thus controlling the temperature. These two screws can be seen in Figure 10 along with the stainless steel plate to which the front block is attached. Also visible in Figure 10 are the thermocouple insulators and the tubes for water cooling of the springs in the thermocouple assembly.

The model holder was made of 3/4 in. -thick copper through which passages were machined for water cooling. Overall dimensions of the water-cooled plate were 4-1/2 in. in width and 8-1/4 in. in length. A cutout was provided in the plate for mounting of the blocks and specimens. The cutout was nominally 2-1/4 x 6 in. and was centered with respects to the plate width. The cutout extended from 1-1/2 in. to 7-1/2 from the leading edge of the plate in the flow direction.

Figure 11 shows a set of six specimens mounted in the specimen housing and the assembly in the test cabin. In this photograph, the direction of gas flow is from left to right. The assembly can be seen between the exit nozzle (left of specimens) and the diffuser (right of specimens).

## Temperature Measurement

Thermocouples, infrared pyrometry, and infrared photography were used to determine the temperature response of the specimens during plasma-arc exposures.

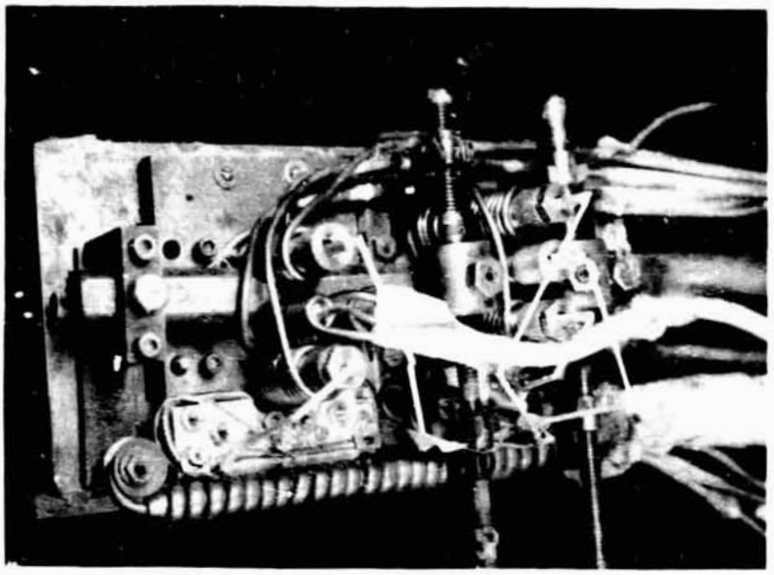

FIGURE 10. BOTTOM VIEW OF SPECIMEN – MODEL HOLDER ASSEMBLY

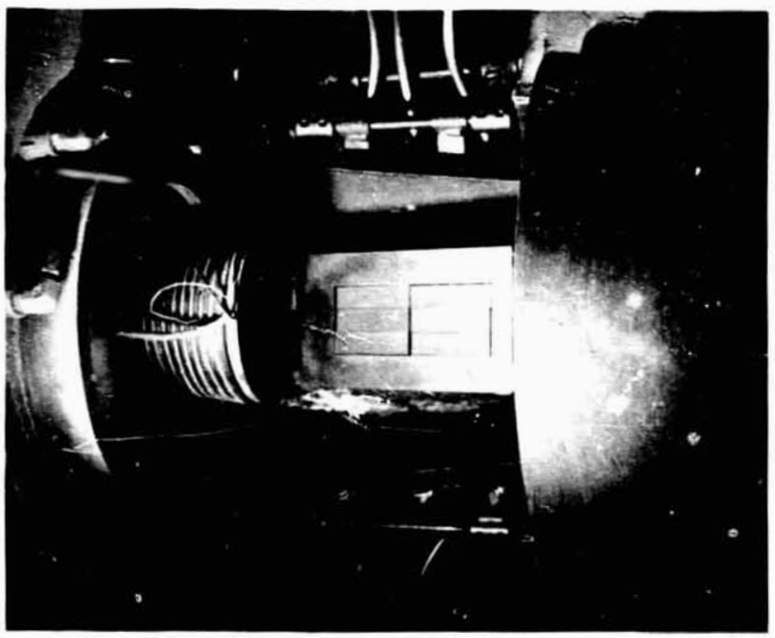

FIGURE 11. VIEW OF A SET OF SIX SPECIMENS IN THE MODEL HOLDER ASSEMBLY PREPARATORY TO ARC EXPOSURE

Thermocouples. For temperature measurement of the cobalt alloys during exposure, a Chromel-Alumel thermocouple was spot welded in the center of the back side of each specimen.

For the coated columbium specimens, a spring-loaded, water-cooled*, Pt/Pt-10 Rh thermocouple was used for the temperature measurement of each specimen. The location of these thermocouples on the underside of the specimens is shown schematically in Figure 12. Also, the same alphabetic specimen identification and orientation illustrated in Figure 12 was used for all of the cobalt and columbium specimens throughout all of the plasma-arc runs. That is, the A, B, or C specimens in a given run always occupied the A, B, or C positions (relative to the arc flow direction) on the forward block of the model holder as shown in Figure 12 and the D, E, or F specimens occupied the corresponding positions on the rear block of the model holder.

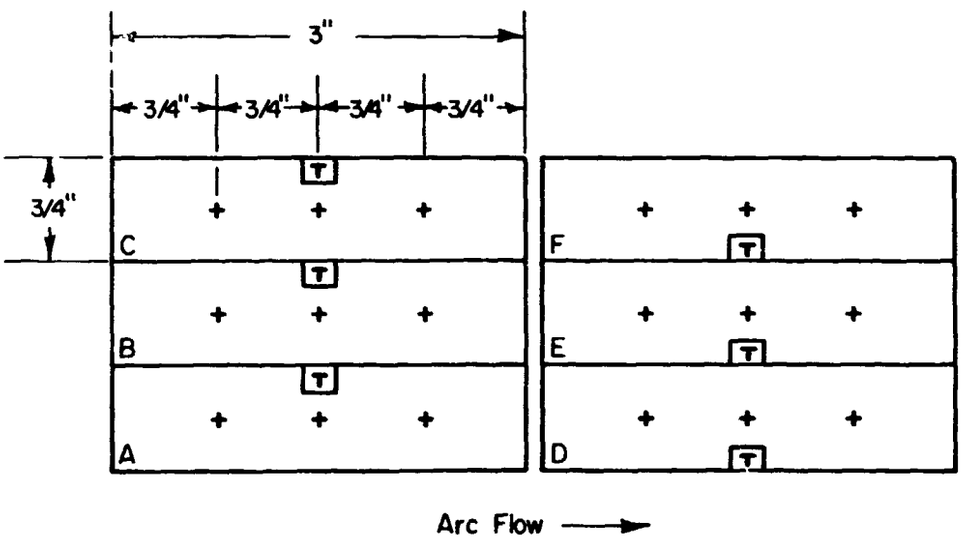


FIGURE 12. SCHEMATIC TOP VIEW SHOWING SAMPLE NOMENCLATURE, ORIENTATION, AND INTENTIONAL DEFECT AND THERMOCOUPLE LOCATIONS IN COATED COLUMBIUM-PLASMA-ARC SPECIMENS

To avoid reactions of the thermocouple material with the specimen's disilicide coating, a 1-mil-thick, 1/8-inch square, iridium foil was attached to the coated columbium using a thin application of Sauereisen No. 8 electrotemp refractory cement. This was found experimentally to be compatible with both R512E and VH109 coatings. The spring-loaded device forces contact of the thermocouple bead against the iridium foil cemented to the underside of the specimen. The beaded ends of the thermocouples and high-purity alumina insulator can be seen in Figure 9.

Experiments were conducted in which the compatibility of the Pt/Pt-10 Rh thermocouple with the Sauereisen cement and iridium foil was determined. It was found that the millivoltage output from the thermocouple was not affected by the presence of the cement or foil for a 2-1/4-hour exposure in air at temperatures of 2500 to 2590 F.

* Water cooling was provided for Run 9 and all succeeding runs.

Other techniques for attaching the thermocouples to the back side of the specimens were explored during the preliminary calibration. These consisted of:

(1) Spot welding the thermcouple bead to a 1-mil-thick iridium foil and cementing the foil to the specimen

(2) Embedding the thermocouple bead and iridium foil in a rigid cement attachment to the specimen

(3) Embedding the thermocouple bead only in a rigid cement attachment to the specimen.

However, none of these techniques provided sufficient mechanical strength to withstand the handling involved in mounting the specimens to the specimen holder assembly.

Infrared Pyrometry. Two recording infrared-radiation (IR) pyrometers were used during the plasma-arc exposures. The pyrometers are manufactured by Ircon Inc., and operate in the spectral range of 2.0 to 2.6$\mu$. One of the pyrometers (control pyrometer) was sighted on the middle specimen in the front row, approximately in the center of the specimen (but not at the defect) and was used for feedback control of the arc heater. This was accomplished using an analog control device preprogrammed to provide the desired surface-temperature history by varying the current to the arc heater. The output of the thermocouple on the front middle specimen was used to initially set the correct pyrometer output voltage since the value of the output signal is dependent on the surface emittance. Using this technique in conjunction with the pyrometer calibration yielded a pyrometer emittance setting of 0.80 to 0.85. Emittance values of 0.8 to 0.85 are in general agreement with previously obtained experimental values for coated columbium alloys*.

The second pyrometer (scanning pyrometer) was used to obtain data on the temperature profile of the specimens. This pyrometer was mounted on a remote-controlled mechanism which permitted the pyrometer to scan over the specimens during the exposure. In this manner, it was possible to obtain from three to four complete scans in the side-to-side and flow directions across each row of defects in each of the six specimens. The voltage output of a positioning potentiometer (which indicated the precise pyrometer scan location) was recorded simultaneously with the pyrometer output voltage. The pyrometer scan speed was adjusted to a maximum compatible with the response characteristics.

The pyrometer temperature-voltage calibration tabulations were experimentally corrected for arc radiation reflected from the specimen surface at operating conditions identical to those used in the specimen exposures. Also, because the pyrometers were mounted on top of the test cabin, it was necessary to correct the signal for radiation absorption by the test-cabin window. This was accomplished experimentally by measuring the change obtained in pyrometer signal with and without the window as a function of specimen temperature.

Infrared Photography. Color infrared pnotographs were taken during the nominal peak-temperature-exposure portion of the cycles to determine the temperature gradients over the entire exposed surface area of the specimens. Kodak 70-mm Ektachrome infrared film was used for these pictures with an 87 C filter over the camera lens. This combination of film and filter limits the radiation detection to a relatively narrow

*Bartsch, K. O., et al., "Investigation of the Emittance of Coated Refractory Metals", AIAA Paper No. 70-68, AIAA 8th Aerospace Sciences Meeting, New York, New York, January 19-21, 1970.

wavelength interval, 0.85 to 0.90$\mu$. An electrically driven Hasselblad camera with a 100-mm planar lens was used for these pictures. Several exposure durations and f-stops were obtained. The Hasselblad camera was mounted on top of the test cabin and was sighted on the specimens through the test-cabin window. The format was sufficiently large to obtain all of the specimen area within each picture.

Calibration of the infrared film was accomplished using a technique similar to that described by Pollack and Hickel.* In this calibration, the density of the film is uniquely related to the source or specimen brightness temperature. In essence, the procedure consists of three key elements: (1) a calculated relationship between the surface temperature and the relative radiant energy, which results in a master distribution curve (MTD curve); (2) an experimentally determined relationship between film density and the relative film exposure energy, which results in a film-response curve (FR curve); and (3) a calibration point which is a known temperature on the specimen surface that can be associated with a corresponding film density. The first two elements are independently determined and are associated with each other by the temperature-density calibration point.

The MTD curve shown in Figure 13 is obtained by calculating the radiant emittance as a function of temperature within the wavelength limits of 0.85 to 0.90$\mu$. Using Wien's approximation of Planck's law the spectral bandwidth radiant emittance is related to temperature by

$$\log W_{\lambda_2-\lambda_1} = \alpha - \frac{1}{T} \quad .$$

The constants required to uniquely define the radiant emittance-temperature relationship for the wavelength band of interest were obtained from results given by Pollack and Hickel. The MTD curve in Figure 13 has been plotted for an assumed spectral bandwidth emissivity of 0.85.

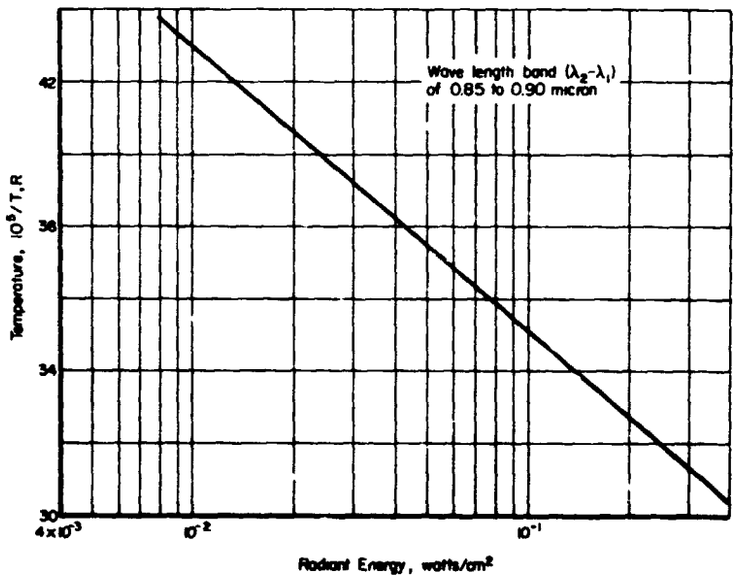


FIGURE 13. MTD CURVE: RADIANT ENERGY AS A FUNCTION OF TEMPERATURE

* Pollack, F. G., and Hickel, R. O., "Surface Temperature Mapping with Infrared Photographic Pyrometry For Turbine Cooling Investigations", NASA TN D-5179 (January, 1969), 45 pp.

The second element of the film calibration is to experimentally generate data which relate the film density to the relative film exposure energy. This was accomplished by exposing the infrared film to a constant-energy, radiation source at various energy levels. The exposure times were also varied and the resulting matrix of film densities were plotted as a function of the relative film exposure energy levels. Figure 14 shows the film response curve generated and the actual data points obtained.

The experimental setup consisted of the constant-temperature tungsten ribbon source (previously calibrated at N. B. S. ), the test-cabin window used during the plasma-arc exposures interposed between the camera and the light source, and the camera. The distances between the camera and window and between the window and light source were established on the basis of the corresponding distances that would be obtained during the plasma-arc exposures. Also, the optical path length through the test-cabin window achieved during the plasma-arc exposures was duplicated during the film calibration by tilting the window. An 87 C filter was placed over the camera lens (same camera and filter as used during the plasma-arc exposures) to obtain the FR curve for the same wavelength interval as was used during the arc-jet tests.

At a given source temperature, the exposure duration was varied to obtain the desired ranges in exposure energy levels and film density. The source temperature was varied to ensure that a unique film-response-relationship exists for the infrared film in the temperature range of interest. Temperatures used in the calibration are indicated in Figure 14. They are within the range of specimen temperatures obtained during plasma-arc testing. It can be seen in Figure 14, that the film density varies slowly at low and high energy levels, corresponding to under- and overexposure of the film, respectively. It can also be seen that the usable relative energy response range for the color infrared film is about 10 (i. e., a tenfold change in energy level. )

With a single known reference temperature or calibration point, Figure 13 can be used to establish an absolute energy scale on Figure 14. This can then be used to relate film density to local temperature variations over the entire photograph.

By coupling the results obtained from selected thermocouples (generally only two or three thermocouples in a given run were free from anomalies), the IR pyrometer scan data, and IR photography, estimates of emittance ranges and changes during dynamic testing were achieved. In most cases, it was possible to estimate emittance of the coating/substrate systems to within ±0. 05 during the arc-jet exposures.

## Temperature and Pressure Profiling

Cobalt Alloys. The simulated time-temperature reentry profiling conditions used in dynamically cycling the cobalt alloys were the same as those used in the static cycling. That is, each plasma-arc run consisted of twelve 5-minute exposures at a nominal peak temperature of 1900 F with nominal heating and cooling periods between cycles of 2 minutes. Typical time-temperature profiles for two specimens during one of these runs are illustrated in Figure 15.

Eighteen specimens were exposed in three runs, each consisting of twelve 5-minute exposures at 1900 F. Complete cycle time-temperature histories for all specimens in these runs are givin in Tables A-8 through A-16, inclusive, in the appendix.

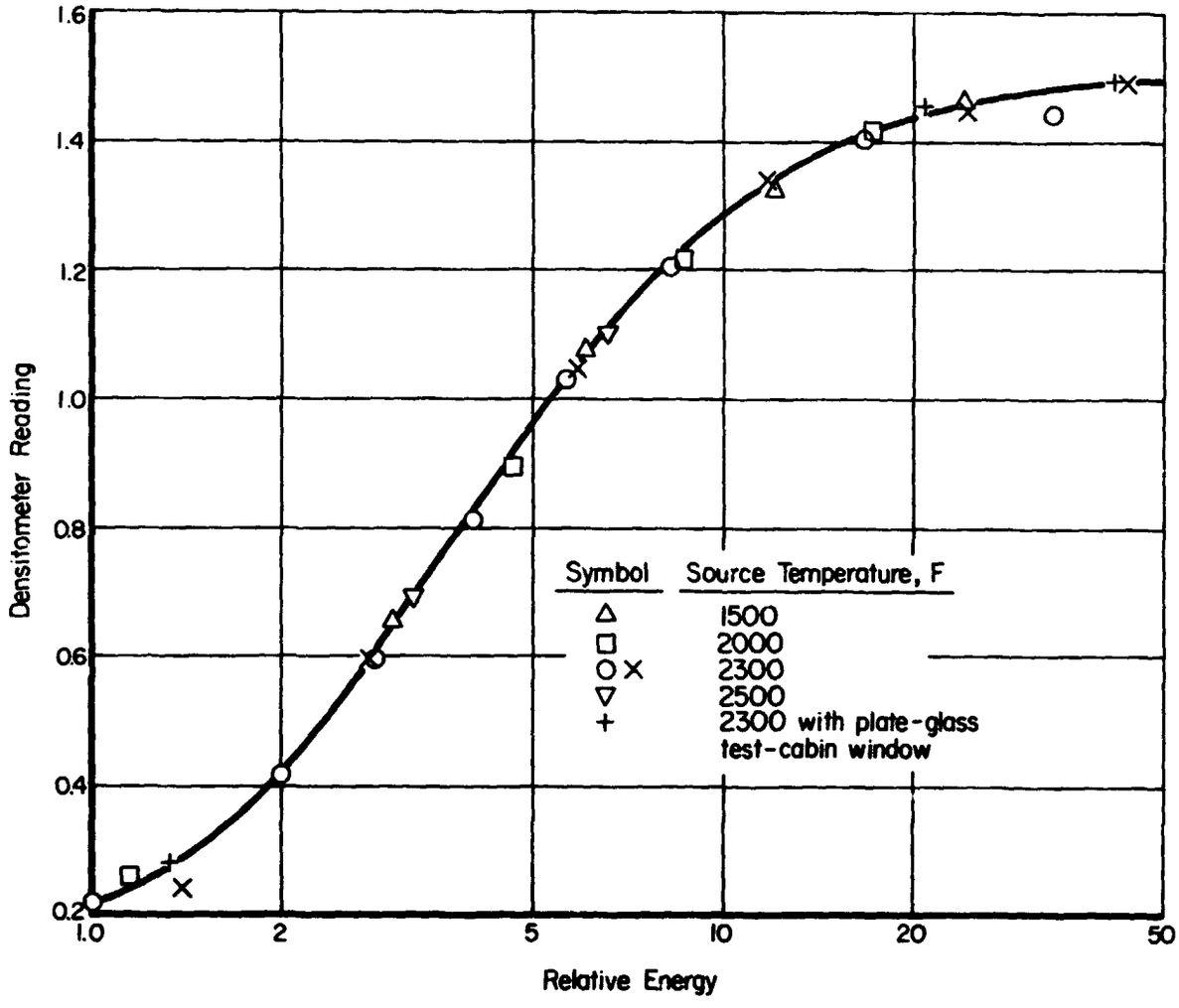


FIGURE 14. FILM RESPONSE CURVE

The nominal versus average time-temperature data for all specimens in each of the three runs are summarized in Table 8. As indicated in Figure 15, the minimum temperature reached by the specimens on cooling between cycles were in the range of 1000 F to 1200 F.

As noted earlier, the center temperature of each specimen during arc exposure was monitored by a thermocouple. These data are summarized in Table 9, which also identifies the compositions and weld conditions of the 18 individual specimens and of the 32 mechanical-property-test specimens which were later prepared from these.

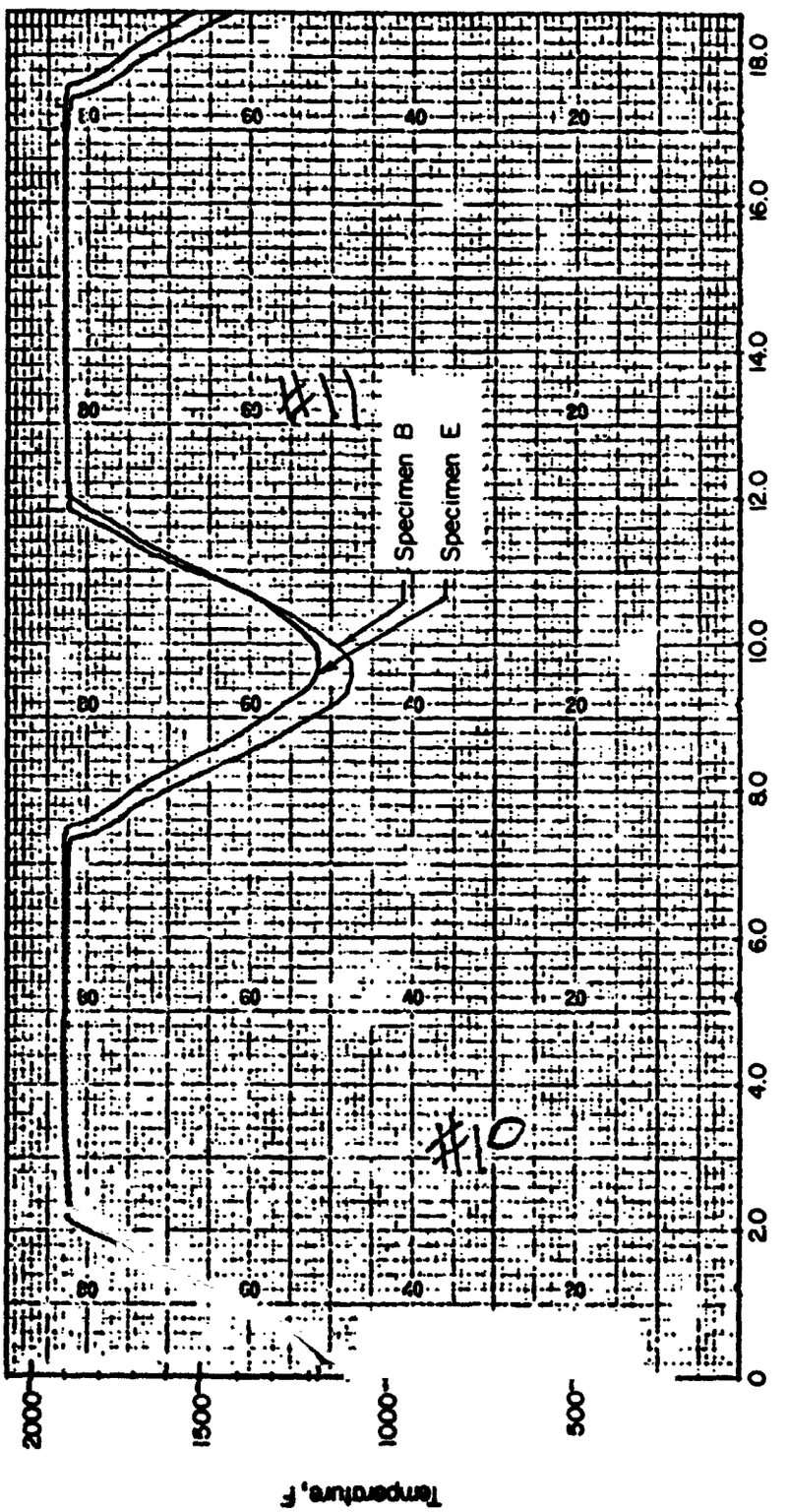


FIGURE 15. SPECIMEN TEMPERATURE PROFILES FOR TWO COBALT ALLOY SPECIMENS DURING DYNAMIC CYCLING AT 1900 F

TABLE 8. SUMMARY OF TIME-TEMPERATURE DATA FOR PLASMA-ARC PROFILING RUNS ON COBALT ALLOYS

| Item | Target Values | Achieved Values in Runs Indicated | | |
|---|---|---|---|---|
| | | 3 | 4 | 5 |
| Number of Cycles | 12 | 12 | 12 | 12 |
| Average Time/Cycle, minutes | | | | |
| Rise to 1900 F | 2 | 2.1 | 1.9 | 1.7 |
| Hold at 1900 F | 5 | 5.3 | 5.2 | 5.5 |
| Decay to <1300 F | 2 | 2.2 | 2.0 | 1.6 |
| Totals | 9 | 9.6 | 9.1 | 8.8 |
| Total Exposure Time, minutes | | | | |
| Rise and Decay | 48 | 51.9 | 46.0 | 40.2 |
| Hold at 1900 F | 60 | 63.1 | 62.9 | 65.7 |
| Time for 12 Cycles | 108 | 115.0 | 108.9 | 105.9 |
| Peak Temperature Control (12 Cycles), F | | | | |
| Minimum Value | -- | 1809 | 1760 | 1810 |
| Maximum Value | -- | 1957 | 1962 | 1976 |
| Average Value | 1900 | 1873 | 1856 | 1866 |

TABLE 9. SUMMARY OF PLASMA-ARC-EXPOSURE TEMPERATURE DATA FOR INDIVIDUAL COBALT-ALLOY SPECIMENS

| | Location | Maximum Center Temperature[a], F | | | Average Gradient[c] F/in. | Mechanical Test Specimens |
|---|---|---|---|---|---|---|
| | | Lowest Cycle | Highest Cycle | Average[b] | | |
| **Run 3** | | | | | | |
| HS188, welded | A | 1841 | 1892 | 1881 | 9 | 57, 58 |
| HS188 | B | 1841 | 1892 | 1882 | 40 | -- |
| HS188 | C | 1855 | 1896 | 1882 | 14 | 59, 60 |
| HS188 | D | 1859 | 1957 | 1904 | 31 | 61, 62 |
| HS188, welded | E | 1809 | 1892 | 1851 | 19 | 63, 64 |
| HS188, welded | F | 1786 | 1892 | 1845 | 23 | 65, 66 |
| **Run 4** | | | | | | |
| L605 | A | 1804 | 1878 | 1837 | 57 | 21, 22 |
| HS188 | B | 1760[d] | 1840[d] | 1809 | 44 | 67, 68 |
| L605, welded | C | 1781 | 1864 | 1819 | 47 | 23, 24 |
| HS188 | D | 1873 | 1962 | 1924 | 54 | 69, 70 |
| HS188, welded | E | 1850[d] | 1920[d] | 1895[d] | 28 | 71, 72 |
| L605 | F | 1820[d] | 1890[d] | 1853[d] | 28 | 25, 26 |
| **Run 5** | | | | | | |
| L605, welded | A | 1828 | 1892 | 1850 | 20 | 27, 28 |
| L605 | B | 1851 | 1888 | 1867 | 45 | - - |
| L605 | C | 1810 | 1948 | 1857 | 15 | 29, 30 |
| L605 | D | 1856 | 1898 | 1876 | 19 | 31, 32 |
| L605, welded | E | 1818 | 1856 | 1840 | 63 | 33, 34 |
| L605, welded | F | 1883 | 1976 | 1922 | 64 | 35, 36 |

(a) Unless otherwise noted, the temperatures cited represent the maximum thermocouple values observed over a nominal 5-minute exposure cycle. See Tables A-11, A-12, and A-13.
(b) Average based on the maximum temperature for 12 exposure cycles.
(c) Average based on the gradients determined in Cycles 1, 6, 9, and 12. See Tables A-14, A-15, and A-16.
(d) Temperatures estimated from pyrometer data because of thermocouple failures.

In the absence of sample distortion under the plasma gas flow, the temperature gradient along each specimen was of the order of 10 to 25 F per inch. This gradient is based on a laminar convective-heat-transfer rate that varies inversely with the square root of distance from the leading edge. However, about half of the exposed cobalt alloys exhibited a noticeable tendency to bow upwards in the arc in the region where peak temperatures were reached, i.e., near their forward edge. This had the undesirable effects of tending to increase the peak temperature and temperature gradient along that particular specimen as well as to disturb the plasma gas flow across the adjacent samples. Where this occurred, the bowing distortion and temperature effects on a given sample were surprisingly consistent throughout the 12 cycles.

The schematic illustration below represents a profile of the front and rear specimens and the flow field generated by the change in slope of the rear specimens relative to

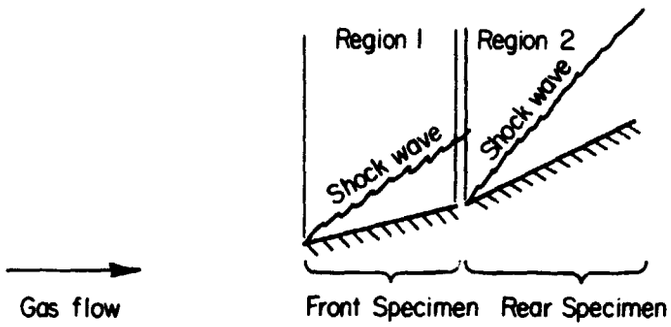


the front specimens. Pressure measurements were made using water-cooled blocks of a configuration identical to that of the specimens. The positioning of the blocks was identical to that used in the actual specimen exposures. From the measured pressures and calculated free-stream properties, the shear stress at the center of the front and rear specimens was calculated. The calculation technique used is that given by Harney and Petrie* and includes a correction for wall-temperature effects. Additional details of the dynamic environmental exposure conditions are given in Appendix B. Shown below are arc-heater operating parameters and the calculated shear stress for the cobalt-alloy exposure conditions.

(1) At maximum temperature (1900 F):

| | |
|---|---|
| Free-Stream Mach Number | 4.5 |
| Total Gas Enthalpy (From Arc-Heater Energy Balance), Btu/lb | 4,460 |
| Heater Reservoir Pressure (Measured), 1 atm | 1.16 |
| Model Surface Pressure (Measured), torr | |
| Region 1 | 11.7 |
| Region 2 | 11.7 |

* Harney, D. J., and Petrie, S. L., "Hypersonic Surface Pressure and Heat Transfer on Slender Bodies in Variable Composition and Nonequilibrium Atmospheres" AFFDL-TR-70-31 (April, 1970), 42 pp.

| | |
|---|---|
| Aerodynamic Shear, psf | |
| Region 1 | ~1.2 |
| Region 2 | ~1.6 |

(2) Minimum temperature without loss of arc was about 1000 F for the front row of specimens and about 1200 F for the back row of specimens. Gas enthalpy minimum was about 1800 Btu/lb.

Apparently, there is a relief in surface pressure from the front to the rear specimens which results in essentially equivalent pressures on the two surfaces.

Columbium Alloys. Two simulated, dynamic, reentry profiling conditions were used for the coated columbium specimens. These were nominally identical in time and temperature to the static cycling conditions previously described. Thus, both profiling conditions incorporated a basic 30-minute cycle which included a ramped heatup to 1450 F, holding at 1450 F for 5 minutes followed by a ramped heatup to either 2500 F or 2350 F, holding for 15 minutes, and then cooling to less than 1300 F. Actual time-temperature curves for the first two 2500 F runs are shown in Figure 16.

Pressure and cold-wall heat-flux measurements were made using water-cooled blocks that simulated the surface geometry of the specimen exposure area during dynamic exposure runs. These calibration blocks bore the same orientations relative to each other, the water-cooled copper base plate, and the plasma stream as was used during actual exposure runs. Pressure and heat-flux data were obtained at arc-heater conditions used for the nominal exposure temperature of 2500 F. Additional details of the dynamic environmental exposure conditions are given in Appendix B which includes results illustrating the effectiveness of the techniques used to measure specimen surface temperatures.

Operating conditions and calculated shear-stress values for the columbium-alloy runs are given below:

| Item | Exposure Temperature, F 1400 | 2350 | 2500 |
|---|---|---|---|
| Free-Stream Mach Number | 4.5 | 4.5 | 4.5 |
| Total Gas Enthalpy (From Arc-Heater Energy Balance), Btu/lb | 2250 | 4700 | 6300 |
| Arc-Heater Reservoir Pressure (Measured), atm | 0.85 | 1.14 | 1.34 |
| Surface Pressure (Measured for 2500 F Condition), torr | | | |
| Region 1 | 10 | 13.5 | 16 |
| Region 2 | 10 | 13.5 | 16 |
| Aerodynamic Shear, psf | | | |
| Region 1 | 1.4 | 1.7 | 1.8 |
| Region 2 | 1.9 | 2.2 | 2.4 |

Results of the heat-flux measurements and comparison of the measured and calculated values are given in Appendix B.

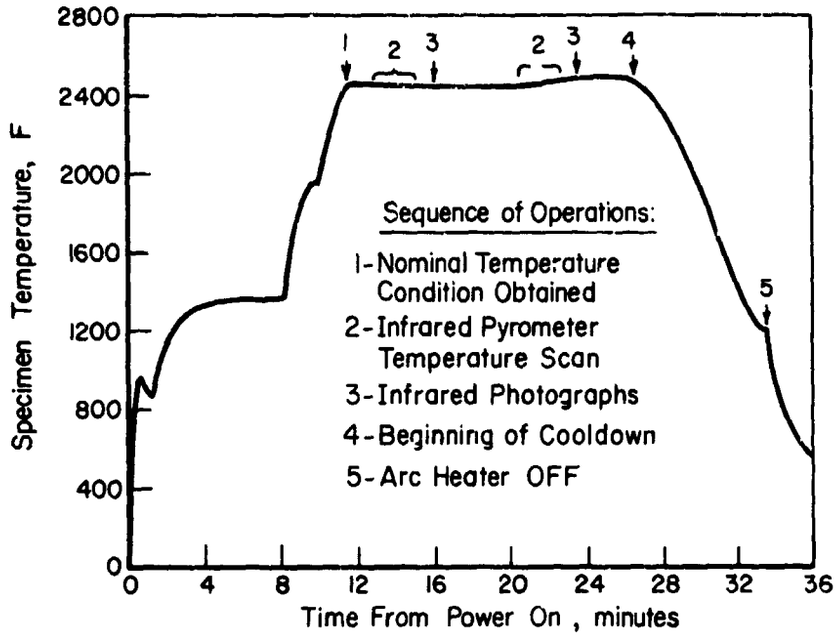


a. Run 8

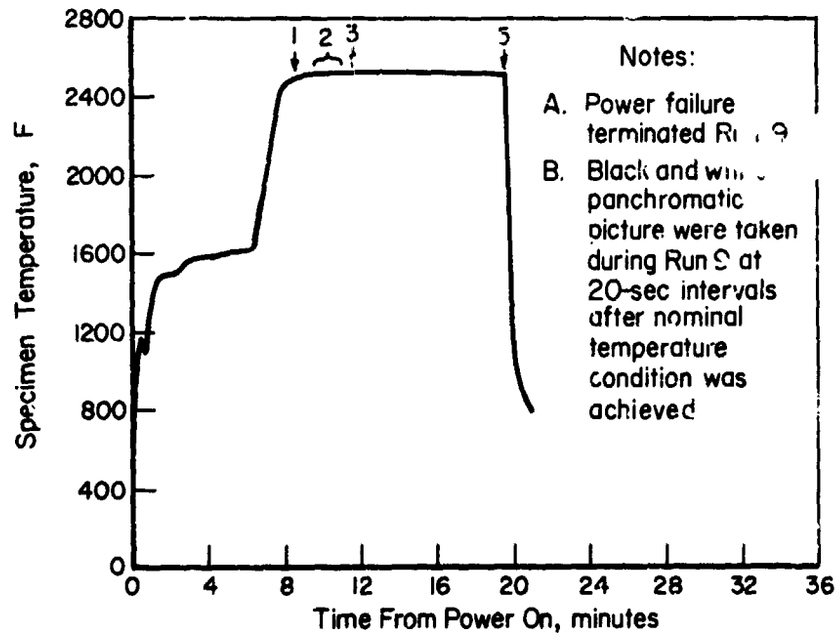


b. Run 9

FIGURE 16. REPRESENTATIVE TEMPERATURE PROFILES FOR INTENTIONALLY DEFECTED COATED COLUMBIUM ALLOY SPECIMENS IN PLASMA-ARC RUNS

Exclusive of calibration runs, eight plasma-arc runs incorporating from one to five cycles at 2350 F or 2500 F were completed. A log of these eight runs in chronological order is given in Table 10 which identifies the coating systems and test condition for each of the individual specimens along with the nominal cyclic-exposure conditions.

As indicated in Table 10, most of the plasma-arc specimens were prepared from substrate alloys having an initial thickness of 25 to 30 mils. While not originally the intent, this expedient was adopted as a result of experiences with nominally 15-mil-thick coated specimens that were used in calibrating the arc conditions for 2350 F prefiling. Here, excessive bowing deflection occurred on several specimens as soon as peak-exposure-temperature conditions were reached. This led to localized disturbances in the plasma gas flow which, in turn, resulted in very severe thermal gradients across the surfaces of the affected specimens. In the absence of gross deflection, typical axial thermal gradients for each row at the peak exposure temperature were on the order of 75 to 100 F per inch. This agrees generally with expectations based on flat-plate laminar-boundary-layer convective-heat-transfer theory.

Complete time and average-center-temperature histories for specimens during each of the cycles on each of the eight runs are given in Tables A-17 and A-18, respectively, in the appendix. The average cyclic time and temperature data for each run are summarized in Table 11. As described later, during several of these runs, temperatures at the individual coating-defect sites varied widely from the nominal intended values. Accordingly, a listing and discussion of these data have been deferred to the Experimental Results section of this report.

## Evaluation

### Cobalt Alloys

The postfiring evaluations on the cobalt-alloy specimens included visual inspection, photographic-appearance documentation, and thickness measurements.

Principal emphasis, however, was placed on mechanical-property evaluations which are to include tensile testing at room temperature, 1400 F*, and 1900 F and creep testing at 1900 F. Figure 17a illustrates the specimen test configuration which was used in these tests. The test-specimen length was limited to 3 inches since this was the maximum length of the individual plasma-arc-test specimen blanks. The test specimens' widths were set at 3/8 inch to provide duplicate specimens from each of the exposed arc-test blanks.

*The 1400 F tensile tests are being performed at NASA-MSFC. The results of these tests were not available at the time of this writing.

TABLE 10. LOG OF COATED COLUMBIUM SPECIMENS EXPOSED TO DYNAMIC CYCLIC PROFILING

| Run | Location | Specimen Conditions: Coating System | Specimen Conditions: Substrate Thickness, mils | Specimen Conditions: Defect Types per Specimen | Cyclic Conditions: Peak Temperature, F | Cyclic Conditions: No. of Cycles |
|---|---|---|---|---|---|---|
| 8 | A | R512E/C129Y | 25 | A, B, C | 2500 | 1 |
| | B | R512E/Cb752 | 25 | Ditto | | |
| | C | VH109/C129Y | 15 | " | | |
| | D | VH109/Cb752 | 25 | " | | |
| | E | VH109/C129Y | 25 | " | | |
| | F | R512E/Cb752 | 15 | " | | |
| 9 | A | R512E/Cb752 | 25 | A, B, C | 2500 | 1 |
| | B | VH109/C129Y | 25 | Ditto | | |
| | C | R512E/C129Y | 25 | " | | |
| | D | R512E/Cb752 | 25 | " | | |
| | E | VH109/C129Y | 25 | " | | |
| | F | VH109/Cb752 | 25 | " | | |
| 11 | A | R512E/FS85 | 30 | A, B, C | 2350 | 3 |
| | B | R512E/Cb752 | 25 | Ditto | | |
| | C | VH109/C129Y | 25 | " | | |
| | D | R512E/FS85 | 30 | " | | |
| | E | R512E/C129Y | 25 | " | | |
| | F | VH109/Cb752 | 25 | " | | |
| 12 | A | R512E/Cb752 | 25 | C | 2350 | 1 |
| | B | R512E/Cb752 | 25 | C | | |
| | C | R512E/Cb752 | 25 | C | | |
| | D | R512E/Cb752 | 25 | C | | |
| | E | R512E/Cb752 | 25 | C | | |
| | F | R512E/Cb752 | 25 | C | | |
| 13 | A | R512E/FS85 | 30 | C | 2350 | 3 |
| | B | R512E/Cb752 | 25 | C | | |
| | C | VH109/C129Y | 25 | C | | |
| | D | R512E/FS85 | 30 | C | | |
| | E | R512E/Cb752 | 25 | C | | |
| | F | VH109/C129Y | 25 | C | | |
| 14 | A | R512E/Cb752 | 25 | C | 2350 | 5 |
| | B | R512E/Cb752 | 25 | None | | |
| | C | R512E/Cb752 | 25 | C | | |
| | D | R512E/Cb752 | 25 | C | | |
| | E | R512E/Cb752 | 25 | None | | |
| | F | R512E/Cb752 | 25 | C | | |

TABLE 10. (Continue

| Run | Location | Specimen Conditions: Coating System | Specimen Conditions: Substrate Thickness, mils | Specimen Conditions: Defect Types per Specimen | Cyclic Conditions: Peak Temperature, F | Cyclic Conditions: No. of Cycles |
|---|---|---|---|---|---|---|
| 15 | A | R512E/FS85 | 30 | C | 2350 | 5 |
| | B | R512E/Cb752 | 25 | C | | |
| | C | VH109/C129Y | 25 | C | | |
| | D | R512E/FS85 | 30 | C | | |
| | E | R512E/Cb752 | 25 | C | | |
| | F | VH109/C129Y | 25 | C | | |
| 16 | A | R512E/FS85 | 30 | C | 2500 | 3 |
| | B | R512E/Cb752 | 25 | C | | |
| | C | VH109/C129Y | 25 | C | | |
| | D | Si/T166/FS85* | 25 | C | | |
| | E | R512E/FS85 | 30 | C | | |
| | F | VH109/C129Y | 25 | C | | |

* For discussion of this specimen, see Appendix C.

TABLE 11. SUMMARY OF TIME-TEMPERATURE DATA FOR DYNAMIC PROFILING RUNS ON INTENTIONALLY DEFECTED COATED COLUMBIUM SPECIMENS

| Item | Target Values | Achieved Values in Runs Indicated | | | | | | | |
|---|---|---|---|---|---|---|---|---|---|
| | | 8 | 9 | 11 | 12 | 13 | 14 | 15 | 16 |
| Number of Cycles | – | 1 | 1 | 3 | 1 | 3 | 5 | 3 | 3 |
| Average Time/Cycle, Minutes | | | | | | | | | |
| Rise to 1450 F | 2 | 3 | 1.6 | 0.4 | 0.2 | 0.3 | 0.2 | 0.3 | 0.2 |
| Hold at 1450 F | 5 | 5 | 4.8 | 5.1 | 5.0 | 5.1 | 5.5 | 5.7 | 5.4 |
| Rise to $T_{max}$ | 2 | 3.5 | 2.3 | 1.7 | 1.8 | 1.6 | 2.0 | 2.7 | 1.9 |
| Hold at $T_{max}$ | 15 | 15.0 | 11.5[b] | 15.6 | 15.4 | 14.5 | 15.0 | 14.8 | 15.1 |
| Decay to <1450 F. | 6 | 7.0 | 2.3[b] | 5.4 | 6.2 | 5.9 | 5.1 | 5.7 | 5.7 |
| Totals | 30 | 33.5 | 22.5 | 28.2 | 27.9 | 27.4 | 27.8 | 29.2 | 28.3 |
| Temperature Control[a] (All Cycles) 1450 F Plateau | | | | | | | | | |
| Minimum Value, F | – | 1320 | – | 1280 | 1200 | 1300 | 1340 | 1270 | 1300 |
| Maximum Value, F | – | 1470 | – | 1470 | 1450 | 1450 | 1600 | 1550 | 1650 |
| Average Value, F | 1450 | 1390 | 1560 | 1365 | 1315 | 1395 | 1490 | 1420 | 1450 |
| $T_{max}$ Plateau | | | | | | | | | |
| Minimum Value, F | – | 2470 | 2470 | 2210 | 2300 | 2210 | 2240 | 2230 | 2420 |
| Maximum Value, F | – | 2510 | 2510 | 2410 | 2380 | 2360 | 2360 | 2380 | 2510 |
| Average Value, F | – | 2495 | 2490 | 2300 | 2335 | 2300 | 2285 | 2315 | 2460 |

(a) Temperature at center of specimen.

(b) Run terminated prematurely owing to momentary power fluctuation.

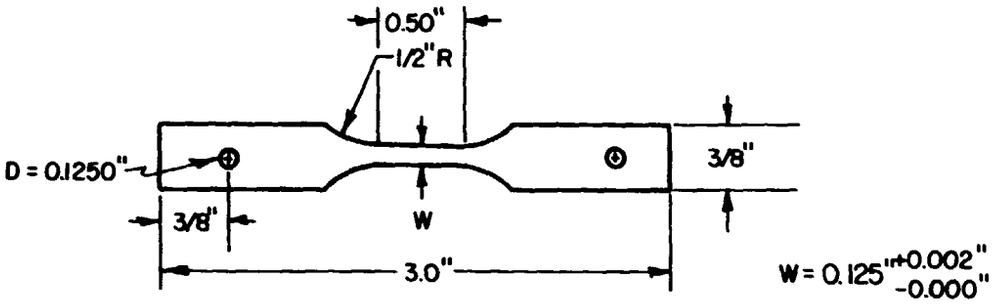


a. Cobalt Alloys

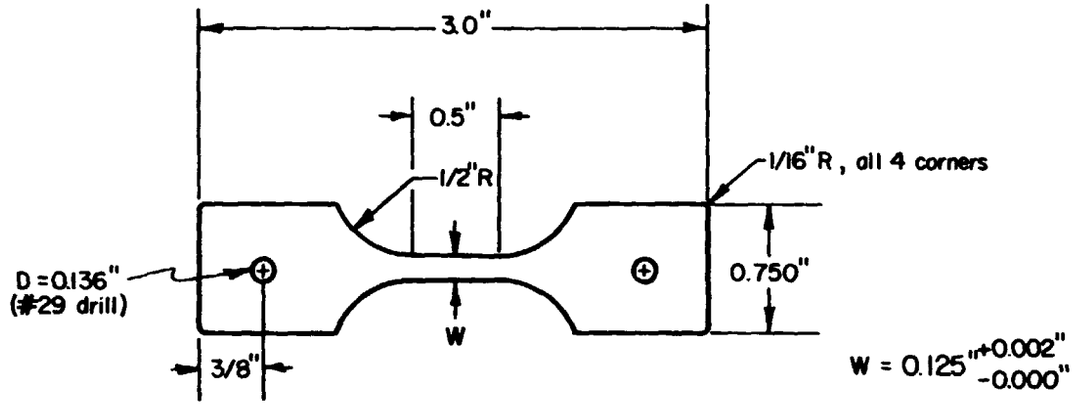


b. Coated Columbium Alloys, Standard Gage

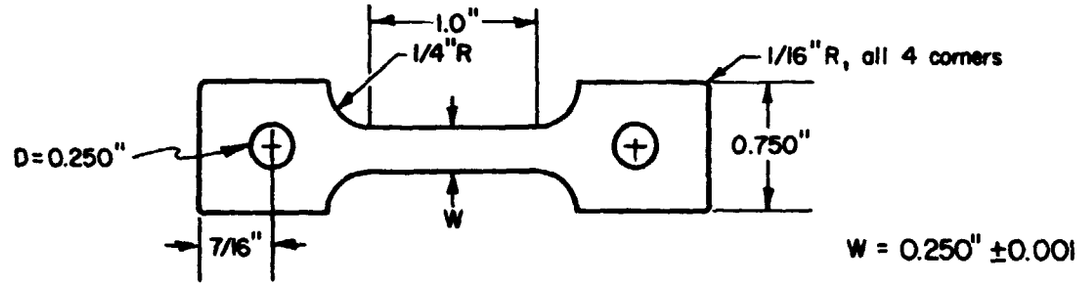


c. Coated Columbium Alloys, Wide Gage

FIGURE 17. TENSILE- AND CREEP-SPECIMEN CONFIGURATIONS

In the room-temperature tensile tests, the nominal strain rate (based on constant crosshead speed) was controlled at 0.01 in./in./min up through the yield load, and then increased to a rate of 0.1 in./in./min to fracture. At elevated temperatures, the nominal strain rate was maintained at a constant value of 0.04 in./in./min throughout each test. In all cases, load-deformation curves were recorded autographically using a LVDT (linear variable differential transformer) which was attached to the specimen grips to measure of strain. All tensile tests were performed in still, dry air.

The creep-testing procedure used was designed primarily to compare the relative effects of the different cyclic-exposure environments on a low level of creep strain (0.5 to 1 percent) in a nominal test exposure time of 12 hours at 1900 F. Because of these moderately long exposures, these tests were carried out in a dynamic vacuum of $10^{-4}$ to $10^{-5}$ mm of mercury. As in tensile testing, creep strain was measured autographically on an x-y recorder through the use of a LVDT attached to the specimen grips. Initial calibrations with direct gaging and optical strain readout showed good reliability and reproducibility for the external-measurement technique.

Selected mechanical-property-test specimens were also subjected to metallographic examination. To preserve the character of the surface on these specimens, all were nickel plated prior to mounting and grinding.

## Coated Columbium Alloys

Coating Thickness and Quality Correlations. All coated specimens were evaluated for coating quality by visual inspection and micrometer thickness measurements. The latter were performed using both flat-tipped and pointed-anvil micrometers, usually by taking thickness measurements in a minimum of three locations on each sample. In addition, approximately 125 of the coated specimens were also subjected to coating thickness measurements using both eddy-current and thermoelectric-probe measurement techniques.

The eddy-current instrument used was a Dermitron Thickness Tester, Model D-2, made by Unit Process Assemblies, Incorporated, of New York, New York. The probe used was the standard Type C (2 megahertz) unit which was supplied with this model.

The thermoelectric probe consisted of a standard, commercial, 40-watt soldering pencil (Ungar Electric Products, Hawthorne, California) equipped with Ungar Tip No. PL-331. The temperature of the probe was maintained at 550 F and a standard probe loading weight (point contact pressure against a laboratory spring balance) of 500 grams was used with a dwell time of 15 seconds before each reading.

In order to compare these three coating-thickness-measurement techniques, seventeen coated tab specimens with nominal coating thicknesses of 1, 3, and 5 mils were evaluated as follows:

(1) A reference line was lightly penciled across the center on the top and bottom surfaces of each specimen.

(2) Thickness measurements were made, using both a pointed tip and flat anvil micrometer, at the exact centers of each specimen.

(3) Five thermoelectric-probe readings were made at five points adjacent to the reference line on the top surface of each specimen.

(4) Dermitron readings were obtained at three of the same points evaluated for probe readings on the top surface of each specimen. Similarly, readings were also made on the bottom surface exactly opposite the top readings.

(5) Each specimen was then sectioned for metallographic examination along the reference line. Minimum and maximum thicknesses of the coating were then determined at each of the points where thermoelectric probe and Dermitron readings had previously been determined.

In all cases, the thicknesses of all coated specimens were found to be significantly less upon measurement with pointed-tip micrometers as compared with measurement using flat-anvil micrometers. These differences were less for the R512E coatings (from 0.8 to 1.1 mils) than for the VH109 coatings for which the differences on the nominal 3-mil-thick coatings varied from 2.5 to 3.8 mils. Metallographic examination confirmed the macroscopic observations which indicated that these discrepancies in thicknesses resulted from coating-thickness variations on a microscopic scale. Representative microstructures of the as-coated systems are shown in Figure 18.

In general, the microstructures of all of the R512E-coated Cb752 specimens were fairly uniform on each specimen as well as from one specimen to another. The structure of this coating system was also consistent with that of the D43 columbium-alloy substrate described by other investigators.* According to this reference source, the thin innermost coating layer consists essentially of unmodified $Cb_5Si_3$. The moderately thick outermost layer consists of essentially unmodified $CbSi_2$. Between these extremes, several layers were identified which are all of the (chromium, iron, columbium)$_5Si_3$ structure but which differ in chemistry.

As applied to the C129Y substrate, the R512E coating structure was similar to that observed on the Cb752 substrate and was equally uniform in thickness.

Microstructures in the VH109 coatings were somewhat more complex and less consistent than those observed in the R512E coatings, as shown by comparisons within Figure 18. Specifically, the innermost layers in all of the VH109 coatings (marked A in Figures 18c and 18d) were fairly consistent in structure and thickness on each of the specimens examined. However, the thickness and number of phases in the outerlying layers of these specimens were variable within a given specimen as well as from specimen to specimen. Also, the thickness of the Cb752 substrate as coated with VH109 showed a pronounced irregularity (as indicated by the curved substrate/coating interface in Figure 18c), which suggests a moderate degree of chemical incompatibility for this coating system.

Despite these thickness irregularities (which are characteristic of all silicide coatings), a reasonably good agreement was found for the maximum as-coated thickness value of each specimen upon comparing the metallographically determined values with those obtained at the same location using pointed micrometers. These data are given in Table 12 for all of the nominal 3-mil-thick coating specimens examined. Also, despite

*Priceman, S., and Sama, L., "Development of Fused Slurry Silicide Coatings for the Elevated-Temperature Oxidation Protection of Columbium and Tantalum Alloys", AFML-TR-68-210, Sylvania Electric Products, Inc., New York, N. Y. (December, 1968).


a. Sample R7-3. R512E Coating on Cb752 Substrate


b. Sample R9-1. R512E Coating on C129Y Substrate

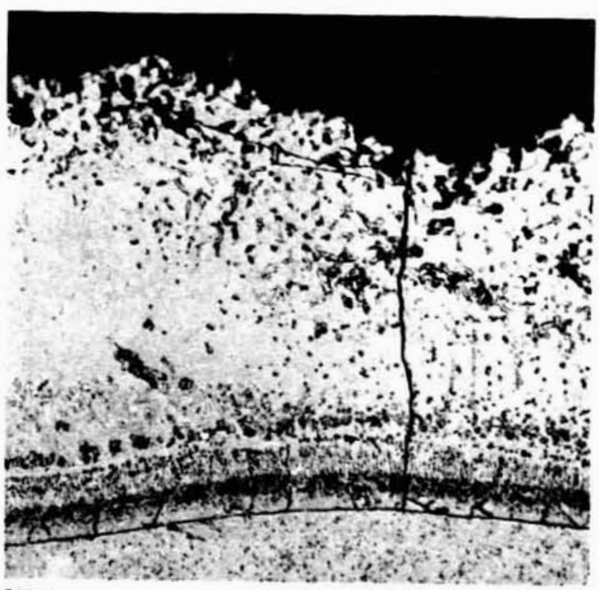


c. Sample V7-3. VH109 Coating on Cb752 Substrate

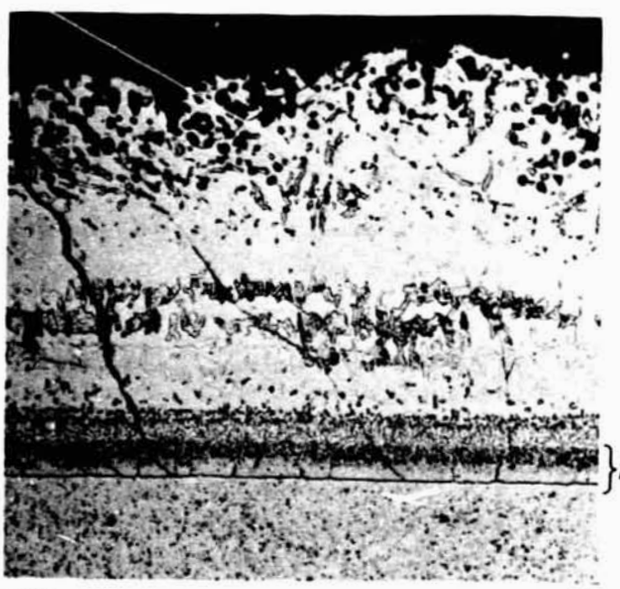


d. Sample V9-3. VH109 Coating on C129Y Substrate

FIGURE 18. REPRESENTATIVE MICROSTRUCTURES IN AS-COATED COLUMBIUM SPECIMENS

All coatings nominally 5 mils thick except for Sample R9-1 where coating was nominally 3 mils thick.

TABLE 12. SUMMARY OF COATING-THICKNESS-MEASUREMENT DATA FOR NOMINAL 3-MIL-THICK COATING ON COLUMBIUM-ALLOY "STANDARD" SPECIMENS

| Sample | Substrate Thickness, mils Initial | Final | Side | Coating Thickness, mils (Metallographic Measurement) Average Minimum | Average Maximum | Grand Average | Total Thickness, mils Metallographic Minimum | Maximum | Average | Point Micrometer | Substrate Consumption, mils/mil of coating |
|---|---|---|---|---|---|---|---|---|---|---|---|
| | | | | | | R512E/Cb752 | | | | | |
| R7-2 | 25.2 | 22.0 | Top | 2.8 | 3.3 | 3.1 | 28.0 | 29.1 | 28.5 | 29.1 | 0.49 |
| | | | Bottom | 3.2 | 3.7 | 3.5 | | | | | |
| | | | | | | 3.2 | | | | | |
| DR-7 | 25.2 | 21.8 | Top | 3.0 | 4.3 | 3.5 | 28.0 | 30.7 | 28.8 | - | 0.49 |
| | | | Bottom | 3.2 | 4.5 | 3.5 | | | | | |
| | | | | | | 3.5 | | | | | |
| | | | | | | R512E/C129Y | | | | | |
| R9-1 | 26.0 | 22.9 | Top | 3.1 | 3.35 | 3.2 | 29.1 | 29.6 | 29.3 | 29.7 | 0.48 |
| | | | Bottom | 3.1 | 3.3 | 3.2 | | | | | |
| | | | | | | 3.2 | | | | | |
| | | | | | | VH109/Cb752 | | | | | |
| V7-3 | 15.0 | 12.1 | Top | 3.5 | 4.4 | 4.0 | 19.5 | 21.8 | 20.5 | 20.4 | 0.35 |
| | | | Bottom | 3.9 | 5.3 | 4.6 | | | | | |
| | | | | | | 4.2 | | | | | |
| V7-4 | 25.2 | 22.6 | Top | 3.7 | 4.5 | 4.1 | 30.3 | 31.7 | 31.0 | 31.0 | 0.31 |
| | | | Bottom | 3.9 | 4.6 | 4.25 | | | | | |
| | | | | | | 4.2 | | | | | |
| | | | | | | VH109/C129Y | | | | | |
| V9-3 | 15.2 | 11.8 | Top | 4.1 | 4.9 | 4.5 | 20.4 | 21.7 | 21.0 | 21.6 | 0.57 |
| | | | Bottom | 4.45 | 5.0 | 4.7 | | | | | |
| | | | | | | 4.6 | | | | | |
| V9-4 | 25.9 | 22.6 | Top | 4.2 | 4.9 | 4.5 | 30.9 | 32.1 | 31.5 | 32.1 | 0.38 |
| | | | Bottom | 4.1 | 4.6 | 4.4 | | | | | |
| | | | | | | 4.5 | | | | | |
| DV-9 | 26.0 | 22.8 | Top | 3.15 | 5.0 | 4.0 | 29.2 | 32.5 | 30.7 | - | 0.41 |
| | | | Bottom | 3.2 | 4.65 | 3.9 | | | | | |
| | | | | | | 3.9 | | | | | |

local variations in coating thickness at any given point, the average coating thicknesses were fairly uniform over both surfaces on all of the specimens examined.

For each of the coated specimen standards examined, calculations were made to determine the amount of substrate consumed for each mil of thickness in the resulting coating. These data are also given in Table 12. As indicated, the R512E coating acted essentially the same with both alloy substrates, i.e., both substrates decreased by about 0.5 mil in thickness for each mil of coating applied at the nominal 3-mil-thick coating level. Surprisingly (in view of the duplex processing involved), less substrate consumption occurred for both alloys with the application of the VH109 coating as compared with the R512E coating.

Later, more extensive measurements were made on these same specimens to assess more accurately the overall (as compared with discrete-point evaluation) coating-substrate reactions. The resulting average factors for substrate consumption during processing to apply nominal 3-mil coatings were determined as follows:

| Coating Systems | Substrate Consumption, mils/mil of coating applied |
|---|---|
| R512E/Cb752 and R512E/C129Y | 0.39 |
| VH109/C129Y and VH109/Cb752 | 0.34 |

As noted above, a good correlation was obtained between the maximum coating-thickness values obtained by metallographic measurements and those obtained by pointed micrometer measurements. This is illustrated for three of the coating substrate systems of interest by the solid curves in Figure 19. The dashed curves, representing minimum and average coating-thickness values, were added to Figure 19 on the basis of the metallographic measurements on these same specimens.

Similarly, a reasonably good agreement was observed between the metallographically determined maximum coating thicknesses for the R512E-coated alloys and those obtained by the Dermitron measurements. This is indicated by the solid curves shown in Figure 20, A and B. Again, dashed curves representing metallographically determined minimum and average coating thicknesses were added to these figures. For the VH109 coatings, the correlation of coating thicknesses with Dermitron readings was less satisfactory, especially for the VH109/Cb752 specimens as shown in C of Figure 20. This is believed to be a combined result of (1) the greater surface roughness of the VH109 coatings (as compared with R512E) and (2) the variable microstructures observed in the VH109 coatings. Thus, the Dermitron relies primarily on variations in the electrical conductivity of the coating which is a function of coating chemistry and, hence, coating microstructure.

Attempts to correlate the metallographically determined coating thicknesses with the values obtained by thermoelectric-probe readings gave the least satisfactory results. This is illustrated by the curves in Figure 21 where the range of probe readings obtained

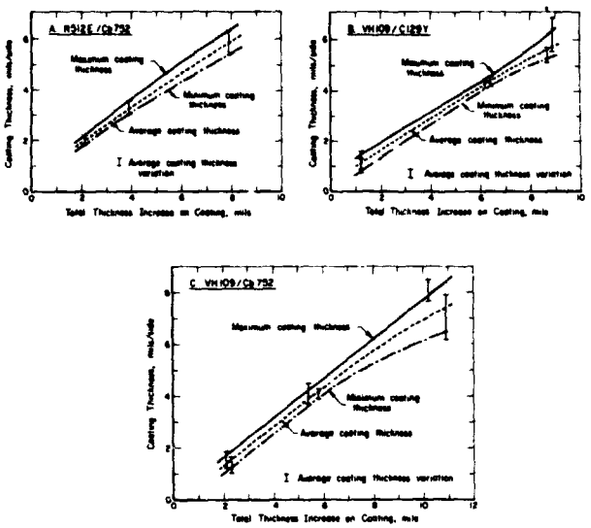

FIGURE 19. CORRELATION OF COATING-THICKNESS INCREASE (AS DETERMINED BY POINT MICROMETER MEASUREMENT) TO COATING THICKNESS

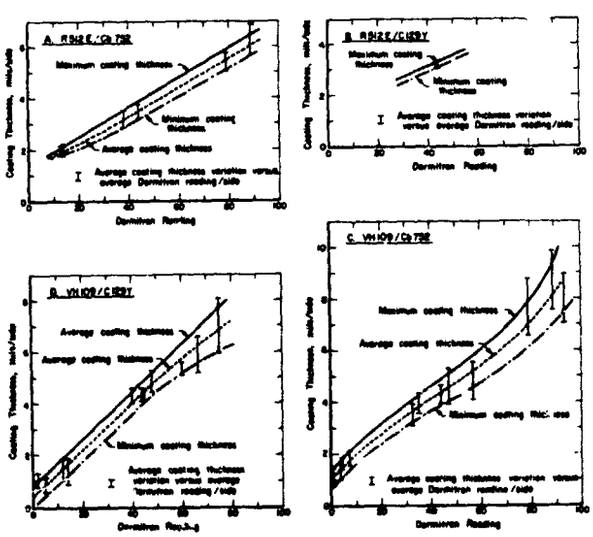

FIGURE 20. CORRELATION OF DERMITRON READINGS TO COATING THICKNESS

at any given point on a coated specimen is indicated by the spread in the dashed curves showing the extremes in the millivoltage readings obtained versus average coating thicknesses as determined metallographically. As is well known, the thermoelectric output at any probe contact point is dependent on coating chemistry and the temperature at the contact point. Preliminary experiments showed that the results obtained were also extremely sensitive to contact pressure and time. Despite attempts to standardize on the equipment and technique used, the results obtained were too erratic to warrant the use of this technique as a means of exercising quality control on coating thickness for fully processed specimens.

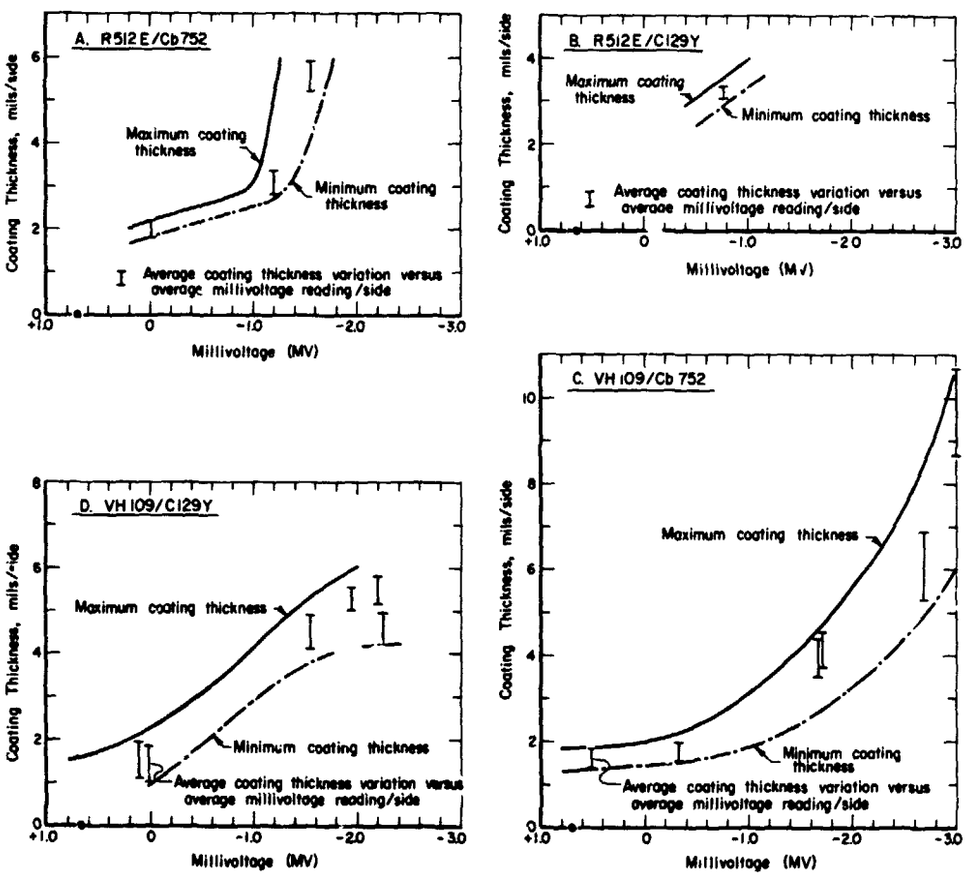


FIGURE 21. CORRELATIONS OF THERMOELECTRIC PROBE MILLIVOLTAGE READINGS TO METALLOGRAPHIC COATING THICKNESS

Because of its applicability to both the R512E and VH109 coatings, the pointed-micrometer measurement technique was favored as the preferred method for estimating coating thicknesses.

Dynamic Test Time-Lapse Photography. As described later, unexpectedly rapid defect growth occurred at the coating's intentional defect sites during the first 2500 F arc exposure of these specimens. Accordingly, for all succeeding arc exposures, a remotely operated Hasselblad camera was mounted over the arc chamber and was used to take a timed sequence of black-and-white panchromatic photographs during any given exposure sequence.

Posttest Physical Appearance. Each of the statically and dynamically cycled specimens was photographed and inspected visually at magnifications through 30X. Where present, the diameters of coating's defect sites were measured optically on the coating's surface. Since preferential substrate oxidation and subsequent undercutting of the coating occurred at many of these defect sites, X-radiography was used to quantitatively assess the extent of substrate oxidation at these locations. Here, contact prints were prepared from the X-ray film and optical methods were used to measure the affected areas.

Many of the cycled specimens were also sectioned for metallographic examination through the coating's intentional-defect site and at selected sections away from the defect sites. In most cases, Tukon hardness traverses were conducted on these sections using a 50-gram load.

Mechanical Properties. The mechanical properties under study for the coated columbium alloys include tensile properties at room-temperature and 2400 F and creep properties at 2400 F. At the time of this writing, however, only the results of the room-temperature tensile tests were available. Figure 17 illustrates the two types of test-specimen configurations which are being used in this work. As was noted earlier in the discussion of the cobalt test-specimens, the overall size of these coated columbium test specimens was limited to the maximum 3/4 by 3-inch size of the plasma-arc exposure blanks. The standard narrow-gage specimen configuration shown in Figure 17b was adopted as the principal means of assessing the effects of contamination introduced (into the center of the reduced section) at an intentional-defect site after various thermal exposures. The wide-gage specimen configuration shown in Figure 17 was used on similarly defected coupons to assess the influence of increasing the ratio of uncontaminated to contaminated areas in specimens after selected thermal exposures.

As described previously, the small Type C (4-mil-diameter through-coating hole) defect was selected as the standard coating defect in these mechanical-property determinations. These defects were introduced in the coated, rectangular coupons prior to thermal exposure, and the test configurations shown in Figure 17 were later machined from the exposed blanks. It was recognized that machining of the test specimens after coating would introduce some additional coating damage. However, the effects of this damage on alloy-substrate properties were not expected to be significant in comparison with those sustained at the coating's intentional-defect sites. To verify this contention, an appropriate number of baseline tensile tests were performed on coated specimens which were (1) coated after machining to the standard tensile-test-specimen configuration before testing, and (2) coated as 3/4 by 3-inch rectangular blanks and machined to the adopted configuration before testing.

All strength properties for the coated specimens were computed on the basis of the alloy-substrate cross-sectional area remaining after coating. In the room-temperature tensile tests, a nominal strain rate of 0.005 in./in./min was used up through the yield load; the rate was then increased to 0.05 in./in./min to fracture.

# EXPERIMENTAL RESULTS

## Cobalt Alloys

### Physical Response to Cycling

Static Environment. Figure 22 illustrates the appearance of the cobalt-alloy specimens after exposure to 12 static, 1900 F profiling cycles. In general, most of the specimens in Runs Co-1 and Co-2 were similar to each other in terms of their basic color (light to medium gray). In comparison, the specimens of Run Co-3 were a slightly lighter shade of gray and also showed traces of blue-green and straw-tan colors toward their upper and lower ends. This apparently reflects the lower total peak-exposure-temperature times which these specimens received (44.9 minutes) as compared with the corresponding times for Runs Co-1 and Co-2 (51.4 and 50.9 minutes, respectively; see Table 4).

Also, five of the nine L605 specimens contained in Runs Co-1 and Co-2 (Specimens C2-C6, inclusively, in Figure 22) displayed a dark spotty pattern across their center sections, suggestive of spalling. This apparently resulted from the slightly higher heating rates accorded to these specimens.* Conversely, none of the HS188 specimens contained in these runs displayed this spotty oxidation characteristic. On the basis of appearance alone, this suggests that the surface oxidation characteristics of the HS188 alloy under static cycling conditions may be superior to those for the L605 alloy. However, thickness measurements on all 20 specimens after their cyclic exposures showed that no significant dimensional changes had occurred in any of these. Thus, longer exposure times would appear required both to confirm this "advantage" and to determine the net effects on the alloy's mechanical properties.

Dynamic Environment. Immediately after the dynamic cyclic exposures, a thin layer of a black, soot-like deposit was noted on the top exposed surface of all of the cobalt-alloy specimens. This deposit was fairly uniformly distributed over all of the specimens in Runs 3 and 5, but displayed the unusual sedimentary pattern on the Run 4 specimens that is illustrated in Figure 23. (Note: The clear, semicircular area near the leading edge of Specimen A in Figure 23 resulted from the inadvertent removal of the deposit by contacting the surface with a finger, i.e., from a fingerprint.) A spectrographic analysis on samples of this deposit (collected from the surfaces of all Run 4 specimens) showed only the presence of all of the major alloying elements in the L605 and HS188 alloys in about the same proportions as these occur in the base compositions. A carbon analysis of this same material showed the carbon content to be 0.1 weight percent. On these bases, the sooty deposit was tentatively identified as a mixed (nonmagnetic), metallic oxide.

After the specimens were wiped with cloth to remove the sooty oxide, inspection disclosed that the top surfaces of all of the cobalt-alloy specimens were similar and fairly uniformly covered with a dull, adherent flat-black oxide. No significant differences in color or texture of this oxide were apparent among the centers of any of these

*It is presumed that L605 Specimen C6 contained in Run Co-2 was heated and cooled more rapidly than the other L605 specimens in this run by virtue of its position in the furnace, i.e., on the outside of the specimen group, facing the susceptor.

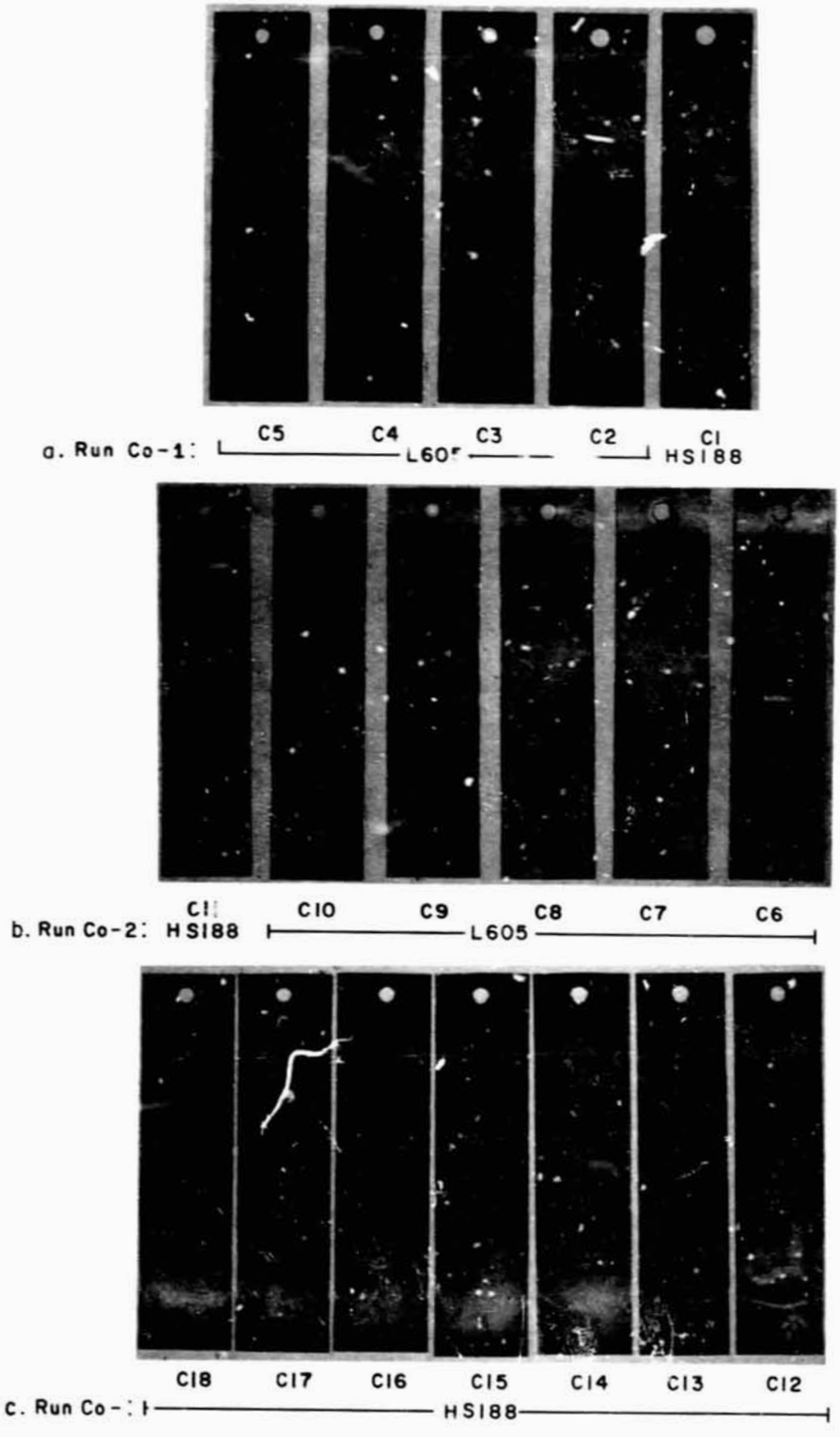


FIGURE 22. APPEARANCE OF COBALT ALLOY SPECIMENS AFTER TWELVE 5-MINUTE EXPOSURES TO 1900 F IN THE STATIC, LOW-PRESSURE ENVIRONMENT

specimens despite the fact that the average peak exposure temperatures differed by as much as 115 F on these individual specimens (see Table 9). Some oxide degeneration had occurred in localized regions (coincident with peak exposure temperatures on the top surfaces at or within 1/2 inch of the leading edges) on Specimens D, E, and F of Run 3 and Specimens D and F of Run 4. In these areas, the thin, residual oxide film tended to display a mixture of greenish and tan colors.

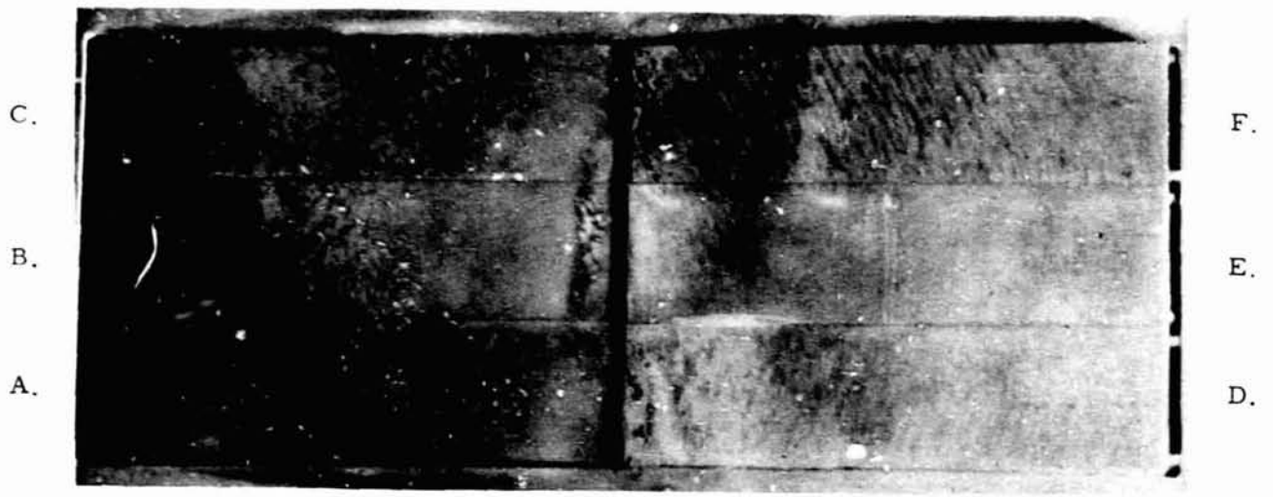


FIGURE 23. TOP VIEW OF COBALT ALLOY SPECIMENS IN MODEL HOLDER AFTER EXPOSURE TO TWELVE DYNAMIC 1900 F CYCLES (RUN 4)

A. L605
B. HS188
C. L605 (welded)
D. HS188
E. HS188 (welded)
F. L605

A slight amount of permanent distortion, i.e., bowing, was retained on the specimens which had occupied the front-row A-B-C positions in each run. It was apparent, however, that most of the distortion which occurred during the arc exposure was a result of thermal stressing, and relatively little permanent distortion remained after the exposures.

Examination of the bottom surfaces of all specimens showed that these essentially retained the dark-gray matte finish which had been imparted by the preoxidation treatment. The exception here was that the edge area of those specimens which had been subjected to a disturbed gas-flow pattern as a result of specimen bowing did develop a thin layer of loose oxide. In contrast to the sooty surface oxide, this nonadherent oxidation product from the bottom surfaces of the specimens was magnetic in all cases.

After removal of the sooty oxide, thickness measurements showed that no significant changes had occurred on 14 of the 16 specimens exposed. Two specimens of HS188 which had been exposed to the two highest average temperatures of 1924 F and 1904 F (Specimens 4D and 3D in Runs 4 and 3, respectively) exhibited the greatest changes in thickness. These thickness increases were, however, only 0.4 and 0.2 mil, respectively.

TABLE 13. EFFECTS OF EXPOSURE ENVIRONMENT ON THE AVERAGE

| Exposure Environment | Test Temp, F | Unwelded Condition: Exposure Conditions: Specimen | Avg. T, F | Time, min: Rise and Decay | $T_{max}$ | Total | Ultimate Strength, ksi | 0.2% Offset Yield Strength, ksi | Elongation in 0.5 Inch, % |
|---|---|---|---|---|---|---|---|---|---|
| | | | | | | | | | L605 Alloy |
| Baseline | RT | 15, 16 | - | - | - | - | 135 | 65.8 | 50 |
| LPE | RT | 89, 90 | 1911 | 57.7 | 50.9 | 108.6 | 132.5 | 62.9 | 50 |
| Arc | RT | 21, 22 | 1837 | 46.0 | 62.9 | 108.9 | 141 | 68.6 | 51 |
| Baseline | 1900 | 11, 12 | - | - | - | - | 19.3 | 18.3 | 12 |
| LPE | 1900 | 84, 86 | 1911 | 57.7 | 50.9 | 108.6 | 20.6 | 17.6 | 19 |
| Arc | 1900 | 29, 30 | 1857 | 40.2 | 65.7 | 105.9 | 20.5 | 17.9 | 12 |
| | | | | | | | | | HS188 Alloy |
| Baseline | RT | 51, 52 | - | - | - | - | 135 | 63.6 | 65 |
| LPE | RT | 103, 104 | 1905 | 66.5 | 44.9 | 111.4 | 132.5 | 60.7 | 59 |
| Arc | RT | 67, 68 | 1809 | 46.0 | 62.9 | 108.9 | 133.5 | 60.7 | 61 |
| Baseline | 1900 | 47, 48 | - | - | - | - | 18.1 | 16.5 | 20 |
| LPE | 1900 | 99, 100 | 1905 | 66.5 | 44.9 | 111.4 | 19.8 | 17.4 | 22 |
| Arc | 1900 | 61, 62 | 1904 | 51.9 | 63.1 | 115.0 | 17.7 | 17.1 | 19 |

(a) W designates weld; PM designates parent metal.
(b) Ratio of welded to unwelded ultimate strength for undressed welds.

TENSILE PROPERTIES OF UNWELDED AND WELDED COBALT ALLOYS

| Welded Condition | | | | | | | | | |
|---|---|---|---|---|---|---|---|---|---|
| Exposure Conditions | | | | | | | | | |
| Specimen | Avg. Temp, T, F | Time, min: Rise and Decay | Time, min: $T_{max}$ | Time, min: Total | Ultimate Strength, ksi | 0.2% Offset Yield Strength, ksi | Elongation in 0.5 Inch, % | Failure Location[a] | Joint Efficiency[b] % |
| 7, 8 | - | - | - | - | 132.5 | 68.9 | 36 | W, W | 98 |
| 81, 82 | 1913 | 56.0 | 51.4 | 107.4 | 126 | 67.5 | 38 | W, PM | 95 |
| 23, 24 | 1819 | 46.0 | 62.9 | 108.9 | 133 | 67.1 | 41 | W, PM | 94 |
| 3, 4 | - | - | - | - | 21.4 | 20.3 | 10 | W, W | 111 |
| 75, 78 | 1913 | 56.0 | 51.4 | 107.4 | 22.6 | 19.9 | 14 | W, W | 110 |
| 27, 28 | 1850 | 40.2 | 55.7 | 105.9 | 23.0 | 21.9 | 11 | PM, W | 112 |
| 43, 44 | - | - | - | - | 135.5 | 65.7 | 52 | PM, PM | 100 |
| 95, 96 | 1905 | 66.5 | 44.9 | 111.4 | 135 | 63.3 | 50 | PM, PM | 102 |
| 65, 66 | 1845 | 51.9 | 63.1 | 115.0 | 135.5 | 62.9 | 52 | PM, PM | 102 |
| 39, 40 | - | - | - | - | 21.1 | 19.0 | 16 | PM, PM | 117 |
| 91, 92 | 1911 | 57.7 | 50.9 | 108.6 | 20.3 | 17.5 | 17 | PM, W | 103 |
| 57, 58 | 1881 | 51.9 | 63.1 | 115.0 | 20.3 | 18.9 | 17 | W, W | 115 |

The emissivity changes during exposure were measured by observing the surface temperature with a single-color pyrometer. This was sighted at one specimen and the output was continually monitored during the 12-cycle exposure. An emissivity setting of 0.83 was used for both the L605 and HS188 alloy. On the basis of this output, a relative emissivity change can be estimated. The results of these data indicate that there was no substantial change in emissivity after surface-temperature variations were accounted for. The indicated variation was within the 2 percent maximum potential error associated with recording of the outputs of the pyrometer and thermocouples and reducing the data.

## Tensile Properties

The tensile properties of both the statically and dynamically cycled cobalt alloys were determined using duplicate specimens at both room temperature and 1900 F. The results for the individual specimens are given in Tables A-19 and A-20 in the appendix. Table 13 lists the average values obtained and relates these properties to the exposure conditions used. These results are conveniently discussed in the paragraphs which follow.

Effects of Welding. The results of the baseline property determinations showed that, at room temperature, the ultimate and yield strengths of both alloys were essentially identical for both the unwelded and welded conditions. However, the unwelded HS188 alloy showed about a 30 percent tensile-elongation advantage over the unwelded L605 (i.e., tensile-elongation values of 65 versus 50 percent, respectively). The room-temperature tensile ductility of both alloys was degraded slightly by welding, and here again, some superiority of the HS188 alloy was indicated. Thus, not only was the as-welded tensile ductility of the L605 decreased to a greater extent (28 percent versus 20 percent reduction for HS188), but the tensile failures in the welded L605 specimens also occurred in the weld joints of this alloy despite the fact that the joints were thicker than the adjacent parent metal.

At 1900 F, the strength and ductility of both unwelded alloys dropped sharply. For comparison purposes, some preliminary 1900 F tensile-property data* for the HS188 alloy (solution treated at 2150 F) are given below:

| Sheet Thickness, in. | Ultimate Strength, ksi | Yield Strength, ksi | Elongation, percent |
|---|---|---|---|
| 0.125 | 29.0 | 18.7 | 80 |
| 0.060 | 27.2 | 16.2 | 66 |
| 0.045 | 28.3 | 16.6 | 55 |
| 0.030 | 28.3 | 16.9 | 38 |

As shown, the tensile ductility of the HS188 alloy at 1900 F decreases markedly with decreasing sheet thickness. Consequently, the low 1900 F tensile ductilities observed in the HS188 and L605 alloys (in the present baseline-condition evaluation) is primarily

*Extrapolated from 1800 F and 2000 F data contained in a preliminary data release from the Cabot Corporation of Kokomo, Indiana, dated January 19, 1970.

believed to be a gage effect resulting from both the low thickness (nominally 0.015 inch) and the small gage size (0.5 inch long by 0.125 inch wide) of the test specimens used.

Similar decreases in the 1900 F tensile properties occurred in both alloys after welding, although the 1900 F weld ductility was less adversely affected than were the strength values. Consequently, the net effects of welding on the 1900 F tensile properties of both alloys were less than observed in these same materials at room temperature.

Effects of Exposure. The effects of the cyclic exposure environments on the room-temperature and 1900 F tensile properties of both alloys in the unwelded and welded conditions are also compared in Table 13. No significant tensile-property differences at either test temperature for any of these exposed specimens were apparent in comparisons with the baseline property data for unexposed material.

## Creep Properties

The results of creep deformation testing on an identical group of baseline and statically and dynamically cycled specimens are given in Table A-21 in the appendix. Some effort was made to apply a statistical analysis to these results. However, for both alloys, the spread in data was too great to assign any statistical significance to the effects of either welding or thermal exposure on the creep behavior of the samples represented. Nonetheless, some behavioristic trends were suggested when the paired results from the duplicate specimens were compared. This is evident from Table 14 which lists these average creep-test values along with the prior thermal histories of the different specimens. The trends suggested by these data are summarized as follows:

(1) The baseline-condition property comparisons suggest that both the HS188 and L605 alloys showed an increase in 1900 F creep-deformation resistance as a result of welding.

(2) Thermal cycling of both the unwelded and welded L605 alloy appears to degrade its 1900 F creep strength slightly. The dynamic environment may have a more severe effect than the static, although temperature effects (i.e., increasing creep-strength degradation with increasing average cyclic peak exposure temperatures) may actually be controlling.

(3) In contrast, thermal cycling of both the unwelded and welded HS188 alloy appears to improve its 1900 F creep-deformation resistance, especially for material cycled in the dynamic environment.

## Metallography

Approximately half of the baseline and thermally exposed tensile- and creep-test specimens were subjected to metallographic examination. In brief, most of these specimens showed many features in common, and only the creep-tested HS188 specimens showed structural changes which appeared related to differences in their thermal-exposure environment.

TABLE 14. CORRELATION OF AVERAGE 1900 F CREEP DEFORMATION BEHAVIOR AND EXPOSURE HISTORY OF COBALT ALLOY SPECIMENS

| Specimen | Exposure Environment | Average Peak Temp, F | Exposure Time, minutes: Heatup and Cooldown | Exposure Time, minutes: Hold at $T_{avg}$ | Exposure Time, minutes: Total | Time, hours, for Indicated Creep Strain[a]: 0.5% | Time, hours, for Indicated Creep Strain[a]: 1.0% | Minimum Creep Rate[a], %/hour |
|---|---|---|---|---|---|---|---|---|
| | | | **L605 Unwelded** | | | | | |
| 9, 10, 18 | Baseline | -- | -- | -- | -- | 5.5 | 14.6 | 0.044 |
| 83, 85 | LPE | 1911 | 58 | 51 | 109 | 3.15 | 9.95 | 0.061 |
| 31, 32 | Arc | 1876 | 40 | 66 | 106 | 3.8 | 11.9 | 0.049 |
| | | | **L605 Welded** | | | | | |
| 1, 2 | Baseline | -- | -- | -- | - | 6.45 | 18.4 | 0.042 |
| 76, 77 | LPE | 1913 | 56 | 51 | 107 | 4.55 | 16.8 | 0.049 |
| 35, 36 | Arc | 1922 | 40 | 66 | 106 | 1.6 | 4.6 | 0.076 |
| | | | **HS188 Unwelded** | | | | | |
| 46 | Baseline | -- | -- | -- | -- | 1.0 | 3.5 | 0.20 |
| 97, 98 | LPE | 1905 | 67 | 45 | 112 | 1.4 | 3.5 | 0.20 |
| 69, 70 | Arc | 1924 | 56 | 63 | 119 | 4.1 | 8.4 | 0.12 |
| | | | **HS188 Welded** | | | | | |
| 37, 38 | Baseline | -- | -- | -- | -- | 2.93 | 5.5 | 0.20 |
| 73, 74 | LPE | 1913 | 56 | 51 | 107 | 2.9 | 7.15 | 0.12 |
| 71, 72 | Arc | 1895 | 56 | 63 | 119 | 5.3 | 10.3 | 0.11 |

(a) Stress level maintained constant at 2.5 ksi.

The common features which showed no relationship to differences in prior thermal-exposure history are noted as follows:

(1) All specimens showed a thin oxide layer less than 0.3 mil thick.

(2) All specimens showed a grain-boundary denuded layer 0.3 to 0.5 mil thick underlying the oxide film. This zone was tentatively ascribed to chromium depletion from the surface oxide-film formation and evidently was formed in the initial 1900 F preoxidation treatment.

(3) The room-temperature tensile fractures in both alloys showed ductile failures for both the unwelded and welded conditions.

(4) The fracture locations in the welded tensile specimens of both alloys were confirmed. That is, tensile fractures in the welded L605 specimens occurred predominantly in the weld metal, while fractures in the welded HS188 specimens occurred predominantly in the parent metal.

(5) The 1900 F tensile failures in the HS188 specimens resulted in internal grain-boundary tearing throughout the reduced test gage section. In contrast, the 1900 F L605 tensile fractures showed grain-boundary tearing from the surface inward, primarily near the fracture region.

The only environmentally associated structural difference noted among all these specimens was found in the 1900 F unwelded series of creep-tested HS188 specimens. Here, both the baseline and statically cycled specimens (Specimens 46 and 98, respectively, in Table 14) showed a large amount of a transversely oriented (relative to the stress axis) grain-boundary phase (illustrated in Figure 24a). In contrast, the dynamically cycled specimen (Specimen 69) displayed little or none of this phase. However, all three welded HS188 creep-test specimens (Specimens 37, 71, and 74 in Table 14) also showed this same phase, though in much lesser amounts than in Specimens 46 and 98. Consequently, the correlation between creep behavior and the quantity of this oriented phase for unwelded specimens is weakened by observations on the welded specimens.

## Coated Columbium Alloys

### Coating Quality and Thickness

Two separate batches of about 125 coated specimens each were prepared over the first year's work. In the first batch (prepared in October, 1970), both the R512E and VH109 coatings were applied to both the Cb752 and C129Y substrate alloys. The second batch (prepared 6 months later) consisted of the R512E coatings on the Cb752 and FS85 alloys and VH109 on C129Y.

In appearance, both coatings were similar in color (light gray). The R512E coating was consistent in texture in both batches, regardless of substrate, as shown in Figures 25 and 26. In comparison, the VH109 coating was noticeably rougher in texture.

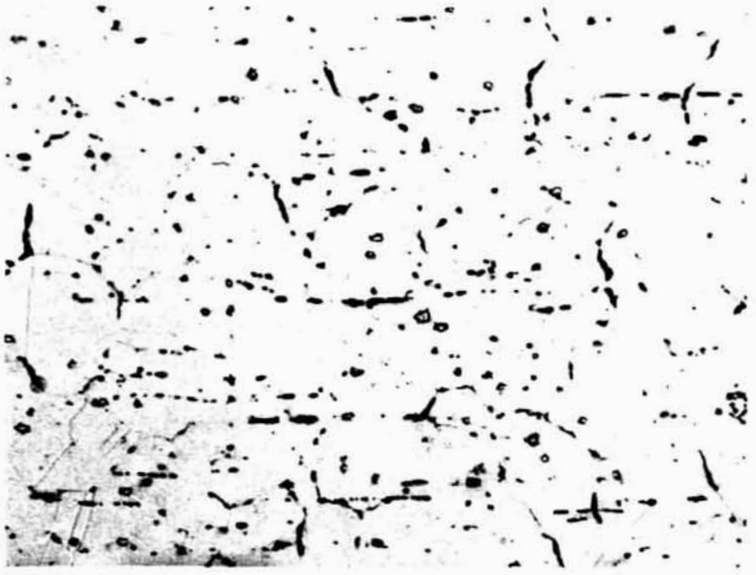

250X 6F462

← Stress →

a. Specimen 46 – Baseline Condition

250X 6F463

← Stress →

b. Specimen 69 – Exposed to Twelve 1900 F Dynamic Profiling Cycles

FIGURE 24. LONGITUDINAL MICROSTRUCTURES CF 1900 F CREEP-TESTED HS188 ALLOY SPECIMENS

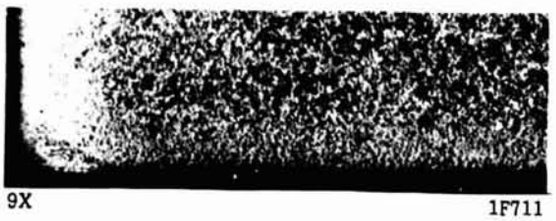

9X 1F711

Top Surface

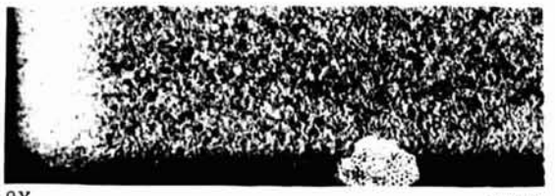

9X 1F712

Top Surface

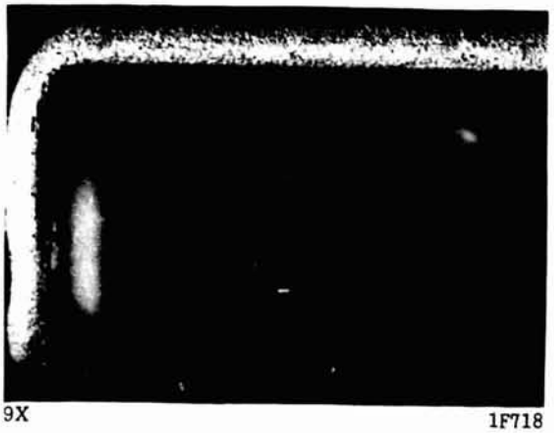

9X 1F718

Edge

a. R512E/Cb752

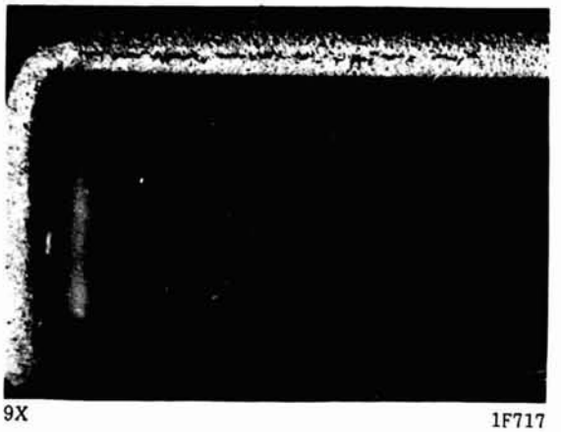

9X 1F717

Edge

b. R512E/C129Y

9X 1F709

Top Surface

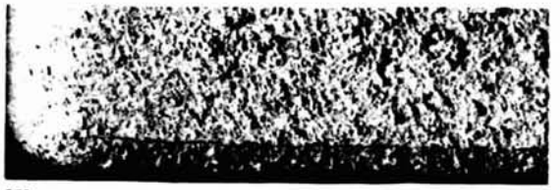

9X 1F710

Top Surface

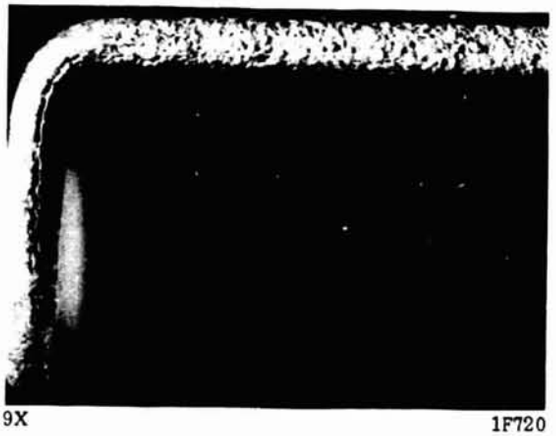

9X 1F720

Edge

c. VH109/Cb752

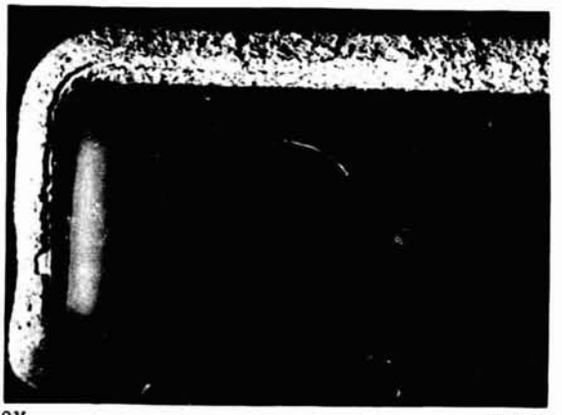

9X 1F719

Edge

d. VH105/C129Y

FIGURE 25. APPEARANCE OF TYPICAL AS-COATED BATCH 1 PLASMA-ARC TEST SPECIMENS

this coating as applied to the C129Y alloy changed markedly in appearance from the first batch to the second. Thus, while the first VH109/C129Y samples had the uniformly spongy texture shown in Figure 25d, the second batch of coatings had a spangled texture, as illustrated in Figure 26b.

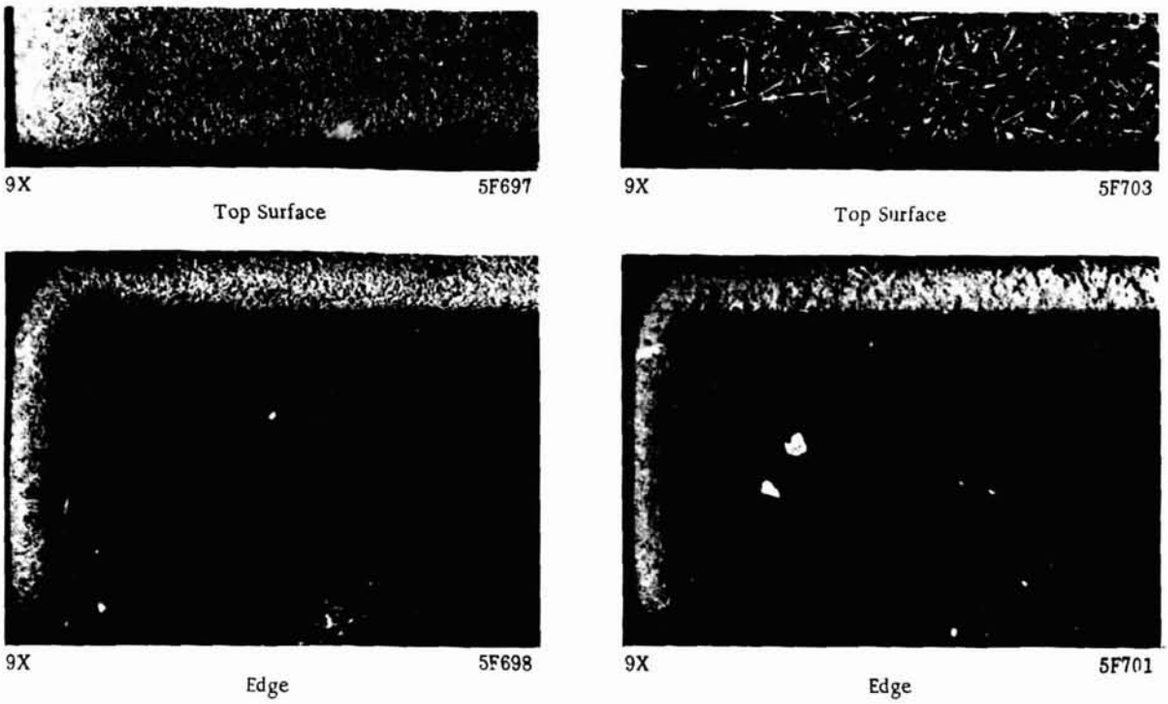


a. R512E/FS85

b. VH109/C129Y

FIGURE 26. APPEARANCE OF TYPICAL AS-COATED BATCH 2 PLASMA-ARC TEST SPECIMENS

Most of the plasma-arc-test specimens had undergone some warpage as a result of the coating processing, especially in the end areas. This apparently resulted from the action of residual stresses (induced in cold forming the end tabs) during the high-temperature sintering treatments* which are used to diffuse these coatings to the columbium-alloy substrate.

Also, as illustrated in Figure 25, some of the VH109-coated plasma-arc-test specimens showed severe coating cracks along the edges of the end tabs. The extent and severity of coating edge cracking on the plasma-arc-test specimens was markedly reduced in the areas away from the end tabs, although some edge cracks were observed on most of the VH109/C129Y, VH109/Cb752, and R512E/C129Y specimens. Similarly, occasional edge cracks were also observed on most of the as-coated VH109/C129Y, VH109/Cb752, and R512E/C129Y tensile-test blanks. In contrast, the freedom from obvious defects in the as-coated R512E/Cb752 and R512E/FS85 specimens was striking.

*For the most part, the processing details used to apply these coatings are proprietary. However, it is known that the R512E formulation (Si-20Cr-20Fe) is applied with a final diffusion treatment of 1 hour at 2580 F. The VH109 formulation incorporates hafnium and tantalum additions along with silicon as the major component. This coating is applied in a duplex process in which two separate diffusion treatments at 2500 F are required.

All of the Batch 1 coated specimens intended for cyclic exposure were subjected to coating-thickness measurements, using the three techniques described earlier, with the results shown in Table 15.

TABLE 15. SUMMARY OF COATING-THICKNESS DATA FOR BATCH 1 COATINGS

| Specimen Type | Initial Thickness, mils | No. of Specimens | Average Coating Thickness: Micrometer Data $\bar{x}$, mils | Micrometer Data s, mil | Dermitron Data (Both Surfaces) $\bar{x}$, mils | Dermitron Data (Both Surfaces) s, mil | Thermoelectric Probe $\bar{x}$, mils |
|---|---|---|---|---|---|---|---|
| | | | R512E/Cb752 | | | | |
| Plasma | 15.6 | 5 | 3.2 | 0.34 | 2.8 | 0.31 | 2.5 |
| Plasma | 25.7 | 4 | 3.0 | 0.27 | 2.7 | 0.20 | -- |
| Tensile | 15.2 | 14 | 3.2 | 0.36 | 3.3 | 0.22 | 2.5 |
| Tensile | 25.5 | 10 | 3.0 | 0.28 | 3.2 | 0.27 | -- |
| All of above | -- | 33 | 3.1 | 0.31 | 3.1 | 0.34 | 5 |
| | | | R512E/C129Y | | | | |
| Plasma | 15.1 | 5 | 3.2 | 0.19 | 2.9 | 0.14 | 2.7 |
| Plasma | 26.1 | 4 | 3.1 | 0.22 | 2.9 | 0.29 | -- |
| Tensile | 14.8 | 4 | 3.2 | 0.20 | 3.2 | 0.14 | 2.9 |
| Tensile | 25.7 | 4 | 3.0 | 0.58 | 3.1 | 0.17 | -- |
| All of above | -- | 17 | 3.1 | 0.21 | 3.0 | 0.24 | 2.8 |
| | | | VH109/Cb752 | | | | |
| Plasma | 15.6 | 5 | 4.7 | 0.61 | 5.0 | 0.66 | 4.5 |
| Plasma | 25.7 | 4 | 3.9 | 0.86 | 4.4 | 0.54 | -- |
| Tensile | 15.2 | 4 | 3.6 | 0.39 | 4.3 | 0.40 | 4.5 |
| Tensile | 25.5 | 4 | 3.5 | 0.24 | 4.2 | 0.41 | -- |
| All of above | -- | 17 | 4.2 | 0.76 | 4.5 | 0.59 | 4.5 |
| | | | VH109/C129Y | | | | |
| Plasma | 15.1 | 5 | 4.1 | 0.25 | 5.3 | 0.32 | 5.2 |
| Plasma | 26.. | 4 | 4.0 | 0.27 | 5.2 | 0.17 | -- |
| Tensile | 14.8 | 14 | 3.3 | 0.24 | 4.9 | 0.36 | 5.0 |
| Tensile | 25.7 | 10 | 3.2 | 0.20 | 4.9 | 0.24 | -- |
| All of above | -- | 33 | 3.7 | 0.46 | 5.0 | 0.34 | 5.1 |

Excellent correlations were observed between the coating-thickness values on the R512E/Cb752 and R512E/C129Y specimens obtained by the pointed micrometer and Dermitron techniques.

The correlation between the values obtained by these techniques on the Vac Hyd coatings was less satisfactory, especially on the C129Y substrate. Specifically, the Dermitron technique gave thickness values which were consistently higher than those indicated by the pointed micrometers. These differences ranged from 0.3 to 0.7 mil greater for the VH109/Cb752 specimens and from 0.8 to 1.7 mils greater for the VH109/C129Y specimens. As noted earlier, this lack of agreement is believed to be a combined result of (1) the greater surface roughness of the VH109 coating and (2) the variable microstructures observed in the VH109-coated specimens which were used as standards to calibrate the Dermitron equipment.

As shown in Table 15, the thermoelectric-probe measurements gave the poorest correlations among the coating thickness measurement techniques that were used.

Both the micrometer and Dermitron measurement techniques showed that the thickness variations for the R512E coatings were about the same for all alloy substrates. Also, the average R512E coating thickness on all substrates conformed very well to the nominal specified level of 3.0 mils. Greater variances in the average thicknesses of the VH109-coated specimens were observed, and the average coating thicknesses on these specimens were from 0.7 to 1.2 mils greater than the nominal specified level.

The results of Dermitron measurements on individual specimens showed generally that, for both coatings, coating uniformity along one surface or from one side to the other of a given sample was within 0.3 mil. However, greater variations from sample to sample were occasionally observed, especially for the VH109 coatings. This is evident from the data of Table 15 as well as from the comparisons below, which represent the extreme values obtained from individual specimens in each of the coating systems evaluated.

| | Measured Coating Values, mils | | | |
|---|---|---|---|---|
| | R512E on | | VH109 on | |
| Coating-Thickness Property | Cb752 | C129Y | Cb752 | C129Y |
| Maximum variation on one side of a specimen | 0.3 | 0.5 | 1.0 | 1.0 |
| Maximum variation from one side to the other | 0.8 | 0.7 | 1.3 | 1.1 |
| Thinnest coating area | 2.8 | 2.4 | 3.4 | 4.6 |
| Thickest coating area | 4.1 | 3.8 | 6.6 | 6.1 |

Coating-thickness estimates for the second batch of coated specimens were determined, using the micrometer technique, with the results shown below.

| | Average Coating Thickness, mils/side | | | | | |
|---|---|---|---|---|---|---|
| | R512E/Cb752 | | VH109/C129 | | R512E/FS85 | |
| | $\bar{x}$ | s | $\bar{x}$ | s | $\bar{x}$ | s |
| Batch 1 | 3.1 | 0.31 | 3.7 | 0.46 | -- | -- |
| Batch 2 | 3.6 | 0.27 | 4.0 | 0.49 | 3.7 | 0.23 |

These results indicate that while coating-thickness uniformity was about the same for both batches, the Batch 2 coatings were somewhat thicker than those in Batch 1.

## Physical Response to Cycling

Static Environment. Figure 27 shows the appearance of the eight intentionally defected coated columbium specimens (Specimens S1 through S8) after one simulated reentry cycle in the static environment which included a 15-minute exposure at 2500 F. In all cases, the specimens were suspended vertically from the large holes provided at


FIGURE 27. APPEARANCE OF INTENTIONALLY DEFECTED COATED COLUMBIUM SPECIMENS AFTER ONE SIMULATED RE-ENTRY CYCLE IN STATIC ENVIRONMENT

Nominal $T_{max}$ of 2500 F, Runs Cb-1 and Cb-2.

one end, and the orientation of the intentional defects (which were spaced 3/4 mil apart) from top to bottom along each specimen in the furnace hot zone was as follows:

Top - Type C, small defect
Center - Type A, through defect
Bottom - Type B, large defect.

Optical measurements at the surfaces of each of the 24 defect sites showed that no measurable changes from the initial defect diameters occurred as a result of the single static profiling exposure. Also, no noticeable oxidation products were observed on any of the exposed Cb752 or C129Y substrate surfaces at the defect sites.

The results of one, three, and five cyclic exposures of fourteen R512E/Cb752 specimens at 2350 F were virtually identical. Thus, none of the single, Type C defects which were centrally located on these specimens (Specimens S9 through S22) showed any measurable change in diameter, and no noticeable oxidation products were observed at these sites.

Dynamic Environment. As shown in Table 10, eight plasma-arc runs were conducted. The first two of these (Runs 8 and 9) consisted of single cyclic exposures at a nominal peak exposure temperature of 2500 F. During both runs, unexpectedly rapid defect growth occurred at many of the coating's intentional-defect sites. So much so, in fact, that the resulting damage was too great to permit the use of 2500 F as a nominal profiling-temperature to assess the extent of mechanical-property degradation with the small arc-test-specimen size adopted. Analyses of these data suggested that while 2500 F was above a critical temperature for rapid defect growth in the dynamic environment, a nominal exposure temperature of 2350 F should be below this critical temperature. Accordingly, the third arc run (Run 11) was carried out for three cycles at 2350 F to confirm this belief. When no visible evidence of specimen damage at defect sites was observed under these conditions, the next four runs (Runs 12 through 15) were carried out to provide specimens for postexposure mechanical-property evaluations. The most recently completed run (Run 16) was intended to evaluate the rate of defect growth in multicyclic exposures at 2500 F.

The detailed results and discussion of these dynamic-exposure data are most conveniently discussed in the chronological order in which they were obtained.

Critical-Temperature Definition. During the peak-temperature-exposure period of Run 8, both visual and photographic data indicated that significant damage occurred rapidly at several of the intentionally defected coating sites. Thus, the first IR photograph revealed that after 4 minutes' exposure the center defect on Specimen 8B (originally a Type A, through defect) was clearly visible. Also, during the second pyrometer scan (carried out at 9 to 11 minutes after peak temperatures were revealed), two of the small Type C defects in the forward positions on Specimens 8B and 8F were clearly visible through the radiation pyrometer. These defect sites as well as others at the centers of Specimens 8B, 8E, and 8F were also clearly shown in the 12-minute IR photograph.

The appearance of these specimens after their single simulated reentry profile cycle is shown in Figure 28. For all of the Run 8 specimens, the defect orientations were the same with respect to arc flow, with the Type C defect being placed forward,

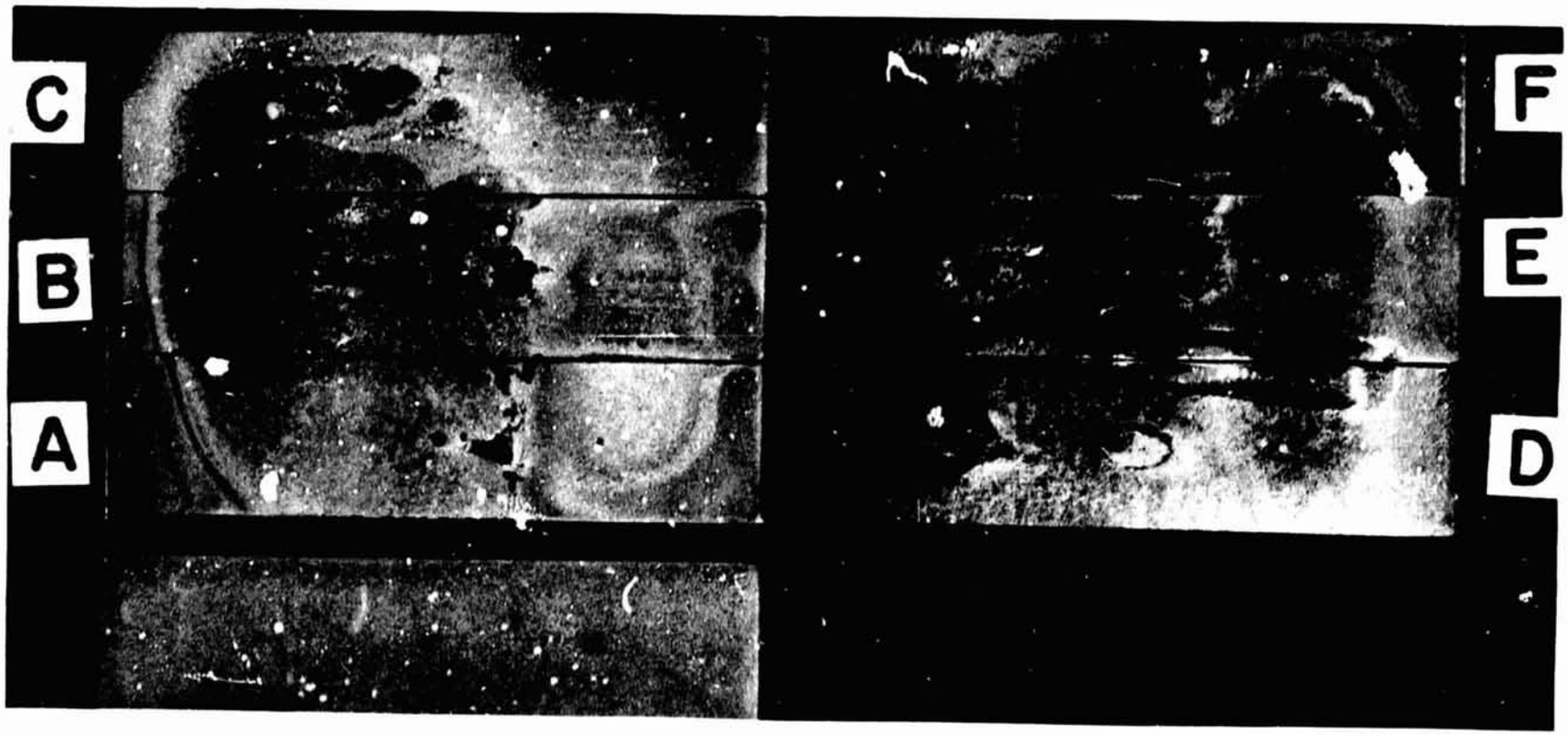


FIGURE 28. TOP VIEW OF INTENTIONALLY DEFECTED COATED COLUMBIUM SPECIMENS AFTER ONE SIMULATED REENTRY CYCLE IN PLASMA ARC FACILITY

| | | | |
|---|---|---|---|
| A. | R512E/C129Y | D. | VH109/Cb752 |
| B. | R512E/Cb752 | E. | VH109/C129Y |
| C. | VH109/C129Y | F. | R512E/Cb752 |

Nominal $T_{max}$ of 2500 F, Run 8.
Note unlettered, unexposed specimen included to show original specimen appearance and defect sizes.

the Type A defect placed at the center, and the Type B defect located to the rear, most downstream location. Comparisons of the exposed defect sites with those of the unexposed specimen in this figure show clearly that severe damage has occurred at more than half of the defect sites as a result of this single cycle. For example, the Type C small defects at 8B-1* and 8E-1* had grown into through holes over 1/8 inch in diameter. Similarly, the original 40-mil-diameter through holes at 8B-2, 8E-2, and 8F-2 had been enlarged to diameters in the range of 100 to 140 mils.

Run 9 was carried out using essentially the same arc conditions as those for Run 8 in order to verify the initiation and growth of gross substrate damage at intentionally defected coating sites at a nominal peak exposure temperature of 2500 F. Two additional features were designed into Run 9. These included the use of timed-sequence photographs and a reversal of the order of defects with respect to the plasma-arc flow direction on two specimens (9D and 9E). A third additional, unintentional difference between these runs resulted from a power outage which prematurely terminated the peak-temperature-exposure period of Run 9 after about 11 minutes and which effectively quenched these specimens from their peak exposure temperatures.

The results of the timed-sequence photographs were quite revealing, particularly from the viewpoint of showing that visible damage at some of the defect sites occurred almost as soon as the nominal peak exposure temperature of 2500 F was achieved. Thus, as illustrated in Figure 29a, within 20 seconds after reaching peak temperature, the presence of an effluent emanating from the Type B defect at the forward end of Specimen 9E was clearly visible as flowing in the downstream direction to a point beyond the center defect on this specimen. In fact, within the first 40 seconds, similar effluent products were noted at or downstream from the following coating system/defect locations:

VH109/C129Y: 9B-1, 9B-2, 9E-1, and 9E-2
R512E/Cb752: 9D-1
VH109/Cb752: 9F-1 .

Further, most of the small Type C defects located at these forward locations had either grown to a visible spot or were discharging an effluent product within a period of 6 minutes after peak temperatures had been achieved. Also, noticeable and measurable defect growth occurred at most** of these locations as the exposure continued. The apparent diameters of these defects were measured from the photographs and plotted as a function of exposure time. Representative results are shown in Figure 30. The final "apparent defect diameters" indicated on Figure 30 were in excellent agreement with the values determined by optical methods on the surface of these samples at the conclusion of the run. The appearance of these specimens after Run 9 is shown in Figure 31.

The reduction of temperature data from thermocouples, radiation pyrometry, and IR photography suggested that rapid flaw growth was related to specific temperatures in the locale of the flaw. These temperatures are given in Table 16 along with the growth

*With this nomenclature, the first number designates the run number and the letter shows specimen position on the model. The last number shows defect position on the specimen, with 1 designating the upstream site, 2 designating the center site, and 3 designating the most downstream site.

**That is, at all front and center locations except those at Sites 9F-1 and 9F-2 which were obscured by an effluent product within 2 minutes at peak temperature.

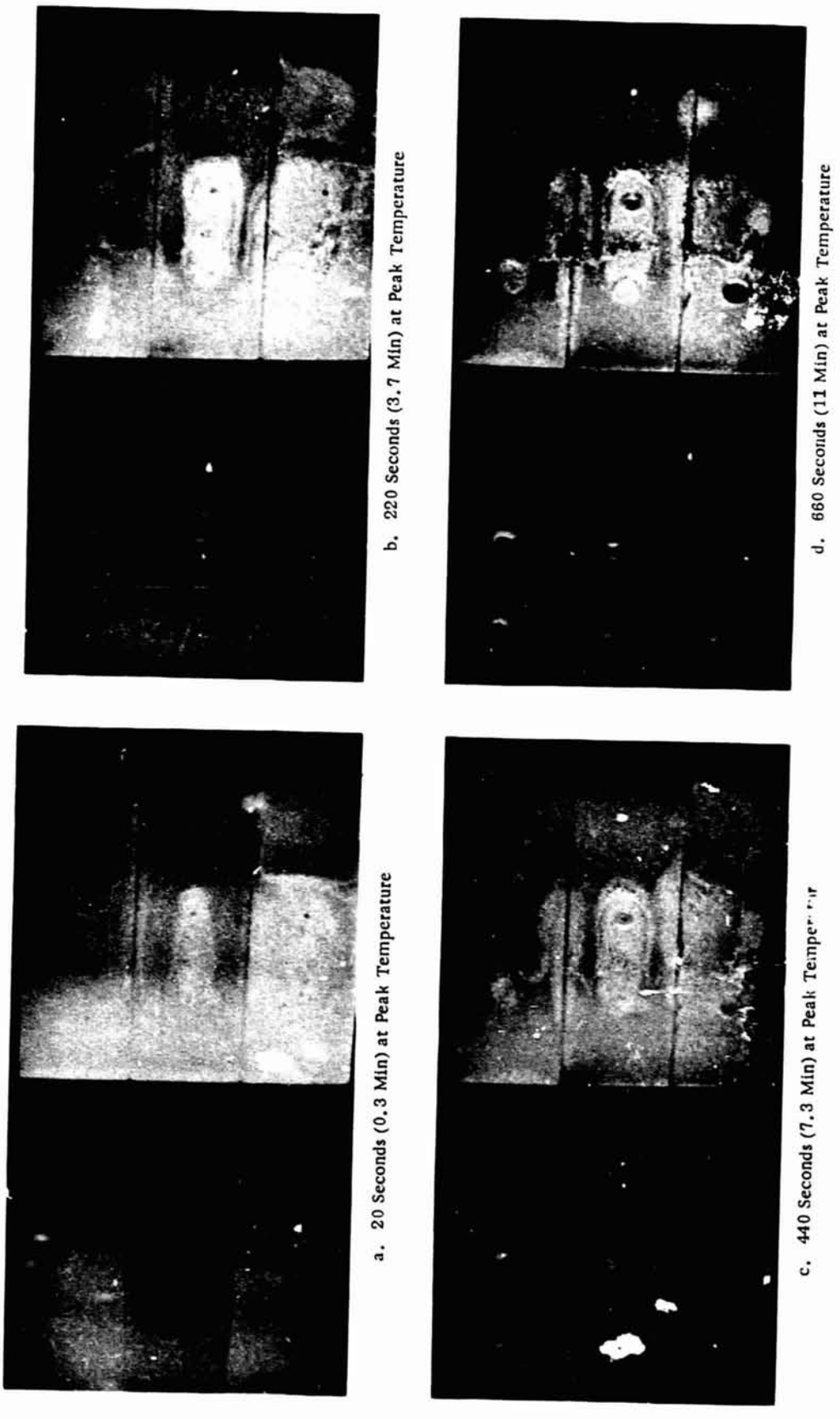


FIGURE 29. SELECTED PRINTS FROM TIMED-SEQUENCE PHOTOGRAPHS TAKEN DURING THE NOMINAL 2500 F PEAK TEMPERATURE EXPOSURE PERIOD OF RUN 9

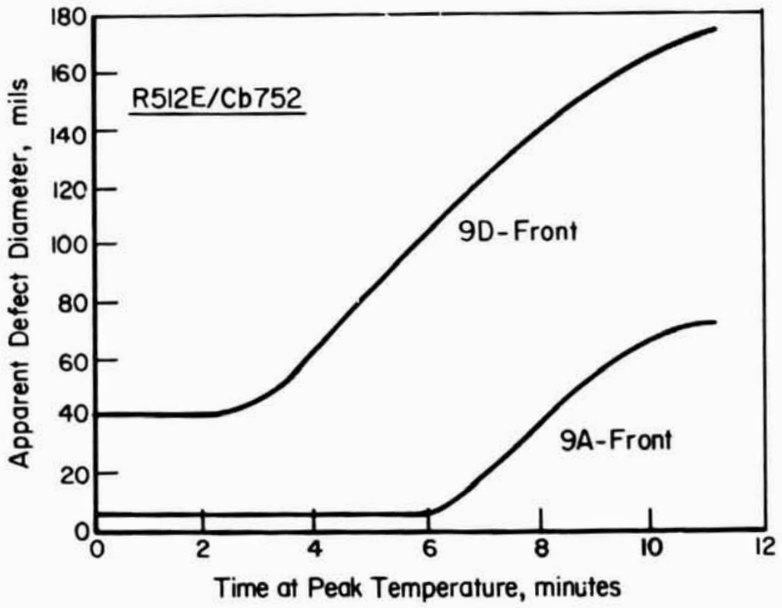


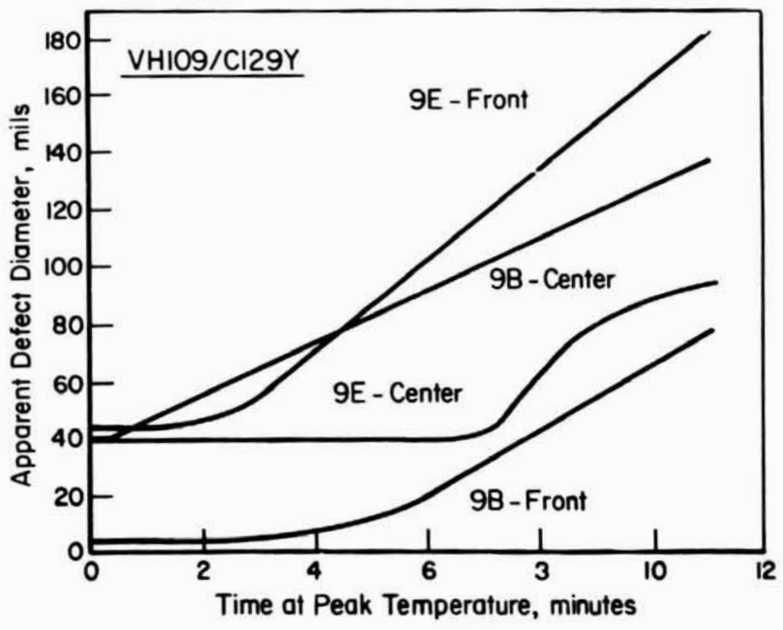


FIGURE 3( APPARENT GROWTH RATES OF DEFECTS ON RUN 9 SPECIMENS AS A FUNCTION OF TIME AT PEAK TEMPERATURE

Data taken from timed-sequence photographs.

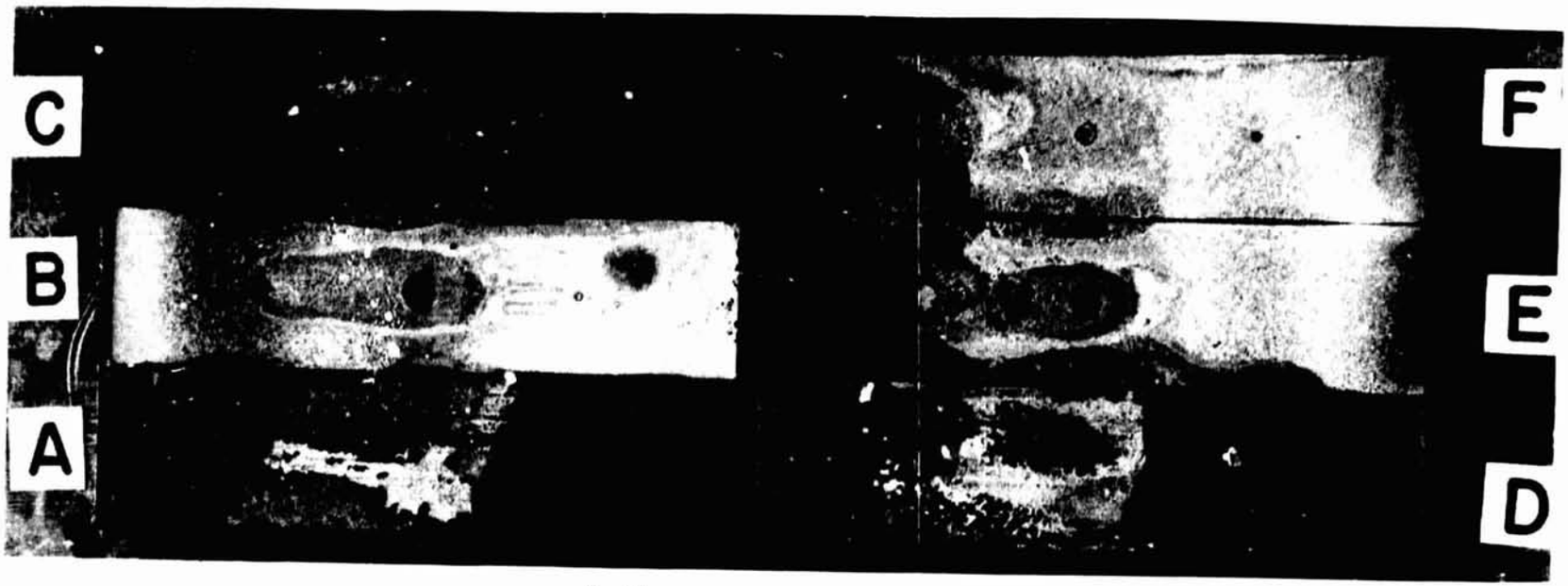


Arc Flow ⟶

FIGURE 31. TOP VIEW OF INTENTIONALLY DEFECTED COATED COLUMBIUM SPECIMENS AFTER ONE SIMULATED REENTRY CYCLE IN PLASMA ARC FACILITY

A. R512E/Cb752
B. VH109/C129Y
C. R512E/C129Y
D. R512E/Cb752
E. VH109/C129Y
F. VH109/Cb752

Nominal $T_{max}$ of 2500 F, Run 9.

TABLE 16. SUMMARY OF FLAW GROWTH AND CONTAMINATION BEHAVIOR OF INTENTIONALLY DEFECTED COATED COLUMBIUM SPECIMENS IN RUNS 8 AND 9

| System | Flaw Type[a] | Defect No. | Estimated Local Temperature, F | Diametral Flaw Growth | | Contamination Depth[c], mils | KHN at 2-Mil Depth |
|---|---|---|---|---|---|---|---|
| | | | | Mils | Mils/Min[b] | | |
| R512E/Cb752 | S | 8B-1 | 2510 | 206 | 14 | 13 | 522 |
| | S | 8F-1 | 2510 | 156 | 10 | 10 | 632 |
| | S | 9A-1 | 2550 | 96 | 8 (19) | -- | -- |
| | S | 9D-3 | 2370 | 3 | 0.3 | 9 | 595 |
| | L | 8B-3 | 2490 | 9 | 0.6 | 23 | 613 |
| | L | 8F-3 | 2470 | 10 | 0.7 | 20 | 1860 |
| | L | 9A-3 | 2440 | 0 | <0.1 | -- | -- |
| | L | 9D-1 | 2540 | 224 | 20 (22) | 7 | 755 |
| | T | 8B-2 | 2510 | 192 | 13 | 21 | 565 |
| | T | 8F-2 | 2510 | 130 | 9 | 21 | 730 |
| | T | 9A-2 | 2510 | 21 | 2 | -- | -- |
| | T | 9D-2 | 2470 | 12 | 1 | 21 | 805 |
| VH109/C129Y | S | 8C-1 | 2520 | 150 | 10 | 10 | 520 |
| | S | 8E-1 | 2510 | 116 | 8 | 9 | 630 |
| | S | 9B-1 | 2580 | 86 | 8 (12) | 4 | 710 |
| | S | 9E-3 | 2410 | 1 | <0.1 | 9 | 920 |
| | L | 8E-3 | 2480 | 7 | 0.5 | 19 | 710 |
| | L | 8C-3 | 2440 | 1 | <0.1 | 11 | 833 |
| | L | 9B-3 | 2450 | 6 | 0.5 | 14 | 1240 |
| | L | 9E-1 | 2610 | 181 | 16 (15) | 4 | 890 |
| | T | 8E-2 | 2510 | 192 | 13 | 8 | 495 |
| | T | 8C-2 | 2480 | 50 | 3 | 21 | 955 |
| | T | 9B-2 | 2470 | 160 | 14 (9) | 7 | 780 |
| | T | 9E-2 | 2510 | 151 | 13 (22) | 2 | 322 |
| R512E/C129Y | S | 9C-1 | 2480 | 155 | 14 (15) | 3 | 650 |
| | S | 8A-1 | 2460 | 16 | 1 | 12 | 550 |
| | L | 9C-3 | 2400 | 5 | 0.4 | 14 | 920 |
| | L | 8A-3 | 2450 | 4 | 0.3 | 18 | 860 |
| | T | 9C-2 | 2470 | 202 | 18 (16) | 6 | 890 |
| | T | 8A-2 | 2470 | 39 | 3 | 18 | 860 |
| VH109/Cb752 | S | 9F-1 | 2625 | 80 | 7 | 7 | 668 |
| | S | 8D-1 | 2500 | 72 | 5 | 18 | 450 |
| | L | 9F-3 | 2390 | 2 | 0.2 | 20 | 1100 |
| | L | 8D-3 | 2470 | 6 | 0.4 | 24 | 860 |
| | T | 9F-2 | 2510 | 11 | 1 | 20 | 860 |
| | T | 9D-2 | 2490 | 30 | 2 | 24 | 550 |

(a) S, L, and T designate small, large, and through defect types, respectively.
(b) Parenthetical values are actual measurements from time-lapse photographs.
(c) Depth below oxide/substrate interface to base hardness plus 50 KHN.

rates determined for the individual defect sites. Note that in a few cases, the actual flaw-growth rates measured from the time-lapse photographs are significantly greater than the nominal values calculated from the "before and after" measurements. This was related to an incubation period prior to rapid flaw growth in these cases, e.g., see curve for 9A-Front defect in Figure 30.

Figure 32 presents a graphical correlation of time-temperature:flaw-growth rates as determined from the Runs 8 and 9 data. These data show that at local temperatures below 2470 F, no rapid flaw growth occurs. From 2470 F through 2510 F, mixed results are indicated, with about half of the flaws growing very rapidly (8 to 22 mils/min), about one-quarter growing at intermediate rates (2 to 4 mils/min), and the balance growing much more slowly (0.2 to 1 mil/min). At temperatures above 2510 F, flaw growth is consistently rapid but with no logical indication of growth-rate dependence on temperature.

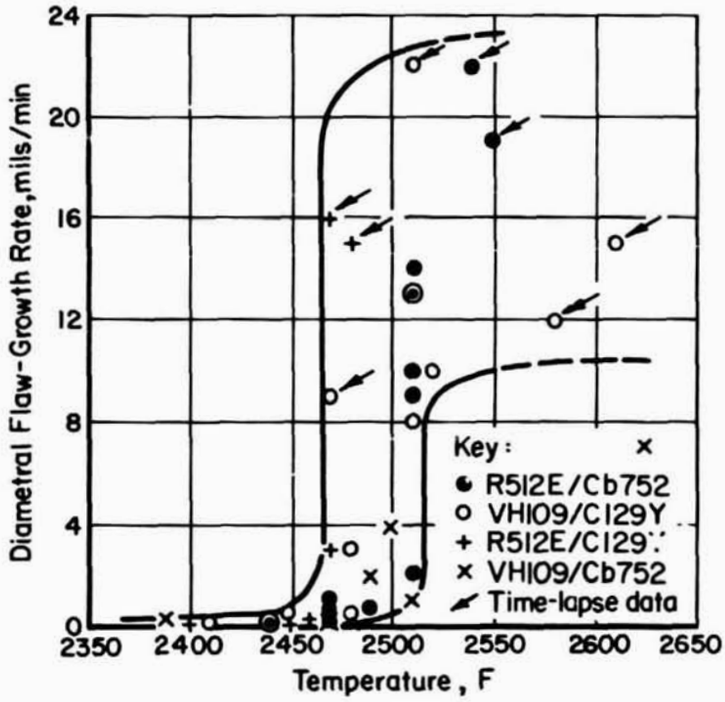


FIGURE 32. CORRELATION BETWEEN DYNAMIC-EXPOSURE TEMPERATURE AND FLAW-GROWTH RATE

As noted earlier, Run 16 was intended to study flaw growth under multicyclic profiling at a nominal peak exposure temperature of 2500 F. Unfortunately, as shown by the temperature data for these specimens in Table A-18, during this run average local defect temperatures did not exceed 2470 F except for two specimens, 16A and 16E. In neither of these cases did any visibly apparent diametral defect growth occur. The only measurable defect growth which occurred during Run 16 (in specimens examined metallographically to date) took place on Specimens 16B and 16F where the initial 4-mil-diameter, small flaws grew to 8 and 28 mils in diameter, respectively. For reference purposes, the coating systems and defect temperatures on these four Run 16 specimens are reproduced below.

| Coating System | Specimen | Estimated Temperature Cycle 1 | Cycle 2 | Cycle 3 | Metallographically Measured Defect Diameter[a], mils |
|---|---|---|---|---|---|
| R512E/Cb752 | 16A | 2500 | 2460 | 2470 | 4 |
| R512E/Cb752 | 16B | 2470 | 2420 | 2420 | 8 |
| R512E/FS85 | 16E | 2510 | 2470 | 2510 | No data yet |
| VH109/C129Y | 16F | 2470 | 2460 | 2450 | 28 |

(a) Initial diameter - 4 mils.

This behavior of the R512E/Cb752 and VH109/C129Y Run 16 specimens is in reasonable agreement with the Run 8 and Run 9 data for these coating systems. However, the fact that no defect growth occurred in the defected R512E/FS85 Run 16E specimen even though this material was exposed to two 2510 F cycles suggests that this coating substrate system may be somewhat more resistant to rapid defect growth than are the others.

Inspection of the data of Table 16 suggests that flaw type is of no significance to flaw-growth rates. Flaw location, either transverse or axial to the plasma flow, is important only as it affects local temperature.

From this analysis, the obvious conclusion is that under dynamic, hypersonic-shear environmental conditions a critical temperature exists below which flaw growth is slow and well behaved, and several cycles are required to cause significant flaw growth. Above this critical temperature, flaws grow rapidly, such that holes as large as 1/8 to 1/4 inch in diameter might be expected in as few as one reentry. Coupling the data depicted in Figure 32 with a reasonable uncertainty of local temperature determination on the order of ±50 F, it appears that the critical temperature lies within the range 2420 F to 2560 F, the most probable being 2490 F for the R512E/Cb752 and VH109/C129Y systems.

Emittance. As described earlier, reduction of thermocouple, scanning pyrometry, and IR photography data from dynamic arc exposures allowed estimates of emittance ranges for the various systems. Despite appreciable scatter in the data, most correlations suggested the following emittance values:

| System | Estimated Normal Spectral Emittance at Nominally 2300 F: Approx. Range | Nominal |
|---|---|---|
| R512E/Cb752 | 0.65 to 0.75 | .73 |
| VH109/C129Y | 0.85 to 0.95 | .91 |
| R512E/FS85 | 0.65 to 0.85 | .75 |

No trends towards higher or lower emittance values with exposure time were observed in any of the runs which included up to five simulated reentry cycles. Because of limited numbers of cycles, and appreciable differences in temperatures within and between runs, the reader is cautioned against treating those data out of context.

Insulation Wash. When dismantling the models after dynamic exposure, limited observations were made concerning effects on the backup zirconia insulation. In Runs 8 and 9, under areas where rapid defect growth had occurred, there was evidence of mild reaction between the insulation and back-side effluent from the defect site. In these

areas, the insulation was hard and rigid, and had a glazed appearance, suggesting perhaps eutectic melting between the zirconia and (basically) $Cb_2O_5$. The worst area observed had eroded to a depth of about 1/16 inch. No attack of the insulation was apparent in any other run.

Subcritical Profiling. Optical measurements were made at the intentionally defected sites on the 30 specimens which had been subjected to subcritical profiling at 2350 F for one to five cycles (see Table 10). These showed that no measurable changes had occurred in the dimensions of these defects as viewed externally. As described later, metallographic sections were prepared through some of the defect sites represented in these runs, e.g., the specimens from Run 11. This showed that some substrate recession had occurred underneath the coatings of a few specimens at the defect site, but the maximum extent of this recession was of the order of 2 mils after three to five cyclic exposures.

## Metallography

Defect Growth. Representative microstructures at two coating-defect sites which had been exposed under subcritical conditions for one dynamic profiling cycle are shown in Figure 33. Under these conditions, a porous "fluffy" oxide (typical of $Cb_2O_5$) was formed over the exposed substrate alloy. "Nongrowing" defects from Runs 8, 9, and 16, with a nominal maximum temperature of 2500 F, typically grew at an assumed* linear rate from 0.1 to 2 mils/minute. Other runs, with a nominal maximum temperature of 2350 F, exhibited defect-growth rates of less than 0.1 mil/minute, and quite frequently less than 0.01 mil/minute. Detailed data are contained in the appendix, Table A-22.

Representative microstructures at three coating defect sites which had been exposed under critical conditions for one dynamic profiling cycle are shown in Figure 34. Here, the oxidation product assumed the form of a dense, glassy oxide containing entrapped gas pockets. In the nominally cycled Run 8 specimens, the color of the glassy product changed from yellow on the exterior surface to a dark blue-black near the oxide/metal interface. In the rapidly cooled Run 9 samples, the glassy oxidation product consisted entirely of the blue-black material which was tentatively identified as a high-temperature allotropic modification of $Cb_2O_5$. The rapid cooling of the Run 9 specimens also resulted in the entrainment of larger gas pockets, as shown by a comparison of Figures 34b and 34c.

As illustrated in Figure 34, the growth of the defects under critical exposure conditions is primarily the result of severe oxidation consumption of the Cb752 and C129Y substrate alloys. This results in undercutting the R512E or VH109 coatings, neither of which appeared to be appreciably degraded during the dynamic exposures. For neither the subcritically nor critically exposed specimen defect sites did there appear to be any fluxing of the coating by the oxidation products evolved.

These observations suggest that the supercritical growth rates are associated with classical "catastrophic" oxidation involving transport through the molten substrate oxide. In general, for columbium alloys under high mass flow of air, coincidence of catastrophic oxidation and autoignition processes is often tacitly assumed. In the present studies, although flaw-growth rates were rapid, they were not of the almost explosive

*This assumption neglects the possibility of a significant incubation period. See p. 71.

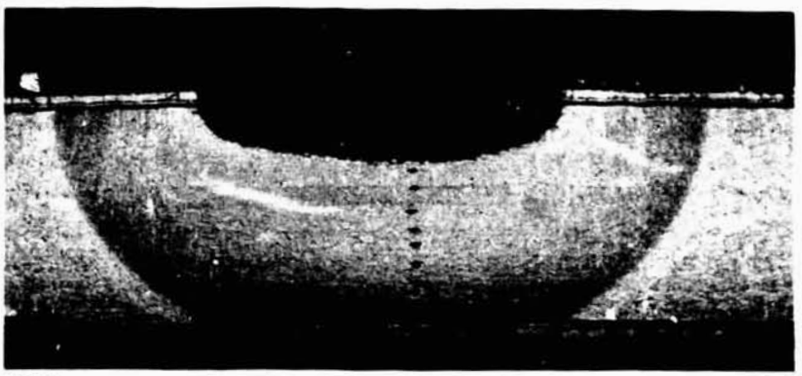

50X Bright Field 5F019

a. Defect 8B-3 on R512E/Cb752; Initially 41 Mils in Diameter by 4 Mils Deep

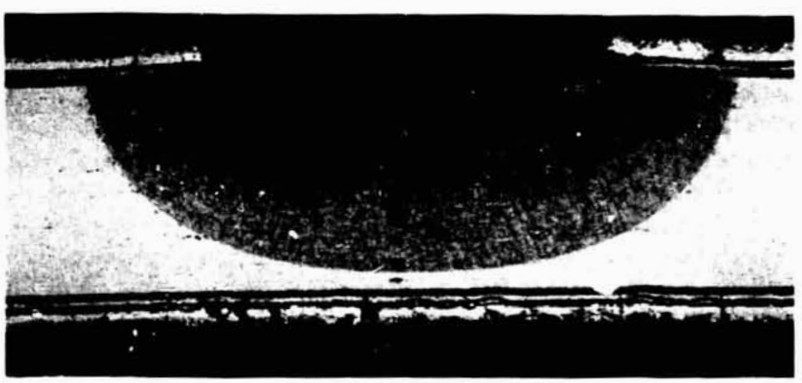

50X Bright Field 5F020

b. Defect 8E-3 on VH109/C129Y; Initially 41 Mils in Diameter by 5.5 Mils Deep

FIGURE 33. LONGITUDINAL SECTIONS THROUGH COATING-DEFECT SITES ON SPECIMENS AFTER ONE DYNAMIC REENTRY PROFILING CYCLE

40X Polarized Light 5F022

a. Defect 8D-1 on VH109/Cb752; Initially 4.7 Mils in Diameter by 5.5 Mils Deep

30X Bright Field 5F025

b. Defect 8E-1 on VH109/C129Y; Initially 4.7 Mils in Diameter by 5.5 Mils Deep

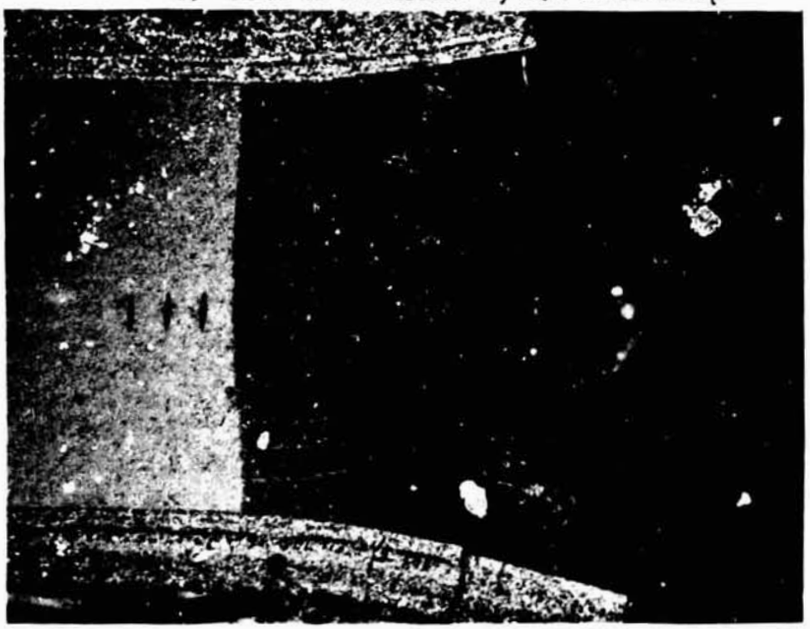

100X Polarized Light 5F016

c. Defect 9B-2 on VH109/C129Y; Initially 39-Mil-Diameter Through-Hole

FIGURE 34. LONGITUDINAL SECTIONS THROUGH COATING-DEFECT SITES ON SPECIMENS AFTER ONE DYNAMIC REENTRY PROFILING CYCLE

Arc flow direction was from left to right.

rapidity associated with autoignition.* The precipitous increase in flaw-growth rate noted at about 2490 F under dynamic conditions, coupled with metallographic observations, indicates that catastrophic oxidation is occurring. If this is true, then the presence of a coating on major surfaces coupled with the heat-sink capacity for the low surface-to-volume ratio (oxidizing surface) represented by a hole edge in thin sheet has a net thermal attenuation effect that results in quenching the expected autoignition reaction.

Defect Contamination Rates. Metallographic evaluation of the extent of contamination was judged by visual observation and by the results of Knoop hardness traverses. Specimens exposed to one dynamic cycle in Runs 8 and 9 where temperatures were subcritical and growth was limited to at most a few mils, and three dynamic cycles in Run 11 were included. Detailed results are given in the appendix, Table A-22. Not included in this but included in the analysis presented here (specific data are presented later in this report) are results of similar analyses for exposed and room-temperature tensile-tested specimens from Runs 12, 13, 14, and 16.

Figure 35 illustrates general contamination features usually observed in the respective substrates. Cb752 showed severe contamination throughout the contamination zone bounded by the dense precipitate ring, as judged both visibly and by hardness traverse. C129Y similarly displayed severe contamination (KHN >300) in the area bounded by the precipitate ring, and additionally showed a low-level contamination zone a few mils thick characterized by hardnesses from 220 to 300 KHN. In this area, grain boundaries etched more heavily than the uncontaminated parent metal. FS85 usually failed to show a precipitate ring. Severe contamination was delineated by staining when etched with $HNO_3$:HF:acetic acid (1:1:1 proportions of reagent acids, about 1-second dip). Beyond the stained, severe contamination ring was a very broad region where, in direct contrast with C129Y, very light grain-boundary etching was the rule. The uncontaminated base metal showed greater propensity to etch at grain boundaries (extreme lower corners in Figure 35). These general features were observed for all defect types.

Table 17 presents a summary of the contamination analysis. The mean contamination rates have been normalized to the estimated 2400 F value by using an Arrhenius adjustment, assuming 28 kcal/mole as the activation energy for the contamination reaction.** For all substrates, the greatest contamination rates were associated with through-hole, Type A, defects. Type B, 40-mil coating defects were somewhat less severe in their contamination effects, and the small Type C defects were still appreciably less. For Cb752 Types A and B defects and for C129Y Type B defects, data fore one and three dynamic exposures show the expected parabolic contamination kinetics (i.e., parabolic rates for one and three cycles are equal). The Type C defects for both substrates and Type A defects for C129Y do not result in parabolic contamination kinetics, as indicated by a significant decrease in contamination rate as the number of expsoure cycles increases. Although data reproducibility (standard-deviation values) is generally quite good, data analysis does not yet suggest for the material/defect combinations in question any single kinetics law. It may be in these cases (C129Y Type A defects and both Type C defects) that the contamination-rate-controlling mechanism is changing from one through five cycles. Obviously, more extended testing is required to resolve contamination/degradation kinetics for small defects.

*Clark, J. W., "The Ignition of Columbium and Selected Alloys", Columbium Metallurgy, Interscience Publishers, New York, New York (1961), pp 615-647.

**The 28 kcal/mole value represents the activation energy for the diffusion of oxygen in columbium alloys based on the work of W. D. Klopp et al, "Studies on the Oxidation and Contamination Resistance of Binary Columbium Alloys", Trans. ASM, 51, pp 256-281, 1959.

100X a. Specimen 11B – Cb752 6F484

100X b. Specimen 11C – C129Y 6F483

100X c. Specimen 11A – FS85 6F485

FIGURE 35. CONTAMINATION ASSOCIATED WITH SMALL, TYPE C DEFECTS PRODUCED IN THREE DYNAMIC CYCLES AT 2350 F NOMINAL MAXIMUM TEMPERATURE (RUN 11)

TABLE 17. SUMMARY OF RESULTS OF CONTAMINATION-ZONE MEASUREMENTS ON DYNAMIC EXPOSURES, RUNS 8, 9, 11

| Substrate | Defect Type(a) | No. of Cycles | Contamination Rate, Adjusted to 2400 F, $mil^2/min$ Mean | Std. Dev. | Pooled Values for Group, $mil^2/min$ Mean | Std. Dev. |
|---|---|---|---|---|---|---|
| Cb752 | A | 1 | 28.4 | 3.0 | 28.9 | 3.4 |
| | | 3 | 29.6 | 5.0 | | |
| | B | 1 | 15.4 | 2.5 | 15.2 | 2.1 |
| | | 3 | 14.6 | 1.8 | | |
| | C | 1 | 7.2(b) | 0.3(b) | | |
| | | 3 | 3.8(b) | 0.6(b) | | |
| | | 5 | 2.8(b) | 0.1(b) | | |
| C129Y | A | 1 | 20.4 | 4.0 | | |
| | | 3 | 9.3 | 1.3 | | |
| | B | 1 | 10.4 | 2.8 | 10.0 | 3.2 |
| | | 3 | 8 | 5.0 | | |
| | C | 1 | 1.6 | 1.2 | | |
| | | 3 | 2.3(b) | 0.6(b) | | |
| FS85 | A | 3 | 52.0 | 1.3 | | |
| | B | 3 | 21.4 | 11.2 | | |
| | C | 3 | 5.4(b) | 1.7(b) | | |

(a) A = 40-mil through-hole
B = 40-mil coating defect
C = 4-mil coating defect.

(b) Includes data from tensile-test specimens.

Also apparent from the data is that for all defect types, FS85 is the least resistant to contamination (only severe contamination for FS85 is used in this analysis – see section on Tensile-Test Results), followed by Cb752, with C129Y displaying the best resistance to contamination.

Specimens that were defected and then exposed to static profiling were also examined metallographically to assess their contamination behavior. Surprisingly, these showed much less severe contamination than did those exposed to dynamic cycling. Table 13 gives some results for specimens examined after one static cycle. Aside from showing little contamination, the results allow no consistent analysis of substrate or defect type, although Cb752 may be inferred to be more contamination proof than C129Y. (Additional data given in the appendix, Table A-23, for up to five statically cycled tensile specimens confirmed the lesser contamination in static versus dynamic cycling.)

Data are not yet available to explain the differences between static- and dynamic-cycling contamination results although temperature and pressure histories were similar in both exposure modes. The other possible variables are environment chemistry and dynamics. These will be investigated in future studies.

TABLE 18. SUMMARY OF CONTAMINATION DATA FOR INTENTIONALLY DEFECTED COATED COLUMBIUM SPECIMENS EXPOSED TO ONE STATIC 2500 F PROFILING CYCLE

| Defect | Coating | Substrate Alloy | Substrate Initial Thickness, inch | Defect Data Type | Defect Data Average Temp, F | Contamination Depth, mils Metallographic Measurements | Contamination Depth, mils Hardness Traverse | KHN at 1-Mil Depth |
|---|---|---|---|---|---|---|---|---|
| | | | | Run Cb-1 | | | | |
| S1-T | R512E | Cb752 | 0.015 | C | 2500 | 6.0 | 6.8 | 668 |
| S1-C | R512E | Cb752 | 0.015 | A | 2500 | 4.0 | 2.2 | 275 |
| S1-B | R512E | Cb752 | 0.015 | B | 2500 | 2.0 | 1.4 | 275 |
| | | | | Run Cb-2 | | | | |
| S7-T | VH109 | C129Y | 0.015 | C | 2490 | 0.6 | 1.6 | 296 |
| S7-C | VH109 | C129Y | 0.015 | A | 2490 | 1.3 | 1.0 | 255 |
| S7-B | VH109 | C129Y | 0.015 | B | 2490 | 0.8 | <1.0 | 242 |
| S8-T | VH109 | C129Y | 0.025 | C | 2490 | 2.0 | 2.0 | 335 |
| S8-C | VH109 | C129Y | 0.025 | A | 2490 | 2.0 | 1.6 | 296 |
| S8-B | VH109 | C129Y | 0.025 | B | 2490 | 0.6 | 1.0 | 260 |

Crack-Contamination Observations. In general, no visual or metallographic evidence of gross coating oxidation failure was observed at sites away from the intentional coating defects in any of the specimens which were cycled for up to 5 exposures in either the dynamic or static environments.* On the other hand, detailed examination of specimen cross sections at locations removed from intentional-defect sites revealed frequent, but mild, substrate contamination associated with the presence of cracks in the coatings of the type illustrated in Figures 36 and 37. Those sections which showed such evidence of crack-associated contamination did so with a frequency on the order of 10 to 20 contaminated sites per inch. In such cases, the contamination depth was on the order of 0.2 to 0.4 mil after one cycle and 2 to 3 mils after three cycles. Not all cross sections of the same specimens showed crack contamination, attesting to the sensitivity to thermal-profiling details. However, sufficient observations of this behavior were made to flag this as a potential problem. One specimen (S6, VH109-coated Cb752, 25 mils thick) also showed severe edge contamination to a depth of 3 to 4 mils without obvious oxidation scaling of the substrate. Figure 38 shows this obvious prefailure site.

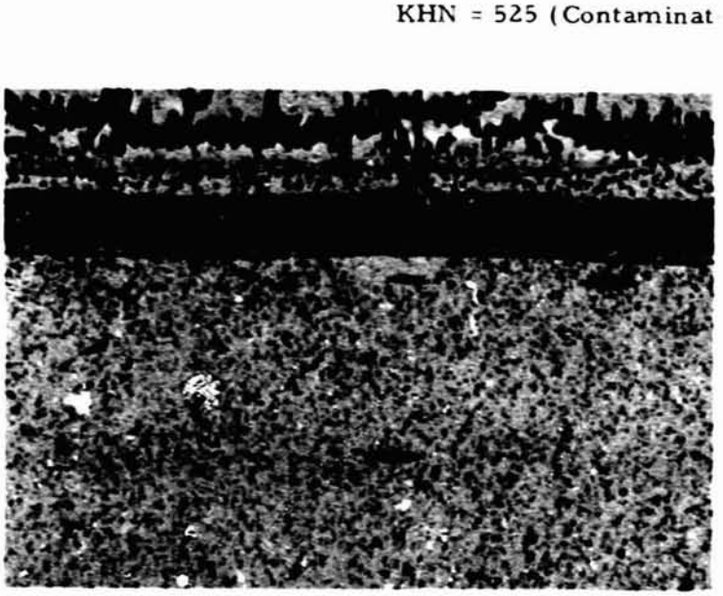


FIGURE 36. CRACK-ASSOCIATED CONTAMINATION IN VH109/C129Y SPECIMEN AS A RESULT OF ONE STATIC SIMULATED 2500 F REENTRY CYCLE EXPOSURE

Note Knoop hardness readings taken using 5-gram load.

Analysis of crack-contamination frequency for single-cycled specimens showed correlation between crack-contamination behavior and cooling rate. Crack contamination was observed more frequently under static-cycling conditions than under dynamic-cycling conditions. Ramp cooling under static conditions is somewhat slower than that under dynamic conditions. Further, in Run 9, a lightning-strike-initiated power outage resulted in quenching of the specimens as previously described. Correlations of cooling rate with frequency of observed crack oxidation are summarized below:

*The single exception to this was the rapid growth of an edge defect in R512E/Cb752 Specimen 9D. See Figure 31.

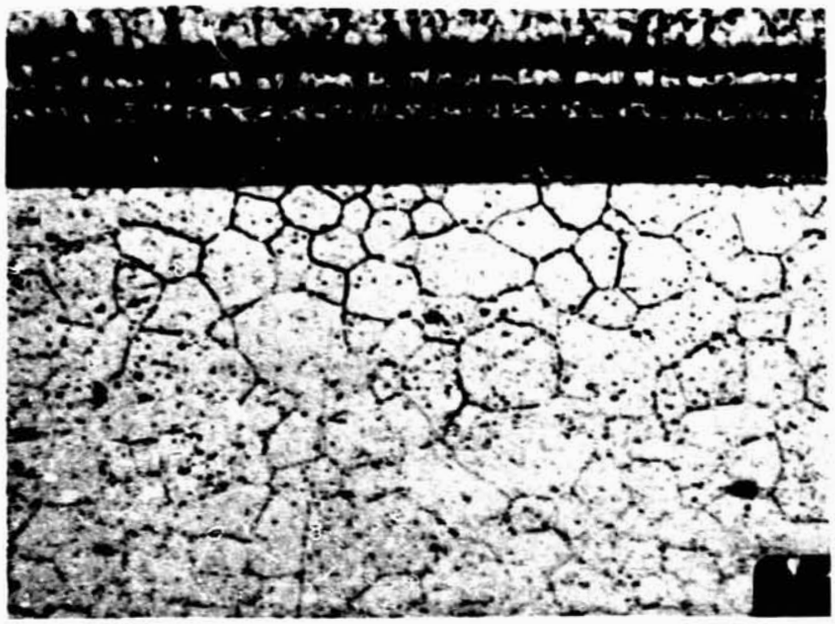

500X a. Specimen 11C – C129Y 6F482

250X b. Specimen 11A –FS85 6F486

FIGURE 37. CRACK CONTAMINATION IN C129Y AND FS85 AFTER THREE DYNAMIC EXPOSURE CYCLES (RUN 11)

| Test | Nominal Cooling Rate, F/sec | No. of Sections Examined | No. of Sections Showing Crack Contamination |
|---|---|---|---|
| Static | 3 | 14 | 5 positive + several other possibles |
| Dynamic - normal | 4-5 | 18 | 2 positive + several other possibles |
| Dynamic - quench | ~60 | 15 | 0 (no indications) |

This correlation indicates a probability that system sensitivity to the occurrence of crack contamination depends strongly upon the thermal profile. The sensitivity of coated columbium to step-down or slow-cycle oxidation testing has long been recognized. For Shuttle, the case of sustained lower temperature thermal loading during maneuvering following peak reentry heating may represent a major challenge.

As shown in Figures 36 and 37, crack contamination was barely noticeable after one cycle, but was appreciably more obvious after three cycles. Thus, it is suggested that this is not merely a transient phenomenon, but may comprise a dominant failure mode. In specimens from Run 11, both C129Y and FS85 showed frequent crack-oxidation signatures. Detailed examination of Cb752 showed only one area in one of six sections examined where crack oxidation occurred. It is suggested that both coating and substrate, probably via thermal-expansion mismatch, are important to this phenomenon. None of the tensile specimens from Runs 12, 13, 14, and 16 showed evidence of crack contamination. Rather than suggesting that crack contamination was absent in the tensile specimens, it is more likely that tensile straining introduces stored energy that affects the etching response of the alloys and obscures the rather sensitive response to etching.

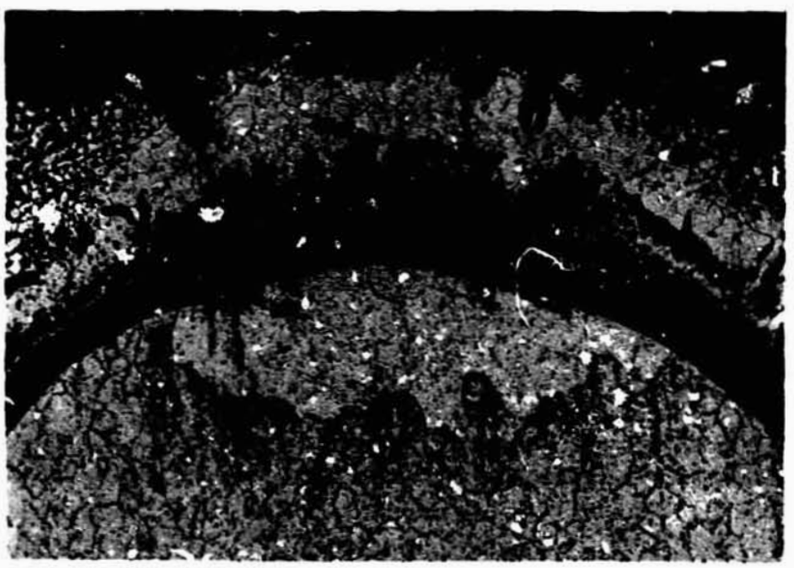

250X 5F748

FIGURE 38. GROSS EDGE CONTAMINATION IN S6 (VH109/Cb752) AFTER ONE STATIC 2500 F SIMULATED REENTRY CYCLE

Considering the frequency of observation of crack contamination, particularly in statically cycled specimens and in C129Y substrates, in only one or three cycles, property degradation attributable to this might be expected in relatively few cycles. However, in results from the NAS 8-26325 program at Battelle involving tensile tests after 5, 10, and 30 static cycles, only 1 out of 30 specimens tested at room temperature after exposure showed embrittlement. Pending further metallographic evaluation of these specimens, it appears that the mild degree of contamination resulting from crack contamination as illustrated in Figure 37 is not degrading to tensile properties at room temperature.

## Tensile Properties

Tensile properties determined at room temperature and test observations are detailed in Table A-24 in the appendix.

Tensile tests and short-time creep tests at elevated temperature are in progress. At this writing, data are too limited to provide useful analysis, and presentation and discussion of results are necessarily deferred to later reporting periods. A particularly troublesome aspect of elevated-temperature tests is that heat-up and soak times prior to testing must be very short to provide meaningful analysis of defect contamination effects.

In the room temperature tests, the R512E/Cb752 system received most emphasis in the first year's effort, with VH109/C129Y and R512E/FS85 receiving lesser emphasis. Because of some differences, results are presented according to system in the following discussion.

Cb752. Table 19 summarizes the significant findings concerning room-temperature tensile properties for the R512E/Cb752 system. Neither yield nor ultimate tensile strengths showed variations that could be attributed to any of the variables examined, which were:

- Substrate thickness
- Gage width of specimen
- Specimen machining/coating sequence
- Static or dynamic exposure of defected or undefected specimens for up to five cycles.

Consequently, all strength values were treated as a single statistical group to arrive at standard deviation values of 1.9 ksi for both yield and ultimate strengths. This respectably low value for standard deviation signifies that the area compensation method and coating and substrate thicknesses were reliable and reproducible to a high degree. Also implicit is that exposure-induced substrate contamination at defect sites within the limits explored is not weakening. Coupled with ductility analysis, it is further implied that defect contamination is either directly strengthening at room temperature or increases the strain-hardening exponent relative to uncontaminated Cb752. In only one case (Specimen 14A, Table A-24) did the decreased ductility associated with defect contamination appear to have a modest effect towards decreased ultimate strength.

TABLE 19. SUMMARY OF ROOM-TEMPERATURE TENSILE PROPERTIES FOR Cb752-BASE SYSTEM

Yield Strength
Mean - 65.0 ksi
Std. Dev.(s) - 1.9 ksi

Ultimate Strength
Mean - 85.0 ksi
Std. Dev.(s) - 1.9 ksi

No significant trends in strength with coating nor exposure.

Elongation and Fracture Analysis

| Condition | Elongation, % | Fracture Location[a] |
|---|---|---|
| Bare, As-Received Sheet (Std. Spec.) | | |
| 15-Mil Thickness | 26, 26 | -- |
| 25-Mil Thickness | 32, 34 | -- |
| As-Coated With R512E | | |
| Machined, Then Coated (Std. Spec.) | | |
| 15-Mil Thickness | 16, 17 | -- |
| 25-Mil Thickness | 22, 26 | -- |
| Coated, Then Machined | | |
| 15-Mil Thickness (Std. Spec.) | 16, 18 | -- |
| 25-Mil Thickness | | |
| Std. Spec. | 28, 25 | -- |
| Wide Spec. | 23, 23 | -- |
| Defected and Exposed (25-Mil Thickness) | | |
| Subcritical Dynamic Exposures | | |
| 1 Cycle (Std. Spec.) | 26, 26 | A, A |
| 3 Cycles | | |
| Std. Spec. | 26, 14 | A, D |
| Wide Spec. (Single) | 17 | D |
| 5 Cycles | | |
| Defected (Std., Wide Spec.) | 14, 16 | D, D |
| Undefected (Single, Std. Spec.) | 25 | -- |
| Static Exposures | | |
| 1 Cycle (Std. Spec.) | 22, 25 | A, A |
| 3 Cycles (Std., Wide Spec.) | 24, 23 | A, A |
| 5 Cycles (Std., Wide Spec.) | 24, 24 | A, A |

(a) In defected specimens, A = away from Defect, D = at defect.

The elongation and fracture analysis summarized in Table 19 shows several significant features. The 15-mil-thick material, in both the as-received and coated conditions, displayed elongation values roughly two-thirds to three-fourths times the values for the 25-mil-thick material. Prior observations in "acceptance certification" of the material did not show this for a different tensile-specimen geometry. This effect is in the direction predicted by classical treatment of $A^{1/2} \cdot L^{-1}$ effects*, but the difference is somewhat greater than might be expected. As shown in Table A-24, the 15-mil-thick material never displayed a yield drop, whereas the thicker material usually did. This suggests some material difference (perhaps stretcher leveling of the thinner material after the final anneal) between the two gages, which may have contributed to the slightly greater-than-expected difference in elongation. Application of the R512E coating effected an approximately 25 to 40 percent decrease in tensile elongation.

Exposure of defected specimens to one subcritical dynamic cycle had no effect on tensile elongation. Duplicate specimens failed at locations away from the defect site. After three dynamic cycles, two of three specimens (one standard and one wide specimen) failed at the defect site with a consequent additional 40 percent loss in tensile elongation. However, substantial ductility remained, and after "pop-in" of brittle fracture (after yielding) in the contaminated region surrounding the defect, failure progressed slowly in a predominantly biaxial shear mode. Thus, brittle fracture that initiated in the contamination zone did not propagate by cleavage through the surrounding uncontaminated substrate. The third defected specimen (standard gage width) that was exposed to three dynamic cycles failed at a location removed from the defect.

One undefected specimen exposed to five subcritical dynamic cycles showed no effects of exposure on elongation. Two defected specimens (one standard and one wide) exposed for five cycles failed at the defect site with consequent reduced ductility. Failure mode appeared virtually identical to that observed for three-cycle-exposed specimens. On the basis of tensile properties, five dynamic-exposure cycles appeared to be no more degrading to defected R512E/Cb752 specimens than were three cycles. This was mildly surprising.

Of the six defected specimens exposed for up to five static cycles, none showed any indication of degraded ductility as a result of exposure. All failed at sites away from the defects. Elongations were comparable to those displayed by coated but unexposed specimens. This result suggests that the extent or level of contamination under Battelle's static-cycling conditions was appreciably less than experienced in the dynamic-cycling exposures.

C129Y. Room-temperature tensile test results for the VH109/C129Y system are summarized in Table 20. In contrast with observations on R512E/Cb752, individual strength data (see Table A-24) appeared to align in three "groups" – uncoated, as-coated, and exposed – and data were grouped accordingly for analysis. Even with this selective grouping, standard deviations of strength were appreciably greater for the VH109/C129Y system than those derived for the more homogeneous values of the R512E/Cb752 system. This variability appears to be related to the coating rather than to the substrate, in agreement with coating-thickness analysis presented earlier. (This observation is also in agreement with the statistically "stronger" comparison between R512E/Cb752 and VH109/C129Y systems under investigation on Contract NAS 8-26325. Data from the Fourth Quarterly Progress Report of that contract are given in Table 21 for comparison.)

*Kula, E. B., and Fahey, N. H., "Elongation in Sheet Tension Specimens", Materials Research and Standards, VI, 631 (1961).

TABLE 20. SUMMARY OF ROOM-TEMPERATURE TENSILE PROPERTIES FOR C129Y-BASE SYSTEM

Strength Summary

| Condition | Yield Strength, ksi | | Ultimate Strength, ksi | |
|---|---|---|---|---|
| | Mean | s | Mean | s |
| As-Received Substrate | 70.7 | 0.46 | 89.1 | 0.49 |
| As-Coated With VH109 | 75.5 | 3.60 | 98.4 | 5.71 |
| Defected and Exposed, Three Subcrit. Dynamic Cycles | 69.8 | 3.27 | 96.6 | 2.57 |

Elongation and Fracture Analysis

| Condition | Elongation, % | Fracture Location[a] |
|---|---|---|
| Bare, As-Received Sheet (Std. Spec.) | | |
| 15-Mil Thickness | 30, 30 | -- |
| 25-Mil Thickness | 35, 32 | -- |
| As-Coated With VH109 | | |
| Machined, Then Coated (25-Mil Thickness, Std. Spec.) | 22, 21 | -- |
| Coated, Then Machined | | |
| 15-Mil Thickness (Std. Spec.) | 18, 18 | -- |
| 25-Mil Thickness | | |
| Std. Spec. | 25, 22 | -- |
| Wide Spec. | 24, 24 | -- |
| Defected, Exposed to Three Subcrit. Plasma Cycles | | |
| Std. Spec. (25-Mil Thickness) | 18, 24 | D, D |
| Wide Spec. (25-Mil Thickness) | 22, 4[b] | D, D[b] |

(a) In defected specimens, A = away from defect, D = at defect.

(b) This value associated with defect oxidation growth to 14-mil radius.

TABLE 21. STATISTICAL ANALYSES OF ROOM-TEMPERATURE TENSILE PROPERTIES FOR C129Y/VH109 AND CB752/R512E AS DETERMINED ON CONTRACT NAS 8-26325

| Alloy/Coating System and Exposure | n | Yield Strength[a], ksi $\bar{x}$ | Yield Strength[a], ksi s | Ultimate Strength[a], ksi $\bar{x}$ | Ultimate Strength[a], ksi s | Elongation, % $\bar{x}$ |
|---|---|---|---|---|---|---|
| C129Y/VH109 As-coated | 20 | 74.77 | 4.423 | 91.44 | 4.480 | 17.3 |
| Cb752/R512E As-Coated | 20 | 63.87 | 1.459 | 82.08 | 3.194 | 17.3 |
| C129Y/VH109 After 5 T/P Cycles | 5 | 72.35 | 2.338 | 87.89 | 2.779 | 17.0 |
| Cb752/R512E After 5 T/P Cycles | 5 | 66.58 | 2.059 | 77.05 | 1.281 | 18.2 |
| C129Y/VH109 After 10 T/P Cycles | 5 | 70.79 | 2.651 | 85.71 | 3.384 | 16.2 |
| Cb752/R512E After 10 T/P Cycles | 5 | 65.78 | 0.411 | 76.98 | 0.262 | 16.2 |

(a) Strength values calculated on basis of unreacted substrate dimensions after coating.

From statistical analysis of the strength data as grouped in Table 20, it was concluded that there are differences among the mean yield and ultimate strengths at the 95 percent level of significance. It appears that coating application increases both yield and ultimate strengths. The most likely physical rationale for this behavior lies in mechanical interaction between coating and substrate.* Upon exposure, yield strength appeared to decrease to about the bare substrate value, but ultimate strength remained close to the as-coated value. Attempts to rationalize this in terms of mechanical interaction would be very tenuous at present, and unjustified on the basis of current knowledge. The observation of different behavior of yield and ultimate strengths upon exposure suggests that the methods used to estimate the amount of residual substrate upon which strength calculations are based are valid, and most likely do not contribute substantially to the observed strength variations.

As with the R512E/Cb752 system, nominal 15-mil-thick C129Y possessed somewhat less ductility than nominal 25-mil-thick material in both coated and uncoated conditions. The differential was generally in line with expectations based on $A^{1/2} \cdot L^{-1}$ empiricism. Both substrate thicknesses showed yield-drop behavior (although inconsistently in the coated condition). Application of the coating decreased elongation to about the same extent as noted for R512E/Cb752.

Four specimens that were defected and then exposed to three dynamic cycles all failed at the defect. One of these was cycled under apparently marginally critical conditions, as defect growth to a 14-mil radius in the three-cycle exposure was apparent from fractographic observations. This specimen exhibited only 4 percent tensile elongation even though the fracture was predominantly ductile. Apparently, virtually all elongation was heterogeneous and confined to the defect locale. The other three specimens failed with relatively large values of elongation, suggesting somewhat greater resistance to degradation in the presence of a coating defect for C129Y as compared with Cb752. This is as might be expected from the previously described contamination kinetics of the two materials.

As was observed with the Cb752 substrate, brittle fracture "pop-in" did not propagate into the surrounding uncontaminated substrate material.

FS85. Limited observations on the R512E/FS85 system's tensile properties are summarized in Table 22. As with the R512E/Cb752 system, strength values were not influenced by coating application or by exposure of defected coated specimens. Standard deviations of strengths were very similar to those exhibited by the R512E/Cb752 system, which indicates good material-system reproducibility.

Tensile-elongation values were again reduced by coating application. Two of three specimens exposed to the subcritical, dynamic environment for three cycles failed at the defect, with reduced elongation, and by the "pop-in" followed by shear mode noted for Cb752. The third specimen failed away from the defect site with normal elongation.

*Allen, B. C., Bartlett, E. S., and Wilcox, B. A., "Elevated Temperature Ductility Minima and Creep Strengthening of Coated and Uncoated Columbium Alloys", AFML-TR-66-89, Part II (February, 1967) (Appendix A).

TABLE 22. SUMMARY OF ROOM-TEMPERATURE TENSILE PROPERTIES FOR FS85-BASE SYSTEM

Yield Strength
Mean - 66.0 ksi
Std. Dev.(s) - 1.7 ksi

Ultimate Strength
Mean - 87.2 ksi
Std. Dev.(s) - 2.0 ksi

No significant trends in strength with coating or exposure.

Elongation and Fracture Analysis

| Condition (All 30-Mil Substrate) | Elongation, % | Fracture Location[a] |
|---|---|---|
| Bare, As-Received Sheet (Std. Spec.) | 30, 30 | -- |
| As-Coated With R512E (Std. Spec.) | | |
| Machined, Then Coated | 24, 25 | -- |
| Coated, Then Machined | 25, 25 | -- |
| Defected, Exposed to Three Subcritical Plasma Cycles | | |
| Std. Spec. | 12, 24 | D, A |
| Wide Spec. (Single) | 12 | D |

(a) In defected specimens, A = away from defect, D = at defect.

Microscopic Observations and Measurements. Point-micrometer traverses of width and thickness across the defect area were made on specimens that failed at locations away from the defect. The purpose was to determine whether defect contamination restricted plastic flow at and near the defect site. The results of this survey for dynamically cycled specimens are tabulated below, with reductions in area based on estimated residual substrate dimensions assuming no plastic flow in the coating:

| System | No. of Cycles | Estimated Reduction in Area at Defect, % | Estimated Reduction in Area About 1/8 in on Both Sides of Defect, % | Ratio of Defect R. A. to "Near-Defect" R. A. |
|---|---|---|---|---|
| R512E/Cb752 | 1 | 12.4, 14.8 | 18.4, 18.4 | 0.7, 0.8 |
| Ditto | 3 | 9.5 | 24.0 | 0.4 |
| R512E/FS85 | 3 | 15.9 | 21.4 | 0.8 |

It is thus apparent that defect contamination resulting from dynamic exposures of one to three cycles does have a notable effect in restricting deformation in cases where actual failure at the defect does not occur. As might be expected, with increased exposure (one versus three cycles for Cb752) the degree of restriction increases. This analysis also suggests that the contamination tolerance regarding effects on mechanical properties may be greater for FS85 than for Cb752. This tentative conclusion was also predictable.

Similar analysis for statically cycled specimens of R512E/Cb752 was less rigorous. In three cases (involving both a one-cycle-exposed specimen and a three-cycle-exposed specimen), micrometer traverses showed no evidence of heterogeneous deformation associated with defect contamination. For two specimens (a three-cycle specimen and a five-cycle specimen), coating spall precluded meaningful analysis. For the remaining five-cycle-exposed specimen, the following results were obtained:

| | |
|---|---|
| Defect Reduction in Area, % | 17.4 |
| Surrounding-Area Reduction in Area, % | 28.5 |
| Ratio | 0.6 |

This restrictive effect of contamination from five of Battelle's static cycles is similar to that noted from only one dynamic cycle. In summary, this brief analysis reinforces the tensile-failure-mode indication that static cycling is less deleterious than dynamic cycling, at least in the exposure modes as conducted in this study.

Microscopic examination of defects where failure occurred away from defect sites showed, in general, that defects exposed under dynamic conditions retained a round geometry and exhibited the expected white substrate oxide at their bases. Those exposed to one or three static cycles were elongated, again showing little restriction to plastic flow attributable to the associated contamination. Defects in specimens exposed to five static cycles were round (restricted deformation in the defect locale), and one of these two specimens exhibited a crescent-shaped hole, roughly 10 mils from tip-to-tip and 6 mils deep, where partial substrate fracture had occurred.

Fractographic examination was conducted on fracture surfaces of specimens that failed at defect sites. In every case fracture topography was distinctive and unique to to the specific substrate material.

Figure 39 exhibits scanning electron micrographs showing the defect-associated fracture surface of two R512E/Cb752 specimens. Cb752 defect-contamination fractures are characterized by

(1) A distinct inner zone surrounding the defect where the most severely contaminated metal failed by transgranular cleavage. At higher magnifications, characteristic river markings were readily apparent.

(2) Surrounding the cleavage zone is a coplanar region in which the grain structure of the base metal is apparent. At higher magnification, this region had a dimpled appearance that is characteristic of ductile fracture, despite the fact that the fracture plane in this region, as well as in the cleavage region, was normal to the applied tensile stress.

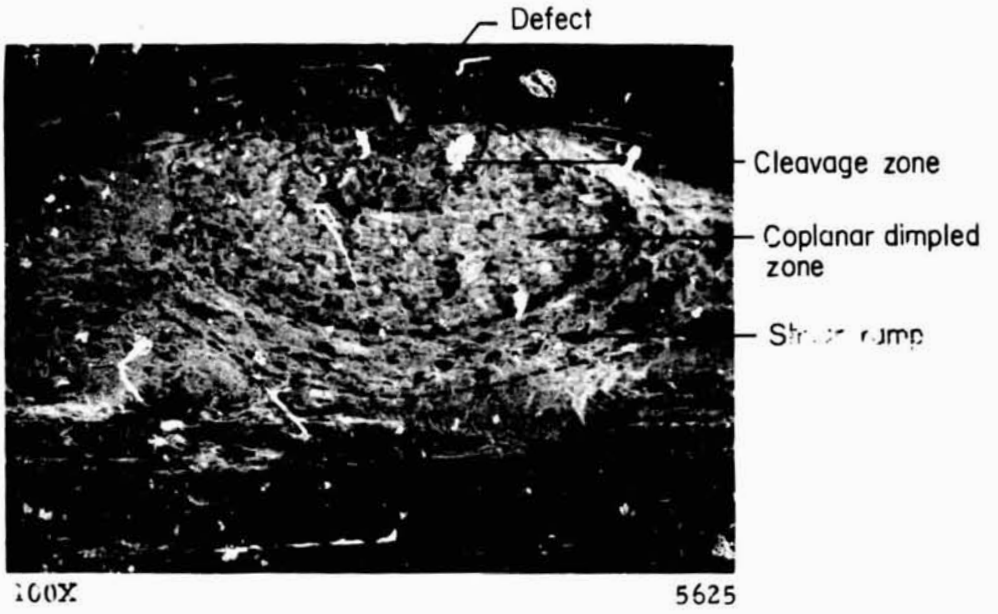


a. Specimen 13E – 3 Dynamic Cycles

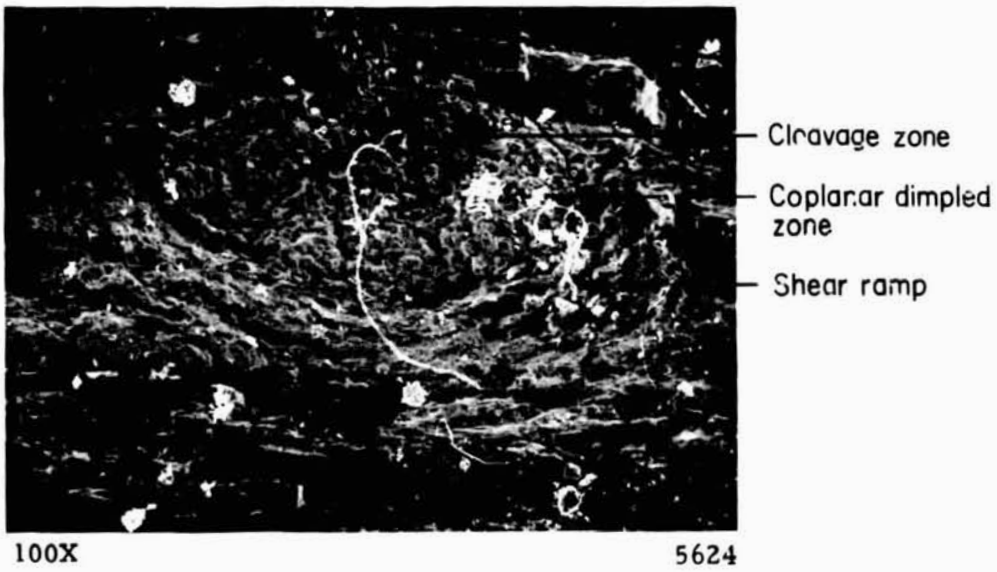


b. Specimen 14A – 5 Dynamic Cycles

FIGURE 39. SCANNING ELECTRON FRACTOGRAPHS OF R512E/Cb752 TENSILE SPECIMENS FAILED AT DEFECT-CONTAMINATION SITES

(3) Outside the coplanar, ductile-fracture area, a shear-transition slope blending with the surrounding uncontaminated shear-failure area was observed.

Figure 40 shows the fracture pattern typical of defect-contamination-induced failure in C129Y. One fractograph is of the defect that exhibited substantial growth during dynamic cycling. Note that the cleavage zone in this case is about twice the thickness of that associated with the "stable", subcritical defect (magnification ratio of the fractographs is 2:1). This supports the prior observations that contamination coefficients associated with the small, stable, 4-mil defects are substantially less than those for larger, or in this case, grown defects. Defect-contamination fracture in C129Y is markedly different from that exhibited by Cb752 in that no indication of the coplanar, dimpled zone could be found. The shear-slope transition occurred directly upon termination of the cleavage fracture zone.

Defect-contamination fractures in FS85 appeared as intermediate between the distinct presence and total absence of the coplanar, dimpled zone in Cb752 and C129Y, respectively. Figure 41 suggests greater similarity to the fracture behavior of Cb752 than to that of C12.Y. While FS85 did display the "grainy" dimpled zone characteristic of Cb752, this was not coplanar with the cleavage zone, but provided the sloped transition between the cleavage and surrounding normal-shear-failure region. The boundary defining the cleavage zone was not so regular and distinct in FS85 as it was in either Cb752 or C129Y.

Estimates were made of radii of the different fracture zones. Results are summarized in Table 23. The fracture-zone definition most likely represents that region

TABLE 23. CONTAMINATION ZONE THICKNESS IN DYNAMIC-EXPOSED, DEFECTED COATED COLUMBIUM ESTIMATED FROM FRACTOGRAPHIC EXAMINATION

| System | No. of Exposure Cycles | Estimated Average Thickness, mils, of Cleavage Zone | Dimpled Zone | Total Defect-Affected Fracture |
|---|---|---|---|---|
| R512E/Cb752 | 3 | 3.3 | 6.9 | 10.2 |
| | 5 | 3.8 | 7.2 | 11.0 |
| VH109/C129Y | 3 | 5.1[a] | 0 | 5.1[a] |
| R512E/FS85 | 3 | 9.6[b] | 11.2 | 20.8 |

(a) Excluding specimen with "grown" defect.
(b) Questionable estimate.

of the total contamination zone that has been sufficiently contaminated to increase the ductile-to-brittle transition temperature under slow-strain conditions to the vicinity of room temperature or above. This will be some fraction of the total contamination zone. It does, however, represent a fairly important characterization of property degradation.

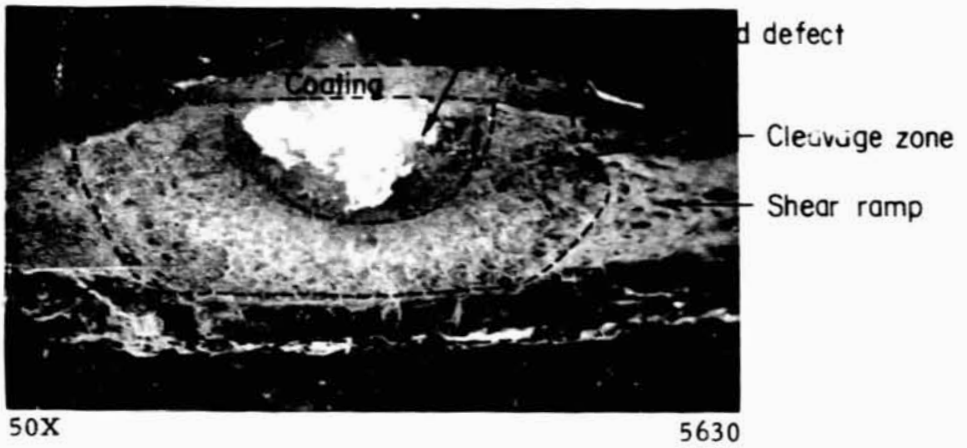


a. Specimen 16F – 3 Dynamic Cycles

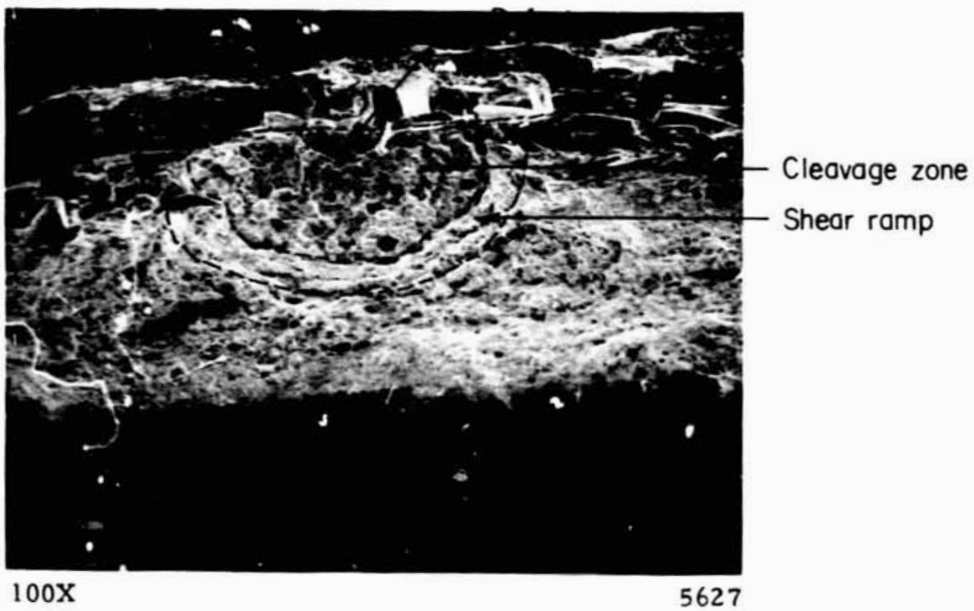


b. Specimen 13F – 3 Dynamic Cycles

FIGURE 40. SCANNING ELECTRON FRACTOGRAPHS OF VH109/C129Y TENSILE SPECIMENS FAILED AT DEFECT-CONTAMINATION SITES

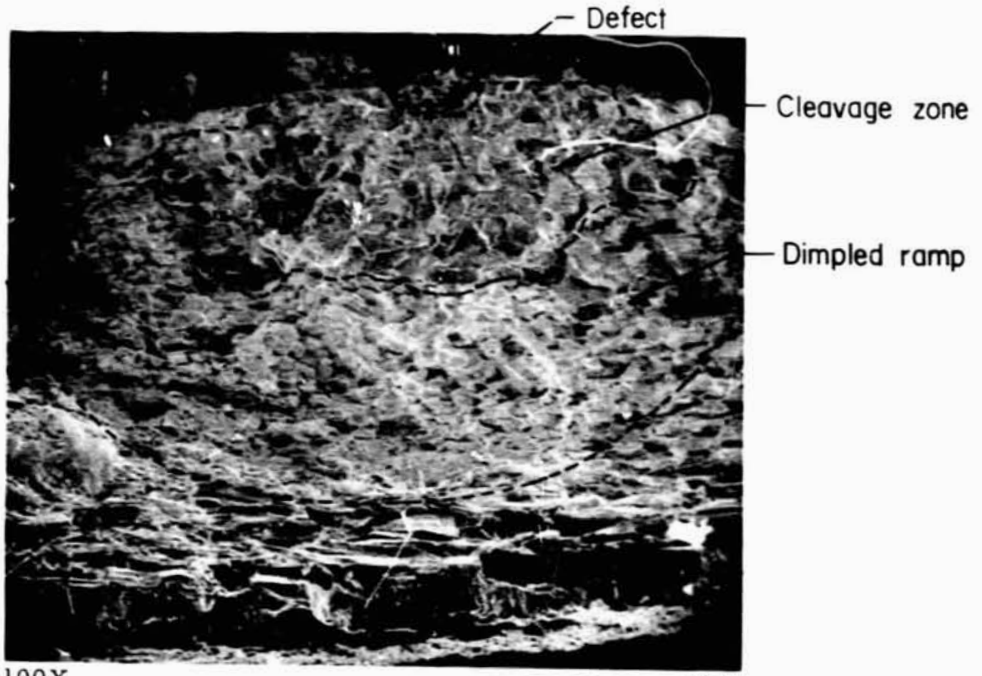


a. Specimen 13A – Dynamic Cycles

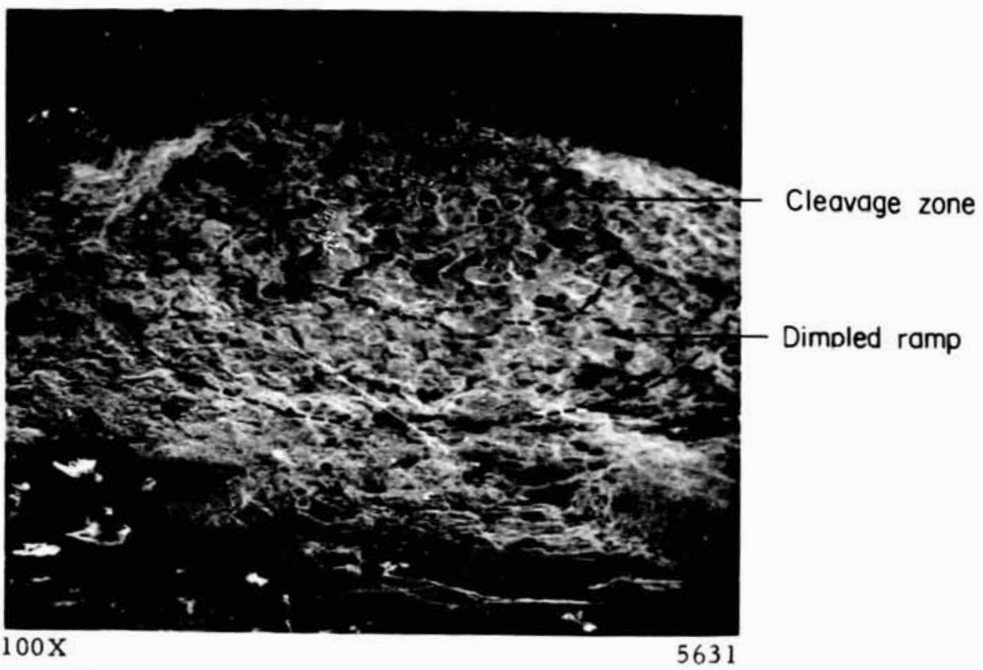


b. Specimen 13D – Dynamic Cycles

FIGURE 41. SCANNING ELECTRON FRACTOGRAPH OF R512E/FS 85 TENSILE SPECIMENS FAILED AT DEFECT-CONTAMINATION SITES

Within this constraint, relative comparisons of exposure effects are valid. Points of interest are enumerated below:

(1) The additional degradation of Cb752 exposed to five cycles compared with three cycles is only about one-half what would be predicted by assuming parabolic degradation kinetics from the onset of contamination.

(2) Coupling the observations of Table 23 with analysis of tensile elongation for Cb752 and C129Y, it is apparent that both the cleavage and dimpled fracture zones contribute to mechanical-property degradation. Thus, despite a somewhat larger cleavage fracture zone, the tensile elongation of C129Y was less affected by exposure than was that for Cb752.

(3) In similar vein, FS85, with appreciably larger cleavage and dimpled zones than Cb752, exhibited not much more degradation in elongation in three cycles than did Cb752. Thus, the coplanar disposition of the dimpled zone for Cb752 appears to be the more degrading to elongation. Stated another way, considering the total defect-affected fracture area, FS85 is more tolerant of contamination than is Cb752. This tends to counteract the somewhat superior contamination resistance of Cb752 relative to FS85.

Metallography. The tensile-specimen gage sections were longitudinally sectioned and prepared for metallographic examination. Attempts were made to grind and polish to the centers of defect areas. In 15 of the 20 specimens, the sections examined were reasonably on target.

Figures 42, 43, and 44 illustrate contamination zones surrounding defects following exposure and tensile testing of selected materials. Typically, a zone of heavy precipitate outlined the region of severe contamination. In the case of the Cb752 substrate, no further mild contamination region was observed. For C129Y, mild contamination was suggested by more heavily etched grain boundaries in a region surrounding the severe-contamination zone than were observed in the normal C129Y structure. In the case of FS85, mild contamination was suggested by decreased etching sensitivity of grain boundaries. In all cases, the etchant was $HNO_3$:HF:acetic acid in a 1:1:1 volume ratio of reagent-grade acids; typical etching time was about 1 second (dip and rinse). These observations were in excellent agreement with those from Runs 8, 9, and 11.

Detailed results of metallographic analyses are given in the appendix, Table A-23. Results are summarized in Table 24. These results show several features, as follows:

(1) C129Y is more contamination resistant than Cb752, which in turn is more contamination resistant than FS85.

(2) Observations on these tensile specimens generally confirmed those for other dynamically exposed, small-defect areas.

(3) Contamination at small defect sites apparently does not progress by a simple parabolic relationship. (Checks showed no evidence of incomplete defect penetration prior to exposure – in only one case was there an appreciable amount of subsilicide oxidation product identifiable.)

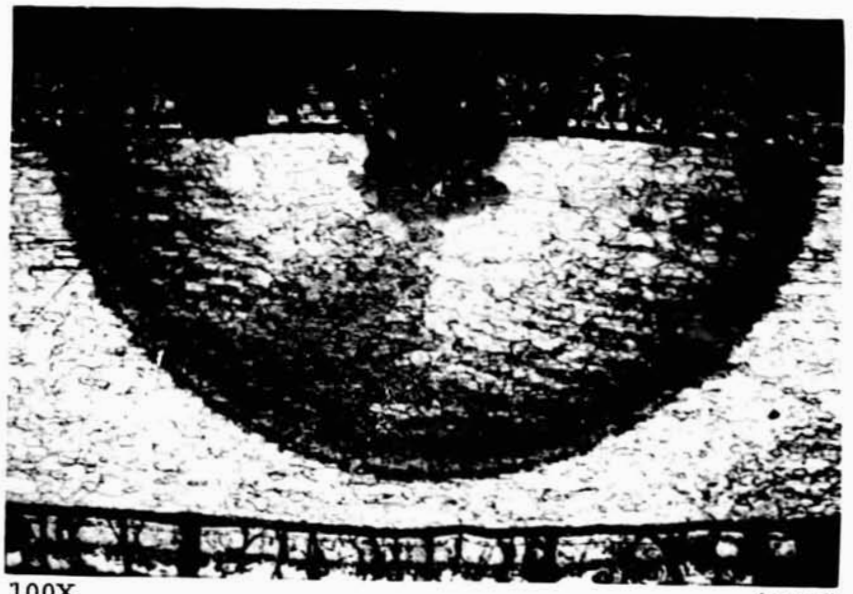

100X 6F478

FIGURE 42. TENSILE SPECIMEN 16B

R512E/Cb752 tested after three dynamic exposure cycles. Failed away from defect. Note defect grew in size to about 8 mils in diameter, allowing somewhat greater contamination than normal for a "stable" defect. Note also "bulge" in thickness caused by contamination hardening.

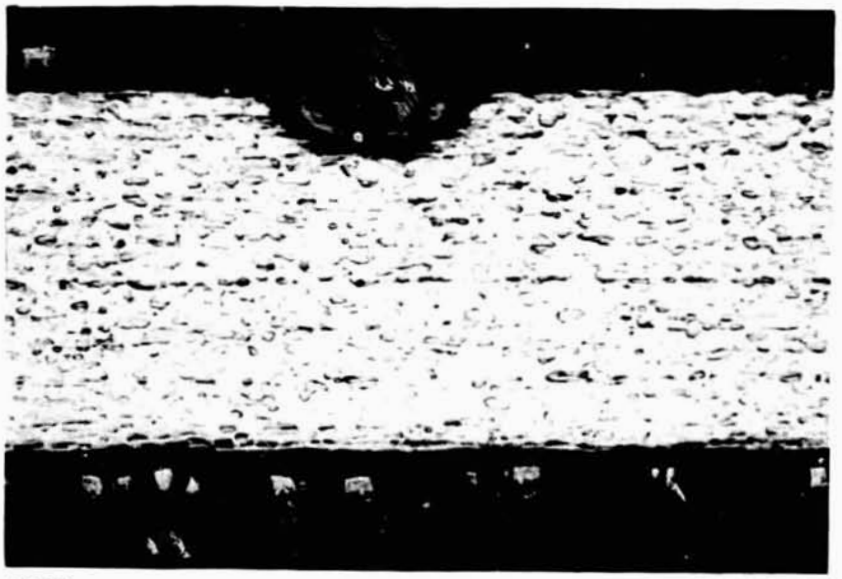

100X 6F477

FIGURE 43. TENSILE SPECIMEN S16

R512E/Cb752 tested after three static cycles. Note small contamination zone and lack of effect on homogeneous deformation.

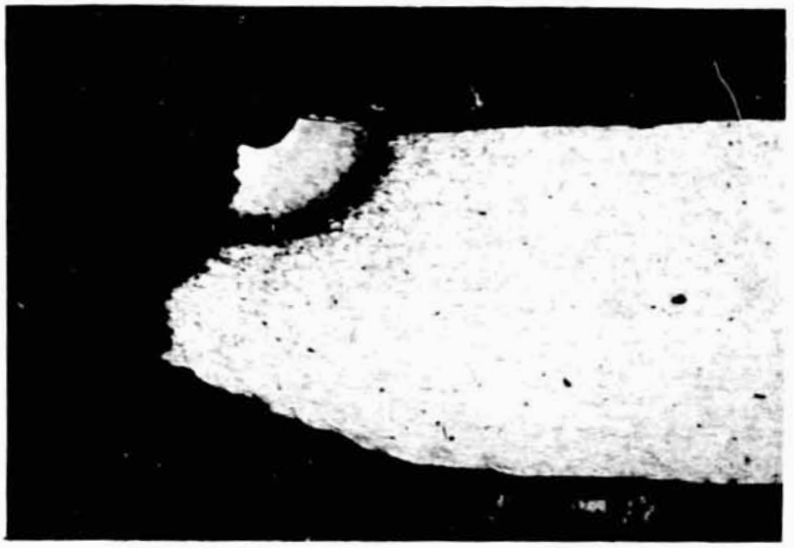

100X 6F479

FIGURE 44. TENSILE SPECIMEN 16C

VH109/C129Y tested after three dynamic exposure cycles. Failed at defect. Note (1) lack of deformation in contamination zone, (2) cleavage limited to "severe" contamination region, (3) good residual ductility in metal surrounding contamination zone, and (4) "mild" contamination zone (heavy-etching grain boundary region surrounding "heavy precipitate" area).

(4) Contamination resulting from Battelle's static cycling exposure is much less severe than that experienced as a result of dynamic cycling.

(5) Where tensile fracture occurred at defects, the total cleavage plus coplanar, dimpled region for Cb752 corresponded quite well to the depth of contamination indicated metallographically, but was somewhat less than that suggested by microhardness traverse. For C129Y, cleavage occurred within severely contaminated metal. For FS85, the extent of cleavage was somewhat less than that of severe contamination, but the mixed dimpled area extended beyond even the slightly contaminated zone.

TABLE 24. SUMMARY OF METALLOGRAPHY FOR DEFECTED-AND-EXPOSED TENSILE SPECIMENS

| | | Average Contamination Depth[a], mils by: | | | | Fracture-Feature Depth, mils | | |
|---|---|---|---|---|---|---|---|---|
| | | Visual | | Microhardness Traverse | | | Dimpled | |
| System | Exposure | Severe | Total | >300 KHN | >250 KHN | Cleavage | Coplanar | Total |
| R512E/Cb752 | 1 ~ dynamic | 9.3 | 9.3 | 9.5 | -- | | (Away) | |
| R512E/Cb752 | 3 ~ dynamic | 10.8 | 10.8 | 7 1 | 13.4 | 3.3 | 6 9 | 10.2 |
| R512E/Cb752 | 5 ~ dynamic | 11.4 | 11.4 | 11.8 | -- | 3.8 | 7.2 | 11.0 |
| R512E/Cb752 | 3 ~ static | 2.5 | 2.5 | -- | -- | | (Away) | |
| R512E/Cb752 | 5 ~ static | 6.4 | 6.4 | -- | -- | -- | -- | 7.5[b] |
| VH109/C129Y | 3 ~ dynamic | 4.7 | 7.8 | 6.3 | 6.7 | 5.1 | -- | 5.1 |
| R512E/FS85 | 3 ~ dynamic | 13.6 | 15.1 | -- | -- | 9.6 | 11.2[c] | 20.8[c] |

(a) Excludes data for "growing" defects from Run 16.
(b) Partial fracture at defect noted for one specimen.
(c) Dimpled zone is not coplanar with cleavage zone.

Not included in Table 24 are data from two specimens from Run 16 (16B-R512E/Cb752, and 16F-VH109/C129Y) where modest defect growth resulted from cycling. Apparently the somewhat enlarged defects resulted in contamination rates greater than those characteristic of small, stable defects. In these cases, progressing from one to three cycles caused contamination behavior in line with what would be expected from parabolic kinetics based on earlier data.

## INTERIM CONCLUSIONS

Results obtained to date under Contract NAS 8-26205, as presented in this report, allow statement of several tentative conclusions. Several of these are of obvious considerable importance to applications of metallic TPS materials to the space shuttle. Major conclusions, some of which must still be regarded as tentative pending confirmation being sought in continuing studies, are as follow:

(1) The cobalt alloys, L605 and HS188, showed no property degradation in 12 low-pressure cycles to maximum temperature of 1900 F in either static or dynamic exposure modes. It is tempting to conclude that the dynamic, low-pressure shuttle reentry environment will not seriously degrade the oxidation protection mechanism inherent in these alloys. However, the relatively short time of total exposure, coupled with the findings of others relative to stress-cycle performance of nickel-base alloys, demands caution in reaching too sweeping a conclusion.

(2) The critical temperature of about 2490 F indicated for coated, defected columbium alloys under dynamic, hypersonic-shear conditions is not reproduced in static environments, at least in the tests conducted at Battelle. This implies a definite overshoot limit relative to coated-columbium utilization in space shuttle TPS (2400 F is generally considered the maximum "columbium area" temperature) that has not been apparent from prior static testing.

(3) Coated-columbium-substrate contamination kinetics vary according to defect type and size, and to substrate composition. Small defects, such as typify random coating failures, permit contamination at appreciably lower rates than do large, mechanical-damage-type defects. Further, small defect contamination kinetics appear to be governed by physical laws resulting in higher order reactions than parabolic. Large defects appear to be associated with parabolic kinetics, as would be expected.

(4) Contamination introduced by the presence of coating defects is not immediately degrading to room-temperature tensile ductility, but as the contamination-zone dimension increases to roughly one-half the sheet thickness or more, contamination serves as a source for brittle cleavage cracks at low temperature. The surrounding uncontaminated metal, however, tends to arrest brittle-fracture propagation, at least with the low-rate of load application in the tension test.

(5) At subcritical temperatures in dynamic exposures, substrate-surface-recession rates are substantially less than 0.1 mil/min.

(6) The difference between contamination, and, hence, degradation kinetics in static- versus dynamic-exposure modes (in exposures conducted at Battelle) may be attributed to either chemical or physical differences in the environments. It is most important that the reasons for this difference be identified. If physical, extreme caution will be required in translating static-test-evaluation results to predicted space-shuttle performance for coated columbium.

(7) Intrinsic crack oxidation (unintentional defects) observed in several specimens appear to be reasonably well tolerated, at least regarding the effects of a few exposures on room-temperature tensile properties.

(8) Emittance of coated columbium alloys is reasonably high, and appears stable through at least five simulated, dynamic reentry exposures.

(9) For limited exposure cycling, some second-order differences among the different coated columbium systems are apparent. Additional data will be required to adequately establish trade-offs to select preferred systems.

## FUTURE WORK

Continuation of this program has been authorized for an additional 12-month period. In addition to resolution of numerous important questions posed by the data thus far obtained, the data base will be expanded to include the following:

(1) Dynamic exposures for up to five cycles on undefected and defected R512E/Cb752, VH109/C129Y, and R512E/FS85 in unwelded and welded conditions to establish subcritical defect-contamination degradation-kinetic comparisons for room- and elevated-temperature tensile tests and creep tests, and additionally to confirm and further evaluate the significance of supercritical exposure on multicycle defect growth and mechanical properties of one selected system.

(2) Static-exposure series similar in scope to Item (1) above.

(3) Pending resolution of contamination-kinetics differences between static- and dynamic-exposure modes, evaluation in progressive testing of the following factors:

| Variable | No. of Systems |
|---|---|
| Cross-section effects to five cycles | 3 |
| Inter-exposure vibration | 2 (selected) |
| Coating-repair effectiveness after various prior exposures | Ditto |
| Various exposure/defect sequences | " |
| Extended cycling degradation (to 30 cycles) of mechanical properties | 1 (selected) |
| Extended cycling defect and repair sequences | Ditto |
| Effects of stressed exposure on undefected and defected specimen property degradation | " |

* * * * *

Data upon which this report is based are contained in Laboratory Record Books Nos. 28201, 28297, 28551, 28712, 28774, 28871, and 29043.

# APPENDIX A

## DETAILED TEST DATA FOR INDIVIDUAL SPECIMENS

# APPENDIX A

## DETAILED TEST DATA FOR INDIVIDUAL SPECIMENS

TABLE A-1. STATIC CYCLE TIME HISTORIES FOR RUN CO-1

| Cycle | Time, minutes | | |
|---|---|---|---|
| | To Rise | At $T_{max}$ | To Decay |
| 1 | 2.40 | 3.65 | 2.40 |
| 2 | 2.40 | 4.15 | 2.40 |
| 3 | 2.30 | 4.20 | 2.40 |
| 4 | 1.50 | 4.90 | 2.40 |
| 5 | 2.50 | 4.00 | 2.60 |
| 6 | 2.65 | 3.75 | 2.55 |
| 7 | 2.50 | 4.00 | 2.50 |
| 8 | 2.10 | 4.40 | 2.60 |
| 9 | 2.65 | 3.75 | 2.55 |
| 10 | 1.65 | 4.90 | 2.60 |
| 11 | 1.60 | 4.85 | 2.65 |
| 12 | 1.70 | 4.85 | 2.35 |
| Totals | 25.95 | 51.40 | 30.00 |

TABLE A-2. STATIC CYCLE TIME HISTORIES FOR RUN CO-2

| Cycle | Time, minutes | | |
|---|---|---|---|
| | To Rise | At $T_{max}$ | To Decay |
| 1 | 4.75 | 4.15 | 2.50 |
| 2 | 2.50 | 4.00 | 2.35 |
| 3 | 2.65 | 3.95 | 2.40 |
| 4 | 2.65 | 3.95 | 2.40 |
| 5 | 1.50 | 5.05 | 2.50 |
| 6 | 1.60 | 4.85 | 1.95 |
| 7 | 2.25 | 3.70 | 2.50 |
| 8 | 1.70 | 4.85 | 1.90 |
| 9 | 2.70 | 3.90 | 2.45 |
| 10 | 2.40 | 4.20 | 2.50 |
| 11 | 1.70 | 4.70 | 2.60 |
| 12 | 2.90 | 3.60 | 2.30 |
| Totals | 29.30 | 50.90 | 28.35 |

TABLE A-3. STATIC CYCLE TIME HISTORIES FOR RUN CO-3

| Cycle | Time, minutes | | |
|---|---|---|---|
| | To Rise | At $T_{max}$ | To Decay |
| 1 | 4.95 | 3.80 | 2.55 |
| 2 | 2.65 | 3.85 | 2.95 |
| 3 | 2.65 | 3.80 | 2.95 |
| 4 | 3.45 | 3.75 | 2.50 |
| 5 | 2.50 | 3.90 | 2.40 |
| 6 | 2.90 | 3.65 | 2.55 |
| 7 | 2.90 | 3.65 | 2.55 |
| 8 | 3.00 | 3.55 | 2.50 |
| 9 | 2.85 | 3.75 | 2.50 |
| 10 | 2.50 | 3.80 | 2.50 |
| 11 | 2.85 | 3.65 | 2.55 |
| 12 | 2.80 | 3.75 | 2.00 |
| Totals | 36.00 | 44.90 | 30.50 |

TABLE A-4. STATIC CYCLE TIME HISTORIES FOR RUN CO-4

| Cycle | Time, minutes | | |
|---|---|---|---|
| | To Rise | At $T_{max}$ | To Decay |
| 1 | 4.00 | 4.65 | 2.45 |
| 2 | 2.95 | 3.55 | 2.35 |
| 3 | 2.55 | 4.25 | 2.35 |
| 4 | 3.50 | 3.10 | 2.30 |
| 5 | 2.10 | 4.65 | 2.45 |
| 6 | 1.70 | 4.90 | 2.40 |
| 7 | 1.80 | 4.80 | 2.50 |
| 8 | 1.70 | 4.90 | 2.35 |
| 9 | 1.75 | 4.90 | 2.65 |
| 10 | 1.75 | 4.85 | 2.50 |
| 11 | 1.75 | 4.85 | 2.00 |
| Totals | 25.55 | 49.40 | 26.30 |

TABLE A-5. MAXIMUM CENTER TEMPERATURE FOR GROUP OF COBALT-ALLOY SPECIMENS DURING STATIC CYCLING

| Run | No. of Specimens | Temperature, F, Cycle 1 | 2 | 3 | 4 | 5 | 6 | 7 | 8 | 9 | 10 | 11 | 12 |
|---|---|---|---|---|---|---|---|---|---|---|---|---|---|
| Co-1 | 5 | 1920 | 1910 | 1915 | 1940 | 1905 | 1900 | 1900 | 1905 | 1900 | 1920 | 1920 | 1920 |
| Co-2 | 6 | 1925 | 1900 | 1930 | 1900 | 1920 | 1925 | 1905 | 1920 | 1900 | 1900 | 1935 | 1900 |
| Co-3 | 7 | 1935 | 1900 | 1905 | 1900 | 1905 | 1900 | 1900 | 1905 | 1905 | 1900 | 1905 | 1900 |
| Co-4 | 2 | 1915 | 1905 | 1900 | 1908 | 1904 | 1903 | 1905 | 1915 | 1910 | 1910 | 1905 | - - |

TABLE A-6. STATIC CYCLE TIME HISTORIES OF COATED COLUMBIUM ALLOY SPECIMENS

| Run | Cycle | Time, minutes: Rise to 1450 F | Hold at 1450 F | Rise to Tmax | Hold at $T_{max}$ | To Decay | Total |
|---|---|---|---|---|---|---|---|
| Cb-1 | 1 | 1.7 | 5.3 | 2.0 | 14.3 | 8.3 | 32.1 |
| Cb-2 | 1 | 2.1 | 5.1 | 2.2 | 15.3 | 7.9 | 32.6 |
| Cb-3 | 1 | 2.4 | 4.0 | 2.9 | 15.1 | 4.0 | 28.4 |
| Cb-4 | 1 | 0.7 | 5.5 | 3.1 | 14.9 | 8.4 | 32.6 |
| | 2 | 0.4 | 5.6 | 2.7 | 15.3 | 8.7 | 32.7 |
| | 3 | 0.5 | 5.0 | 3.1 | 14.9 | 4.0 | 27.5 |
| Cb-5 | 1 | 2.4 | 4.4 | 3.0 | 14.9 | 9.0 | 33.7 |
| | 2 | 0.6 | 5.1 | 2.9 | 15.0 | 8.9 | 32.5 |
| | 3 | 0.6 | 5.1 | 2.8 | 15.0 | 8.9 | 32.4 |
| | 4 | 0.8 | 4.9 | 2.9 | 15.6 | 8.1 | 32.3 |
| | 5 | 0.7 | 5.0 | 2.7 | 15.7 | 3.7 | 27.8 |

TABLE A-7. AVERAGE CENTER TEMPERATURE FOR GROUPS OF SPECIMENS DURING STATIC EXPOSURE CYCLING

| Run | Average Temperature[a], F, During Cycle Indicated: Cycle 1 Low[b] | Cycle 1 High[c] | Cycle 2 Low | Cycle 2 High | Cycle 3 Low | Cycle 3 High | Cycle 4 Low | Cycle 4 High | Cycle 5 Low | Cycle 5 High | Average Low | Average High |
|---|---|---|---|---|---|---|---|---|---|---|---|---|
| Cb-1 | 1440 | 2500 | -- | -- | -- | -- | -- | -- | -- | -- | 1440 | 2500 |
| Cb-2 | 1443 | 2490 | -- | -- | -- | -- | -- | -- | -- | -- | 1443 | 2490 |
| Cb-3 | 1437 | 2352 | -- | -- | -- | -- | -- | -- | -- | -- | 1437 | 2352 |
| Cb-4 | 1457 | 2358 | 1427 | 2357 | 1434 | 2357 | -- | -- | -- | -- | 1440 | 2358 |
| Cb-5 | 1440 | 2358 | 1438 | 2356 | 1436 | 2358 | 1441 | 2353 | 1428 | 2356 | 1437 | 2356 |

(a) Average of five values spaced at 1 to 3-minute intervals.
(b) Low designates nominal 1450 F plateau.
(c) High designates $T_{max}$ plateau.

TABLE A-8. DYNAMIC CYCLE TIME HISTORIES FOR RUN 3 COBALT ALLOYS

| Cycle | Time, minutes | | |
|---|---|---|---|
| | To Rise | At $T_{max}$ | To Decay |
| 1 | 2.10 | 6.20 | 2.60 |
| 2 | 2.20 | 5.10 | 2.04 |
| 3 | 2.20 | 5.00 | 2.10 |
| 4 | 2.20 | 4.80 | 2.30 |
| 5 | 2.20 | 6.20 | 2.00 |
| 6 | 2.00 | 5.80 | 2.30 |
| 7 | 2.00 | 5.60 | 2.15 |
| 8 | 2.00 | 4.80 | 2.08 |
| 9 | 2.20 | 4.00 | 2.30 |
| 10 | 2.20 | 5.20 | 2.20 |
| 11 | 2.10 | 5.60 | 2.20 |
| 12 | 2.10 | 4.80 | 2.00 |
| Totals | 25.55 | 63.10 | 26.30 |

TABLE A-9. DYNAMIC CYCLE TIME HISTORIES FOR RUN 4 COBALT ALLOYS

| Cycle | Time, minutes | | |
|---|---|---|---|
| | To Rise | At $T_{max}$ | To Decay |
| 1 | 1.80 | 5.00 | 1.70 |
| 2 | 1.70 | 5.30 | 1.90 |
| 3 | 1.70 | 4.90 | 1.80 |
| 4 | 1.80 | 5.40 | 2.00 |
| 5 | 2.00 | 5.80 | 2.00 |
| 6 | 1.70 | 5.30 | 2.00 |
| 7 | 1.80 | 5.00 | 2.00 |
| 8 | 2.00 | 5.50 | 2.00 |
| 9 | 1.90 | 4.90 | 2.00 |
| 10 | 2.00 | 5.80 | 2.10 |
| 11 | 2.00 | 5.00 | 2.00 |
| 12 | 2.10 | 5.00 | 2.00 |
| Totals | 22.50 | 62.90 | 23.50 |

TABLE A-10 DYNAMIC CYCLE TIME HISTORIES FOR RUN 5 COBALT ALLOYS

| Cycle | Time, minutes | | |
|---|---|---|---|
| | To Rise | $T_{max}$ | To Decay |
| 1 | 1.7 | 5.1 | 1.6 |
| 2 | 1.66 | 5.6 | 1.74 |
| 3 | 1.62 | 5.1 | 1.84 |
| 4 | 1.68 | 5.8 | 1.72 |
| 5 | 1.78 | 5.34 | 1.84 |
| 6 | 1.64 | 5.54 | 1.74 |
| 7 | 1.48 | 5.54 | 1.78 |
| 8 | 1.66 | 5.44 | 1.84 |
| 9 | 1.64 | 5.14 | 1.52 |
| 10 | 1.72 | 4.76 | 1.46 |
| 11 | 1.80 | 7.10 | 0.30 |
| 12 | 2.14 | 5.26 | 2.36 |
| Totals | 20.48 | 65.70 | 19.74 |

TABLE A-11. MAXIMUM CENTER TEMPERATURE OF SPECIMENS DURING RUN 3

| Specimen | Temperature, F | | | | | | | | | | | |
|---|---|---|---|---|---|---|---|---|---|---|---|---|
| | Cycle | | | | | | | | | | | |
| | 1 | 2 | 3 | 4 | 5 | 6 | 7 | 8 | 9 | 10 | 11 | 12 |
| A | 1841 | 1855 | 1864 | 1887 | 1887 | 1892 | 1892 | 1892 | 1892 | 1892 | 1892 | 1892 |
| B | 1841 | 1887 | 1892 | 1887 | 1887 | 1887 | 1887 | 1887 | 1887 | 1878 | 1878 | 1887 |
| C | 1855 | 1855 | 1869 | 1896 | 1887 | 1878 | 1887 | 1887 | 1896 | 1896 | 1896 | 1878 |
| D | 1859 | 1892 | 1929 | 1957 | 1929 | 1901 | 1901 | 1892 | 1901 | 1892 | 1892 | 1901 |
| E | 1809 | 1859 | 1873 | 1892 | 1873 | 1841 | 1859 | 1841 | 1841 | 1832 | 1841 | 1845 |
| F | 1786 | 1841 | 1855 | 1892 | 1873 | 1845 | 1845 | 1841 | 1841 | 1841 | 1841 | 1841 |

TABLE A-12. MAXIMUM CENTER TEMPERATURE OF SPECIMENS DURING RUN 4

| Specimen | Temperature, F — Cycle 1 | 2 | 3 | 4 | 5 | 6 | 7 | 8 | 9 | 10 | 11 | 12 |
|---|---|---|---|---|---|---|---|---|---|---|---|---|
| A | 1832 | 1821 | 1821 | 1804 | 1832 | 1841 | 1841 | 1832 | 1845 | 1841 | 1859 | 1878 |
| B | 1760(a) | 1800(a) | 1815(a) | 1800(a) | 1805(a) | 1820(a) | 1820(a) | 1815(a) | 1815(a) | 1815(a) | 1820(a) | 1840(a) |
| C | 1781 | 1754 | 1799 | 1799 | 1836 | 1836 | 1836 | 1827 | 1827 | 1827 | 1836 | 1864 |
| D | 1873 | 1873 | 1882 | 1891 | 1919 | 1929 | 1957 | 1929 | 194[illegible] | 1957 | 1962 | 1962 |
| E | 1877 | 1850 | 1887 | – | – | 1900(a) | – | – | 191[illegible](a) | – | – | 1920(a) |
| F | 1820(a) | – | – | – | – | 1870(a) | – | – | 1870(a) | – | – | 1890(a) |

(a) Temperatures were estimated from pyrometer data.

TABLE A-13. MAXIMUM CENTER TEMPERATURE OF SPECIMENS DURING RUN 5

| Specimen | Temperature, F — Cycle 1 | 2 | 3 | 4 | 5 | 6 | 7 | 8 | 9 | 10 | 11 | 12 |
|---|---|---|---|---|---|---|---|---|---|---|---|---|
| A | 1892 | 1865 | 1856 | 1838 | 1847 | 1847 | 1838 | 1828 | 1856 | 1828 | 1847 | 1856 |
| B | 1888 | 1860 | 1870 | 1870 | 1860 | 1860 | 1870 | 1851 | 1851 | 1879 | 1888 | 1851 |
| C | 1948 | 1883 | 1874 | 1883 | 1847 | 1847 | 1847 | 1838 | 1856 | 1828 | 1828 | 1810 |
| D | 1898 | 1870 | 1889 | 1870 | 1870 | 1880 | 1880 | 1856 | 1856 | 1889 | 1880 | 1870 |
| E | 1836 | 1856 | 1836 | 1827 | 1836 | 1836 | 1846 | 1818 | 1856 | 1846 | 1846 | 1836 |
| F | 1976 | 1956 | 1938 | 1920 | 1920 | 1920 | 1920 | 1883 | 1929 | 1902 | 1911 | 1892 |

TABLE A-14. TEMPERATURE GRADIENTS OVER CENTER REGION OF SPECIMENS DURING RUN 3

| Cycle | Gradient, F/inch | | | | | |
|---|---|---|---|---|---|---|
| | A | B | C | D | E | F |
| 3 | 8 | 41 | 5 | 24 | 9 | 9 |
| 6 | 10 | 41 | 14.5 | 36.5 | 11 | 31.5 |
| 9 | 9 | 41 | 15 | 28 | 31.5 | 27 |
| 12 | 9.5 | 37 | 21 | 35 | 23 | 23 |
| Average | 9 | 40 | 14 | 31 | 19 | 23 |

TABLE A-15. TEMPERATURE GRADIENTS OVER CENTER REGION OF SPECIMENS DURING RUN 4

| Cycle | Gradient, F/inch | | | | | |
|---|---|---|---|---|---|---|
| | A | B | C | D | E | F |
| 3 | 52 | 37 | 51 | 36 | 29 | -- |
| 6 | 71 | 53 | 49 | 85 | 32.5 | 29.5 |
| 9 | 44.5 | 42 | 35 | 54 | 26 | 25 |
| 12 | 60.5 | 42 | 53.5 | 39 | 26.5 | 28 |
| Average | 57 | 44 | 47 | 54 | 28 | 28 |

TABLE A-16. TEMPERATURE GRADIENTS OVER CENTER REGION OF SPECIMENS DURING RUN 5

| Cycle | Gradient, F/inch | | | | | |
|---|---|---|---|---|---|---|
| | A | B | C | D | E | F |
| 3 | 13 | 32.5 | 26 | 19 | 61 | 58 |
| 6 | 19 | 54 | 17 | 24 | 62 | 69 |
| 9 | 25 | 45 | 6 | 16 | 61 | 73 |
| 12 | 21 | 50 | 9 | 17 | 67 | 56 |
| Average | 20 | 45 | 15 | 19 | 63 | 64 |

TABLE A-17. DYNAMIC CYCLE TIME HISTORIES FOR COATED COLUMBIUM ALLOYS

| Run | Cycle | Time, minutes: Rise to 1450 F | Hold at 1450 F | Rise to $T_{max}$ | Hold at $T_{max}$ | To Decay | Total |
|---|---|---|---|---|---|---|---|
| 8 | 1 | 3 | 5 | 3.5 | 15.0 | 7.0 | 33.5 |
| 9 | 1 | 1.6 | 4.8 | 2.3 | 1 .5[a] | 2.3[a] | 22.5 |
| 11 | 1 | 0.7 | 5.0 | 1.7 | 16.3 | 5.5 | 29.2 |
| | 2 | 0.2 | 5.0 | 1.2 | 15.5 | 3.7 | 25.6 |
| | 3 | 0.2 | 5.2 | 2.2 | 15.1 | 6.9 | 29.6 |
| 12 | 1 | 0.2 | 5.0 | 1.8 | 15.4 | 6.2 | 27.9 |
| 13 | 1 | 0.2 | 5.0 | 1.9 | 15.0 | 5.8 | 27.9 |
| | 2 | 0.2 | 5.0 | 1.9 | 14.2 | 5.8 | 27.1 |
| | 3 | 0.4 | 5.2 | 1.1 | 14.2 | 6.2 | 27.1 |
| 14 | 1 | 0.2 | 6.3 | 1.8 | 15.4 | 5.8 | 29.5 |
| | 2 | 0.2 | 5.6 | 2.0 | 14.9 | 4.2 | 26.9 |
| | 3 | 0.2 | 5.3 | 1.8 | 15.0 | 5.0 | 27.3 |
| | 4 | 0.2 | 5.2 | 2.2 | 14.8 | 4.7 | 27.1 |
| | 5 | 0.2 | 5.2 | 2.0 | 15.0 | 5.8 | 28.2 |
| 15 | 1 | 0.2 | 6.0 | 3.5 | 14.0 | 5.3 | 29.0 |
| | 2 | 0.4 | 5.5 | 2.2 | 15.4 | 6.0 | 29.5 |
| | 3 | 0.4 | 5.6 | 2.3 | 15.0 | 5.9 | 29.2 |
| 16 | 1 | 0.2 | 5.8 | 1.9 | 15.3 | 5.9 | 29.1 |
| | 2 | 0.4 | 5.3 | 1.6 | 15.0 | 5.6 | 27.9 |
| | 3 | 0.0 | 5.2 | 2.2 | 15.2 | 5.6 | 28.2 |

(a) Run terminated prematurely owing to momentary power fluctuation at local power station.

TABLE A-18. AVERAGE CENTER TEMPERATURES FOR INDIVIDUAL COATED COLUMBIUM SPECIMENS DURING DYNAMIC EXPOSURE CYCLING

| | | Average Temperature, F, for Specimens Indicated | | | | | | | | | | | | | |
|---|---|---|---|---|---|---|---|---|---|---|---|---|---|---|---|
| | | A | | B | | C | | D | | E | | F | | Average | |
| Run | Cycle | Low[a] | High[b] | Low | High | Low | High | Low | High | Low | High | Low | High | Low | High |
| 8 | 1 | -- | 2470 | 1320 | 2510 | -- | 2480 | -- | 2490 | 1470 | 2510 | -- | 2510 | 1390 | 2495 |
| 9 | 1 | -- | 2510 | -- | 2470 | -- | 2470 | -- | 2470 | -- | 2510 | -- | 2510 | 1560 | 2490 |
| 11 | 1 | 1400 | 2370 | 1470 | 2410 | 1300 | 2330 | 1380 | 2330 | 1310 | 2370 | 1280 | 2300 | 1355 | 2350 |
| | 2 | 1400 | 2260 | 1450 | 2360 | 1310 | 2350 | 1410 | 2240 | 1300 | 2320 | 1340 | 2260 | 1370 | 2300 |
| | 3 | 1390 | 2210 | 1460 | 2320 | 1320 | 2310 | 1390 | 2210 | 1300 | 2240 | 1340 | 2200 | 1365 | 2250 |
| | Avg. | 1395 | 2280 | 1460 | 2365 | 1310 | 2335 | 1395 | 2260 | 1305 | 2310 | 1320 | 2255 | 1365 | 2300 |
| 12 | 1 | 1200 | 2300 | 1450 | 2330 | 1320 | 2350 | 1230 | 2360 | -- | 2380 | 1370 | 2300 | 1315 | 2335 |
| 13 | 1 | 1375 | 2350 | 1400 | 2300 | 1380 | 2290 | 1300 | 2340 | -- | 2360 | 1400 | 2270 | 1370 | 2320 |
| | 2 | 1430 | 2320 | 1420 | 2290 | 1320 | 2220 | 1450 | 2310 | -- | 2300 | 1450 | 2210 | 1415 | 2275 |
| | 3 | 1450 | 2340 | 1430 | 2370 | 1320 | 2250 | 1410 | 2350 | -- | 2300 | 1400 | 2220 | 1400 | 2305 |
| | Avg. | 1420 | 2335 | 1415 | 2320 | 1340 | 2255 | 1385 | 2335 | -- | 2320 | 1415 | 2233 | 1395 | 2300 |
| 14 | 1 | 1400 | 2280 | 1480 | 2280 | 1470 | 2310 | 1500 | 2310 | 1510 | 2320 | 1560 | 2270 | 1485 | 2295 |
| | 2 | 1430 | 2250 | 1500 | 2260 | 1390 | 2260 | 1540 | 2270 | 1570 | 2260 | 1540 | 2240 | 1495 | 2255 |
| | 3 | 1440 | 2290 | 1520 | 2320 | 1370 | 2290 | 1520 | 2360 | 1580 | 2330 | 1540 | 2290 | 1495 | 2315 |
| | 4 | 1430 | 2270 | 1500 | 2240 | 1350 | 2280 | 1510 | 2320 | 1580 | 2290 | 1530 | 2270 | 1485 | 2280 |
| | 5 | 1450 | 2240 | 1510 | 2240 | 1340 | 2240 | 1510 | 2320 | 1600 | 2300 | 1520 | 2290 | 1490 | 2270 |
| | Avg. | 1430 | 2265 | 1500 | 2270 | 1385 | 2275 | 1515 | 2315 | 1570 | 2300 | 1540 | 2270 | 1490 | 2285 |
| 15 | 1 | 1300 | 2370 | 1470 | 2340 | 1310 | 2290 | 1350 | 2380 | 1500 | 2330 | 1550 | 2320 | 1415 | 2340 |
| | 2 | 1300 | 2310 | 1500 | 2340 | 1360 | 2330 | 1270 | 2320 | 1520 | 2250 | 1500 | 2280 | 1410 | 2305 |
| | 3 | 1350 | 2290 | 1550 | 2330 | 1390 | 2360 | 1330 | 2300 | 1530 | 2230 | 1510 | 2280 | 1445 | 2300 |
| | Avg. | 1315 | 2325 | 1505 | 2335 | 1355 | 2325 | 1315 | 2335 | 1520 | 2270 | 1520 | 2295 | 1420 | 2315 |
| 16 | 1 | 1390 | 2500 | 1510 | 2470 | 1480 | 2440 | 1450 | 2450 | 1650 | 2510 | 1560 | 2470 | 1505 | 2475 |
| | 2 | 1380 | 2460 | 1430 | 2420 | 1370 | 2420 | 1300 | 2430 | 1570 | 2470 | 1460 | 2460 | 1420 | 2445 |
| | 3 | 1390 | 2470 | 1410 | 2420 | 1350 | 2450 | 1310 | 2450 | 1590 | 2510 | 1490 | 2450 | 1425 | 2460 |
| | Avg. | 1385 | 2475 | 1450 | 2435 | 1400 | 2435 | 1355 | 2445 | 1605 | 2495 | 1505 | 2460 | 1450 | 2460 |

(a) Low designates nominal 1450 F plateau.

(b) High designates $T_{max}$ plateau.

TABLE A-19. TENSILE PROPERTIES OF UNWELDED COBALT ALLOYS

| Specimen | Exposure Environment | Test Temperature, F | Ultimate Strength, ksi | 0.2% Offset Yield Strength, ksi | Elongation in 0.5 Inch, % |
|---|---|---|---|---|---|
| | | L605 Alloy | | | |
| 15 | Baseline | RT | 135 | 65.8 | 50 |
| 16 | " | RT | 135 | 65.8 | 50 |
| 11 | " | 1900 | 18.5 | 17.7 | 14 |
| 12 | " | 1900 | 20.0 | 19.1 | 10 |
| 89 | LPE | RT | 133 | 62.1 | 52 |
| 90 | " | RT | 132 | 63.7 | 48 |
| 84 | " | 1900 | 19.1 | 16.2 | 20 |
| 86 | " | 1900 | 22.0 | 18.9 | 18 |
| 21 | ARC | RT | 141 | 68.3 | 52 |
| 22 | " | RT | 141 | 68.9 | 50 |
| 29 | " | 1900 | 21.7 | 18.8 | 12 |
| 30 | " | 1900 | 19.2 | 16.9 | 12 |
| | | HS188 Alloy | | | |
| 51 | Baseline | RT | 135 | 63.3 | 66 |
| 52 | " | RT | 135 | 63.8 | 64 |
| 47 | " | 1900 | 17.4 | 15.9 | 22 |
| 48 | " | 1900 | 18.8 | 17.0 | 18 |
| 103 | LPE | RT | 132 | 60.9 | 60 |
| 104 | " | RT | 133 | 60.5 | 58 |
| 99 | " | 1900 | 19.1 | 17.4 | 20 |
| 100 | " | 1900 | 20.5 | 17.4 | 24 |
| 67 | ARC | RT | 133 | 60.9 | 60 |
| 68 | " | RT | 134 | 60.5 | 62 |
| 61 | " | 1900 | 16.6 | 16.6 | 26 |
| 62 | " | 1900 | 18.8 | 17.6 | 12 |

TABLE A-20. TENSILE PROPERTIES OF WELDED COBALT ALLOYS

| Specimen | Exposure Environment | Test Temp, F | Ultimate Strength, ksi | 0.2% Offset Yield Strength, ksi | Elongation in 0.5 Inch, % | Failure Location[a] |
|---|---|---|---|---|---|---|
| | | | L605 Alloy | | | |
| 7 | Baseline | RT | 132 | 68.3 | 36 | W |
| 8 | " | RT | 133 | 69.4 | 36 | W |
| 3 | " | 1900 | (b) | (b) | 10 | W |
| 4 | " | 1900 | 21.4 | 20.3 | 10 | W |
| 81 | LPE | RT | 124 | 67.2 | 28 | W |
| 82 | " | RT | 128 | 67.8 | 48 | PM |
| 75 | " | 1900 | 21. | 19.6 | 14 | W |
| 78 | " | 1900 | 23. | 20.1 | 14 | W |
| 23 | ARC | RT | 132 | 65.8 | 44 | W |
| 24 | " | RT | 134 | 68.3 | 38 | PM |
| 27 | " | 1900 | 23.0 | 21.9 | 10 | PM |
| 28 | " | 1900 | 28.7[c] | 24.8[c] | 12 | W |
| | | | HS188 Alloy | | | |
| 43 | Baseline | RT | 136 | 66.2 | 52 | PM |
| 44 | " | RT | 135 | 65.2 | 52 | PM |
| 39 | " | 1900 | 21.3 | 19.4 | 16 | PM |
| 40 | " | 1900 | 20.9 | 18.6 | 16 | PM |
| 95 | LPE | RT | 135 | 63.3 | 50 | PM |
| 96 | " | RT | 135 | 63.3 | 50 | PM |
| 91 | " | 1900 | 18.5 | 16.0 | 18 | PM |
| 92 | " | 1900 | 22.0 | 18.9 | 16 | W |
| 65 | ARC | RT | 135 | 62.4 | 52 | PM |
| 66 | " | RT | 136 | 63.3 | 52 | PM |
| 57 | " | 1900 | 21.5 | 20.2 | 16 | W |
| 58 | " | 1900 | 19.1 | 17.5 | 18 | W |

(a) W designates weld, while PM designates parent metal.
(b) Load values not obtained owing to RF interference.
(c) Tested at strain rate of 0.2 in./in./min.

TABLE A-21. 1900 F CREEP DEFORMATION BEHAVIOR OF COBALT-ALLOY SPECIMENS

| Specimen | Exposure Environment | Welded? | Stress, ksi | Time, hours, for Indicated Creep Strain | | Test Discontinued at | | Minimum Creep Rate, %/hour |
|---|---|---|---|---|---|---|---|---|
| | | | | 0.5% | 1.0% | Strain, % | Time, hours | |
| | | | L605 Alloy | | | | | |
| 17 | Baseline | No | 3.0 | 1.7 | 5.1 | 2.6 | 21.1 | 0.092 |
| 9 | Baseline | No | 2.5 | 8.3 | 21.2 | 0.88 | 16.6 | 0.037 |
| 18 | Baseline | No | 2.5 | 5.5 | 15.3 | 1.0 | 15.3 | 0.047 |
| 10 | Baseline | No | 2.5 | 2.7 | 7.2 | 1.92 | 15.0 | 0.048 |
| 31 | Arc | No | 2.5 | 2.3 | 9.4 | 1.22 | 11.9 | 0.05 |
| 32 | Arc | No | 2.5 | 5.3 | 14.3 | 1.0 | 14.3 | 0.048 |
| 83 | LPE | No | 2.5 | 3.0 | 9.3 | -- | 22.0 | 0.06 |
| 85 | LPE | No | 2.5 | 3.3 | 10.6 | 1.4 | 17.0 | 0.061 |
| 1 | Baseline | Yes | 2.5 | 7.4 | 17.5 | 1.1 | 18.5 | 0.05 |
| 2 | Baseline | Yes | 2.5 | 5.5 | 19.2 | 1.0 | 19.2 | 0.033 |
| 35 | Arc | Yes | 2.5 | 2.6 | 5.7 | 1.67 | 12.6 | 0.09 |
| 36 | Arc | Yes | 2.5 | 0.6 | 3.5 | 1.5 | 9.9 | 0.062 |
| 76 | LPE | Yes | 2.5 | 6.4 | 24.0 | 1.0 | 24.0 | 0.026 |
| 77 | LPE | Yes | 2.5 | 2.7 | 9.6 | 1.0 | 9.6 | 0.072 |
| | | | HS188 Alloy | | | | | |
| 45 | Baseline | No | 3.0 | 0.8 | 1.75 | 8.8 | 20.0 | 0.25 |
| 46 | Baseline | No | 2.5 | 1.0 | 3.5 | 4.0 | 15.4 | 0.20 |
| 69 | Arc | No | 2.5 | 4.7 | 9.4 | 1.08 | 9.8 | 0.11 |
| 70 | Arc | No | 2.5 | 3.5 | 7.4 | 2.0 | 14.5 | 0.13 |
| 97 | LPE | No | 2.5 | 2.5 | 5.6 | 1.04 | 5.9 | 0.16 |
| 98 | LPE | No | 2.5 | 0.3 | 1.4 | 4.7 | 14.9 | 0.23 |
| 37 | Baseline | Yes | 2.5 | 5.2 | 8.5 | 1.2 | 9.9 | 0.12 |
| 38 | Baseline | Yes | 2.5 | 0.65 | 2.5 | 3.6 | 10.8 | 0.28 |
| 71 | Arc | Yes | 2.5 | 5.8 | 12.3 | 1.0 | 12.3 | 0.078 |
| 72 | Arc | Yes | 2.5 | 4.8 | 8.3 | 1.8 | 12.5 | 0.14 |
| 73 | LPE | Yes | 2.5 | 3.8 | 7.3 | 1.2 | 8.8 | 0.13 |
| 74 | LPE | Yes | 2.5 | 2.0 | 7.0 | 1.4 | 9.6 | 0.10 |

TABLE A-22. SUBSTRATE CONTAMINATION DATA FOR SUBCRITICALLY EXPOSED DEFECT SITES AFTER DYNAMIC EXPOSURE

| Specimen | Substrate | No. of Cycles | Avg Max Temp, F | Time at Max Temp, min | Defect Type[a] | Defect Location[b] | Defect Surface Recession Rate, mil/min | Contamination Depth[c], mils | | Max Contamination Hardness, KHN | Relative Contamination Rate, $mil^2$/min | Equivalent Contamination Rate at 2400 F[d], $mil^2$/min |
|---|---|---|---|---|---|---|---|---|---|---|---|---|
| | | | | | | | | Severe | Total | | | |
| 8D-2 | Cb752 | 1 | 2485 | 15 | A | C | 1.0 | -- | 24 | 550 | 38.4 | 29.0 |
| 9D-2 | Cb752 | 1 | 2470 | 11-1/2 | A | C | 0.5 | -- | 21 | 805 | 38.3 | 31.1 |
| 9F-2 | Cb752 | 1 | 2510 | 11-1/2 | A | C | 0.5 | -- | 20 | 860 | 34.8 | 25.1 |
| 11B-2 | Cb752 | 3 | 2365 | 47 | A | C | 0.07 | 30 | 33 | 1560 | 23.2 | 26.0 |
| 11F-2 | Cb752 | 3 | 2255. | 47 | A | C | 0.02 | 18 | 31 | 1575 | 20.5 | 33.1 |
| 8B-3 | Cb752 | 1 | 2490 | 15 | B | R | 0.3 | -- | 16 | 613 | 17.0 | 13.0 |
| 8D-3 | Cb752 | 1 | 2475 | 15 | B | R | 0.2 | -- | 16 | 860 | 17.0 | 13.6 |
| 8F-3 | Cb752 | 1 | 2470 | 15 | B | R | 0.3 | -- | 18 | 1860 | 21.5 | 17.5 |
| 9F-3 | Cb752 | 1 | 2390 | 11-1/2 | B | R | 0.1 | -- | 14 | 1100 | 17.0 | 17.6 |
| 11B-1 | Cb752 | 3 | 2445 | 47 | B | F | 0.03 | 24 | 29 | 1000 | 17.9 | 15.8 |
| 11F-3 | Cb752 | 3 | 2170 | 47 | B | R | 0.04 | 14 | 17 | 1575 | 6.1 | 13.3 |
| 9D-3 | Cb752 | 1 | 2370 | 11-1/2 | C | R | 0.1 | -- | 10 | 595 | 6.7 | 7.4 |
| 11B-3 | Cb752 | 3 | 2195 | 47 | C | R | 0.006 | 7 | 10 | 800 | 2.1 | 4.2 |
| 11F-1 | Cb752 | 3 | 2225 | 47 | C | F | 0.01 | 7 | 9 | 860 | 1.7 | 3.0 |
| 8A-2 | C129Y | 1 | 2470 | 15 | A | C | 1.3 | -- | 18 | 860 | 21.6 | 17.6 |
| 8C-2 | C129Y | 1 | 2480 | 15 | A | C | 1.7 | -- | 21 | 955 | 29.4 | 23.2 |
| 11C-2 | C129Y | 3 | 2335 | 47 | A | C | 0.04 | 16 | 18 | 800 | 6.9 | 8.5 |
| 11E-2 | C129Y | 3 | 2310 | 47 | A | C | 0.05 | 17 | 19 | 800 | 7.7 | 10.3 |
| 8A-3 | C129Y | 1 | 2455 | 15 | B | R | 0.1 | -- | 12 | 860 | 9.6 | 8.1 |
| 8E-3 | C129Y | 1 | 2485 | 15 | B | R | .2 | -- | 13 | 710 | 10.2 | 7.9 |
| 9B-3 | C129Y | 1 | 2450 | 11-1/2 | B | R | 0.3 | -- | 12 | 1240 | 13.7 | 11.8 |
| 9C-3 | C129Y | 1 | 2400 | 11-1/2 | B | R | 0.2 | -- | 12 | 920 | 13.7 | 13.7 |
| 11C-1 | C129Y | 3 | 2375 | 47 | B | F | 0.03 | 13 | 16 | 575 | 5.4 | 5.8 |
| 11E-3 | C129Y | 3 | 2245 | 47 | B | R | 0.000 | 17 | 19 | 800 | 7.7 | 12.8 |
| 8A-1 | C129Y | 1 | 2460 | 15 | C | F | 0.5 | -- | 11 | 550 | 8.1 | 6.8 |
| 9E-3 | C129Y | 1 | 2410 | 11-1/2 | C | R | 0.05 | -- | 10 | 920 | 8.7 | 8.5 |
| 11C-3 | C129Y | 3 | 2195 | 47 | C | R | 0.01 | 7 | 8 | 698 | 1.4 | 2.8 |
| 11E-1 | C129Y | 3 | 2315 | 47 | C | F | 0.004 | 8 | 9 | 545 | 1.7 | 2.2 |
| 11A-2 | FS585 | 3 | 2280 | 47 | A | C | 0.04 | 41 | 50 | 931 | 53.1(35.8)[e] | 78.4(52.9)[e] |
| 11D-2 | FS585 | 3 | 2260 | 47 | A | C | 0.06 | 39 | 48 | 1085 | 48.9(32.3)[e] | 77.3(51.1)[e] |
| 11A-1 | FS585 | 3 | 2225 | 47 | B | F | 0.01 | 28 | 40 | 1300 | 34.0(16.7)[e] | 59.8(29.4)[e] |
| 11D-3 | FS585 | 3 | 2260 | 47 | B | R | 0.000 | 20 | 30 | 800 | 19.2(8.5)[e] | 30.4(13.5)[e] |
| 11A-3 | FS585 | 3 | 2325 | 47 | C | R | 0.000 | 14 | 20 | 1080 | 8.5(4.2)[e] | 10.8(5.3)[e] |
| 11D-1 | FS585 | 3 | 2245 | 47 | C | F | 0.01 | 10 | 18 | 700 | 6.9(2.1)[e] | 11.5(3.5)[e] |

(a) A = 40-mil through-hole.
B = 40-mil coating defect.
C = 4-mil coating defect.

(b) F = Front (upstream)
C = Center
R = Rear (downstream).

(c) Adjusted value based on visual observation and hardness traverse. Severe, where distinguished from mild, relates to areas defined by heavy precipitate ring or KHN values > 300. Measurement direction was normal to specimen surface for C defects, parallel to surface for A and B defects.

(d) Corrected to 2400 F value via an Arrhenius ratio, assuming:
(1) Contamination depth is controlled by oxygen diffusivity in the substrate
(2) Activation energy for contamination of ~28 kcal/mole.

(e) Severe contamination coefficient given in parentheses.

TABLE A-23. DETAILED METALLOGRAPHIC MEASUREMENTS OF DEFECT CONTAMINATION IN FAILED ROOM-TEMPERATURE TENSILE SPECIMENS

| Specimen | System | Type and No. of Exposure Cycles: Dynamic | Static | Failure Location[a] | Metallographic Contamination Depth, mils: Visual: Severe | Visual: Total | Microhardness Traverse: <300 KHN | Microhardness Traverse: <250 KHN | Fracture-Feature Depth, mils: Cleavage | Dimpled: Coplanar | Dimpled: Total | Remarks |
|---|---|---|---|---|---|---|---|---|---|---|---|---|
| 12B | R512E/Cb752 | 1 | | A | 9.3 | 9.3 | 9.5 | (b) | -- | -- | -- | -- |
| 12E | R512E/Cb752 | 1 | | A | -- | -- | -- | -- | -- | -- | -- | Missed defect in met. prep. |
| S9 | R512E/Cb752 | | 1 | A | -- | -- | -- | -- | -- | -- | -- | Ditto |
| S10 | R512E/Cb752 | | 1 | A | -- | -- | -- | -- | -- | -- | -- | " |
| 13B | R512E/Cb752 | 3 | | D | 10.8 | 10.8 | No data | | 3.1 | 7.1 | 10.2 | -- |
| 13E | R512E/Cb752 | 3 | | D | 10.8 | 10.8 | 7.1 | 13.4 | 3.1 | 7.2 | 10.3 | -- |
| 16B | R512E/Cb752 | 3 | | A | 15.7 | 15.7 | No data | | -- | -- | -- | Defect grew to 8 mils in diameter in cycling |
| S15 | R512E/Cb752 | | 3 | A | >3.0 | >3.0 | No data | | -- | -- | -- | Missed defect; caught some contamination |
| S16 | R512E/Cb752 | | 3 | A | 2.1 | 2.1 | No data | | -- | -- | -- | -- |
| 14A | R512E/Cb752 | 5 | | D | 11.4 | 11.4 | 11.8 | (b) | 3.8 | 7.2 | 11.0 | -- |
| 14C | R512E/Cb752 | 5 | | D | 11.4 | 11.4 | No data | | 3.7 | 7.2 | 10.9 | -- |
| S19 | R512E/Cb752 | | 5 | A | -- | -- | No data | | -- | -- | -- | Missed defect in met. prep. |
| S20 | R512E/Cb752 | | 5 | A | 6.4 | 6.4 | No data | | -- | -- | 7.5 | Brittle crack at defect; incomplete failure |
| 13C | VH109/C129Y | 3 | | D | 5.1 | 8.4 | No data | | 5.0 | -- | 5.0 | -- |
| 13F | VH109/C129Y | 3 | | D | 4.6 | 7.2 | 6.3 | 6.7 | 6.0 | -- | 6.0 | -- |
| 16C | VH109/C129Y | 3 | | D | 4.3 | 7.8 | No data | | 3.5 | -- | 3.5 | -- |
| 16F | VH109/C129Y | 3 | | D | 9.6 | 12.0 | No data | | 14 | -- | 14 | Defect grew to 28 mils in diameter in cycling |
| 13A | R512E/FS85 | 3 | | D | 16.8 | 16.8 | No data | | 9.9 | 11.6[c] | 21.5[c] | -- |
| 13D | R512E/FS85 | 3 | | D | 13.2 | 13.2 | No data | | 9.3 | 10.7[c] | 20.0[c] | -- |
| 16A | R512E/FS85 | 3 | | A | 10.8 | 16.2 | No data | | | -- | | -- |

(a) A = tensile fracture occurred away from defect.
D = tensile fracture occurred at defect.

(b) Base hardness remained above 250 KHN, apparently owing to strain hardening.

(c) Dimpled zone not coplanar with cleavage zone.

TABLE A-24. ROOM-TEMPERATURE TENSILE-TEST DATA CORRELATION-COATED COLUMBIUM ALLOYS

| Specimen | System | Orig. Nom. Substrate Thickness, mils | Nominal Specimen Gage Width, in. | Prior Exposure or Condition | 0.2% Offset Yield Strength[a], ksi | Ultimate Strength[a], ksi | Elongation, percent | Yield Drop? | Remarks |
|---|---|---|---|---|---|---|---|---|---|
| 7-22-5 | Cb752 | 15 | 1/8 | As-received substrate | 63.2 | 85.0 | 26 | No | - |
| 7-22-6 | Cb752 | 15 | 1/8 | Ditto | 62.8 | 85.1 | 26 | No | - |
| 7-22-7 | Cb752 | 25 | 1/8 | " | 66.0 | 84.2 | 32 | Yes | - |
| 7-22-8 | Cb752 | 25 | 1/8 | " | 65.5 | 83.5 | 34 | Yes | - |
| B7-1 | R512E/Cb752 | 15 | 1/8 | Tensile specimen machined, then coated | 64.6 | 85.5 | 16 | No | - |
| B7-2 | " | 15 | " | Ditto | 66.9 | 86.9 | 17 | No | - |
| B7-3 | " | 25 | " | " | 64.2 | 83.5 | 24 | Yes | - |
| B7-4 | " | 25 | " | " | 65.0 | 83.7 | 26 | Yes | - |
| B7-5 | " | 15 | " | Coated, then machined | 68.6 | 88.4 | 16 | No | - |
| B7-6 | " | 15 | " | Ditto | 68.2 | 89.9 | 18 | No | - |
| B7-7 | " | 25 | " | " | 66.7 | 86.8 | 28 | Yes | - |
| B7-8 | " | 25 | " | " | - | 86.7 | 25 | - | Grip slippage precluded yield-strength determination |
| B7-9 | " | 25 | 1/4 | " | - | 85.5 | 23 | - | Ditto |
| B7-10 | " | 25 | 1/4 | " | 62.8 | 85.0 | 23 | No | - |
| 12B | " | 25 | 1/8 | Defected, 1 plasma cycle | 65.3 | 84.1 | 26 | Yes | Failure away from defect |
| 12E | " | 25 | " | Ditto | - | 85.5 | 26 | - | Grip slippage, failure away from defect |
| 16B | " | 25 | " | Defected, 3 plasma cycles | 63.3 | 84.8 | 26 | No | Failure away from defect |
| 13F | " | 25 | " | Ditto | - | 84.3 | 14 | - | Grip slippage, failure at defect |
| 13B | " | 25 | 1/4 | Defected, 3 plasma cycles | - | 85.7 | 17 | Yes | Grip slippage, failure at defect |
| 14A | " | 25 | 1/8 | Defected, 5 plasma cycles | 66.2 | 79.9 | 14 | No | Failure at defect |
| 14B | " | 25 | " | Undefected, 5 plasma cycles | 65.1 | 83.8 | 25 | Yes | - |
| 14C | " | 25 | 1/4 | Defected, 5 plasma cycles | 62.9 | 83.3 | 16 | Yes | Failure at defect |
| S9 | " | 25 | 1/8 | Defected, 1 static cycle | (72.1)[b] | 85.8 | 22 | No | Tested at 0.05 $min^{-1}$, failure away from defect |
| S10 | " | 25 | " | Ditto | 67.1 | 86.2 | 25 | Yes | Failure away from defect |
| S15 | " | 25 | " | Defected, 3 static cycle | 62.5 | 86.8 | 24 | Yes | Ditto |
| S16 | " | 25 | 1/4 | Ditto | 62.5 | 87.5 | 23 | Yes | " |
| S19 | " | 25 | 1/8 | Defected, 5 static cycles | 67.6 | 85.8 | 24 | Yes | " |
| S20 | " | 25 | 1/4 | Ditto | - | 85.9 | 24 | Yes | Failure away from defect, "soft" test, no yield strength value |
| | | | | Avg | 65.0 | 85.0 | | | |
| | | | | Std. Dev. (s) | 1.92 | 1.90 | | | |
| 9-38-5 | C129Y | 15 | 1/8 | As-received substrate | 70.6 | 89.7 | 30 | Yes | - |
| 9-38-6 | " | 15 | " | Ditto | 71.1 | 89.1 | 30 | " | - |
| 9-38-7 | " | 25 | " | " | 71.0 | 89.1 | 35 | " | - |
| 9-38-8 | " | 25 | " | " | 70.1 | 88.5 | 32 | | - |
| | | | | Avg | 70.7 | 89.1 | | | |
| | | | | Std. Dev. (s) | 0.46 | 0.49 | | | |
| B9-1 | VH109/C129Y | 25 | " | Tensile spec. machined, then coated | 73.3 | 109.3 | 22 | | - |
| B9-2 | " | 25 | " | Tensile spec. machined, then coated | 81.9 | 100.4 | 21 | " | - |
| B9-3 | " | 15 | " | Coated, then machined | 77.9 | 101.4 | 18 | No | - |
| B9-4 | " | 15 | " | Ditto | 74.8 | 97.4 | 18 | No | - |
| B9-5 | " | 25 | " | " | 72.5 | 91.2 | 25 | No | - |
| B9-6 | " | 25 | " | " | 73.5 | 96.1 | 22 | Yes | - |
| B9-7 | " | " | 1/4 | " | - | 92.2 | 4 | - | Grip slippage |
| B9-8 | " | " | " | " | - | 98.3 | 24 | - | Ditto |
| | | | | Avg | 75.5 | 98.4 | | | |
| | | | | Std. Dev. (s) | 3.61 | 5.71 | | | |
| 13F | " | " | 1/8 | Defected, 3 plasma cycles | 67.2 | 98.1 | 18 | No | Fractured at defect |
| 16C | " | " | " | Defected, 3 plasma cycles | 74.3 | 96.7 | 24 | No | Fractured at defect |
| 13C | " | " | 1/4 | Ditto | 67.6 | 99.0 | 22 | Yes | Fractured at defect |
| 16F | " | " | " | " | 70.2 | (78.6)[b] | 4 | No | Fractured at defect, 14-mil radial defect growth |
| | | | | Avg | 69.8 | 96.6 | | | |
| | | | | Std. Dev. (s) | 3.26 | 2.57 | | | |

TABLE A-24. (Continued)

| Specimen | System | Orig. Nom. Substrate Thickness, mils | Nominal Specimen Gage Width, in. | Prior Exposure or Condition | 0.2% Offset Yield Strength[a], ksi | Ultimate Strength[a] ksi | Elongation, percent | Yield Drop? | Remarks |
|---|---|---|---|---|---|---|---|---|---|
| 85-1 | FS85 | 30 | 1/8 | As-received substrate | – | 88.7 | 30 | – | "Soft" test, unreliable yield-strength value |
| 85-2 | " | " | " | Ditto | 66.6 | 88.5 | 30 | No | – |
| B5-1 | R512E/Cb752 | " | " | Tensile spec. machined, then coated | 64.5 | 85.1 | 24 | " | – |
| B5-2 | " | " | " | Ditto | 64.9 | 86.1 | 25 | " | – |
| B5-3 | " | " | " | Coated, then machined | 67.8 | 89.8 | 25 | " | – |
| B5-4 | " | " | " | Ditto | 67.5 | 89.7 | 25 | " | – |
| 13D | " | " | " | Defected, 3 plasma cycles | 66.5 | 85.7 | 12 | " | Fractured at defect |
| 16A | " | " | " | Ditto | 65.2 | 96.5 | 24 | " | Fractured away from defect |
| 13A | " | " | 1/4 | " | – | 64.6 | 12 | " | Grip slippage, fractured at defect |
| | | | | Avg | 66.0 | 87.2 | | | |
| | | | | Std. Dev. (s) | 1.70 | 2.01 | | | |

(a) Strengths for coated specimens based on cross-sectional area of substrate, with compensation for substrate consumption during coating
(b) Excluded from analysis – see Remarks column.

APPENDIX B

ADDITIONAL DETAILS AND DATA FROM TESTS UNDER DYNAMIC-ENVIRONMENTAL-EXPOSURE CONDITIONS

# APPENDIX B

## ADDITIONAL DETAILS AND DATA FROM TESTS UNDER DYNAMIC-ENVIRONMENTAL-EXPOSURE CONDITIONS

### Environmental Conditions

The environmental conditions for the cobalt-alloy and columbium-alloy nominal-temperature exposures are summarized in Table B-1.

TABLE B-1. ENVIRONMENTAL CONDITIONS FOR COBALT- AND COLUMBIUM-ALLOY EXPOSURES

| Specimen Type | Surface Temperature, F | Free-Stream Mach Number | Heater Reservoir Pressure, atm | Gas Total Enthalpy, Btu/lb | Average Surface Pressure, torr | Surface Shear Stress, psf | |
|---|---|---|---|---|---|---|---|
| | | | | | | Front Specimens | Rear Specimens |
| Cobalt alloy | 1900 | 4.5 | 1.16 | 4460 | 11.7 | 1.2 | 1.6 |
| Coated columbium alloy | 1400 | 4.5 | 0.85 | 2250 | (a) | 1.4 | 1.9 |
| Coated columbium alloy | 2350 | 4.5 | 1.14 | 4700 | (b) | 1.7 | 2.2 |
| Coated columbium alloy | 2500 | 4.5 | 1.34 | 6300 | 16 | 1.8 | 2.4 |

(a) Surface pressure not measured, estimated value is 10 torr.
(b) Surface pressure not measured; estimated value is 13.5 torr.

The free-stream Mach number was calculated for the 5-inch-exit-diameter nozzle using a chemically reacting nozzle-flow program based on the analytic technique developed by Lordi, et al. [B-1], for nonequilibrium expansions of reacting gas mixtures. Also, a laminar-boundary-layer program based on the Cohen and Reshotko [B-2] solution with heat transfer and arbitrary pressure gradient was used.

The heater reservoir pressure was measured experimentally and the gas total enthalpy was determined using the energy-balance technique. Surface pressures and heat-transfer rates were measured experimentally using water-cooled copper blocks which fit into the spaces occupied by the specimens and molybdenum blocks that were used during the material exposures. Both front and rear calorimeter blocks had three pressure taps and two heat-flux calorimeters to determine the axial pressure and heat-transfer-rate distributions. Heat-flux measurements were obtained for the 2500 F columbium-alloy condition; pressure measurements were obtained for the 1900 F cobalt-alloy and 2500 F columbium-alloy conditions. The pressure taps in each block were located approximately 0.29, 1.5, and 2.71 inches from the block leading edge. The heat-flux calorimeters were located approximately 0.90 and 2.10 inches from the leading edge of front and rear blocks.

For the cobalt-alloy condition and specimen orientation, the average pressures on the front and rear calorimeter blocks were within 1 torr of each other, with variations of approximately ±1.5 torr on the front block and ±2.0 torr on the rear. For the 2500 F columbium-alloy condition and specimen configuration, the average pressures on the front and rear blocks were within 0.1 torr of each other, with variations of approximately ±2.5 torr and ±2.7 torr on the front and rear blocks, respectively.

The surface shear stresses for the front and rear specimens were calculated using the technique described by Harney and Petrie[B-3]. In this procedure, which is consistent with the hypersonic-small-disturbance theory, the flow-field equations are formulated in a manner that brings out their explicit dependence on gas thermodynamic and transport properties with minimal dependence on Mach number. The skin-friction coefficient is expressed in terms of surface and free-stream flow properties. Numerical values for these properties were obtained from the solution of the nonequilibrium nozzle flow expansion.

A comparison of the measured and calculated heat-transfer rates for the 2500 F columbium-alloy condition is shown in Table B-2. Also shown in Table B-2 are measured heat fluxes corrected to the specimen wall temperature of 2500 F. These values can be compared with a value of 31 Btu/ft$^2$-sec which was calculated on the basis of reradiation equilibrium at a temperature of 2500 F and an emittance of 0.85. The relationships used to calculate the hot-wall heat-transfer rates were obtained from References (B-3) and (B-4). It can be seen that the calculated heat-transfer rates are in excellent agreement with the measured values.

TABLE B-2. COMPARISON OF MEASURED AND CALCULATED HEAT-TRANSFER RATES FOR 2500 F COLUMBIUM-ALLOY CONDITION

| Calorimeter Location, Distance from Specimen Leading Edge, in. | Calculated Cold Wall Heat Flux, Btu/ft$^2$-sec | | Measured Cold Wall Heat Flux, Btu/ft$^2$-sec | Measured Cold Wall Heat Flux, Corrected to 2500 F, Btu/ft$^2$-sec |
|---|---|---|---|---|
| | Ref. (B-3) | Ref. (B-4) | | |
| | Front Specimen | | | |
| 0.896 | 54.5 | 56.4 | 53.3 | 38.0 |
| 2.104 | 45.0 | 46.0 | 45.3 | 33.0 |
| | Rear Specimen | | | |
| 0.896 | 46.7 | 57.1 | 45.2 | 33.0 |
| 2.104 | 37.6 | 46.4 | 39.2 | 28.0 |

## Typical Results

In this part of Appendix B, experimental results are presented which illustrate the usefulness and accuracy of the techniques used to determine specimen surface temperatures. Typical results are given for the coated columbium-alloy systems since most of the data were obtained for these specimens. Three columbium-alloy coating/substrate systems were considered within the program: R512E/Cb752, R512E/FS85, and VH109/C129Y. In most arc runs, specimens of all three of these systems were exposed simultaneously. Thus, it was necessary to account for differences in surface emittances of the systems in correlating the optical-pyrometer data with those obtained from the thermocouples and in using infrared photography to obtain temperature profiles of the specimens.

### Infrared Pyrometry and Thermocouple Data

A representative trace obtained from the scanning infrared pyrometer is shown in Figure B-1 as a function of location on the specimens. The irregular-shaped curve labeled "pyrometer signal" is the pyrometer output voltage obtained by remotely scanning across three specimens in a direction normal to the gas flow direction. This particular scan was obtained at a location corresponding to the center defects in the specimens in the front row. For known surface emittances, the specimen temperatures can be determined directly from the calibration of the pyrometer.

The other curve shown in Figure B-1 represents the voltage output of a positioning poteniometer which is used to determine the exact scan location on the specimens as a function of time. From the pyrometer output curve, the edges of each of the specimens can be identified. These edge indications are useful in checking the accuracy of the positioning potentiometer and in relating the time-dependent output voltage to location on the specimens. The lack of an instantaneous rise and falloff in pyrometer output at the extreme specimen edge is due to the finite pyrometer object size and the proximity of the water-cooled copper holder to the specimens.

Correlations of the temperatures obtained from the spring-loaded thermocouples with the scanning pyrometer output signals are given in Figures B-2, B-3, and B-4 for the three columbium-alloy systems. The data points were obtained from the thermocouple output (ordinate) and the pyrometer output voltage (abscissa) for scan positions on the specimens corresponding to the thermocouple locations. Also shown in Figures B-2, B-3, and B-4 are calibration curves relating temperature to pyrometer output voltage for different constant emissivities. Although there is appreciable scatter in the data, it appears that the columbium alloy systems exhibit different nominal emittances. The ranges in elevated temperature, normal spectral emittances*, and the nominal values suggested by the correlations are as follows:

| System | Estimated Normal Spectral Emittance | |
|---|---|---|
| | Approximate Range | Nominal Value |
| R512E/Cb752 | 0.65 to 0.75 | 0.73 |
| R512E/FS85 | 0.65 to 0.85 | 0.75 |
| VH109/C129Y | 0.85 to 0.95 | 0.91 |

*Wavelengths from 2.0 to 2.6 microns.

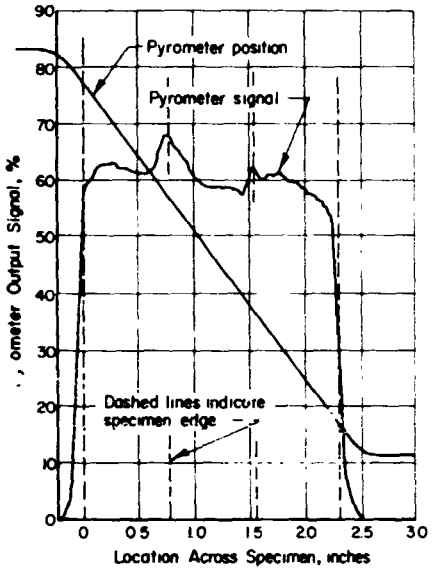


FIGURE B-1. TYPICAL PYROMETER SCAN ACROSS THREE SPECIMENS DURING PLASMA-ARC EXPOSURE

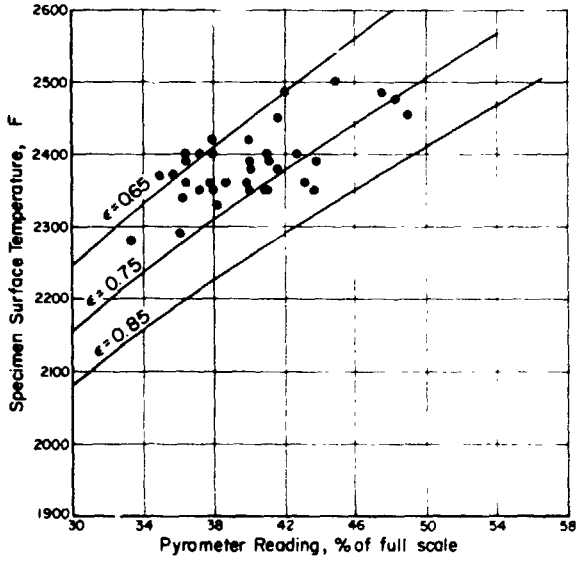


FIGURE B-2. CORRELATION OF THERMOCOUPLE AND PYROMETER DATA FOR R512E/Cb752 SYSTEM

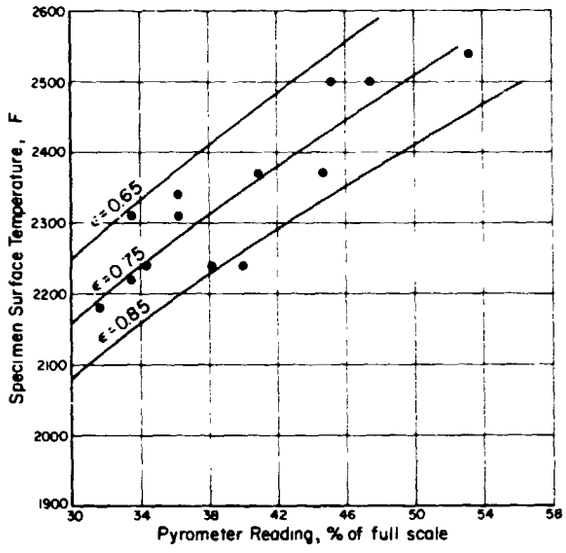


FIGURE B-3. CORRELATION OF THERMOCOUPLE AND PYROMETER DATA FOR R512E/FS85 SYSTEM

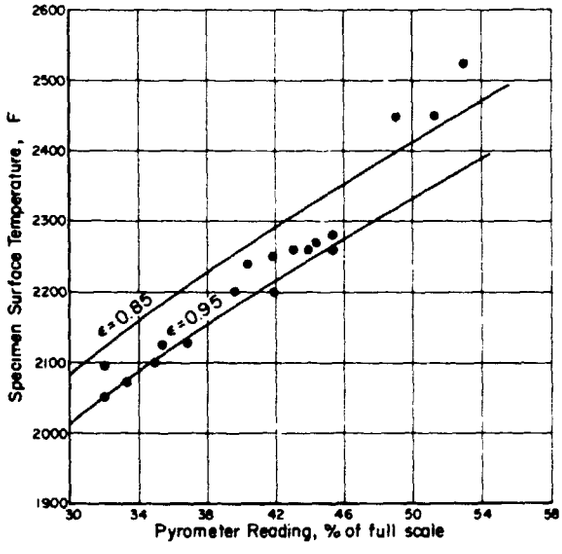


FIGURE B-4. CORRELATION OF THERMOCOUPLE AND PYROMETER DATA FOR VH109/C129Y SYSTEM

No trends toward higher or lower values with exposure time were observed in any of the runs, which included up to five simulated reentry cycles. Because of this and because of the limited numbers of cycles and appreciable differences in temperature within and between runs, no rigorous attempt was made to determine the specimen emittance as a function of number of cycles.

Infrared Photography and Thermocouple Data

In this program, infrared photographs were quite useful in determining a complete temperature profile of the specimens during exposure. Figure B-5 is an infrared photograph taken during one of the 2500 F columbium-alloy runs. Light regions represent hotter areas and dark regions are indicative of cooler areas. From even a cursory observation of the photograph, it is possible to determine local hot spots and colder areas on the specimens. Of course, for accurate temperature determinations, the photographs (actually positive transparencies) are analyzed using a densitometer.

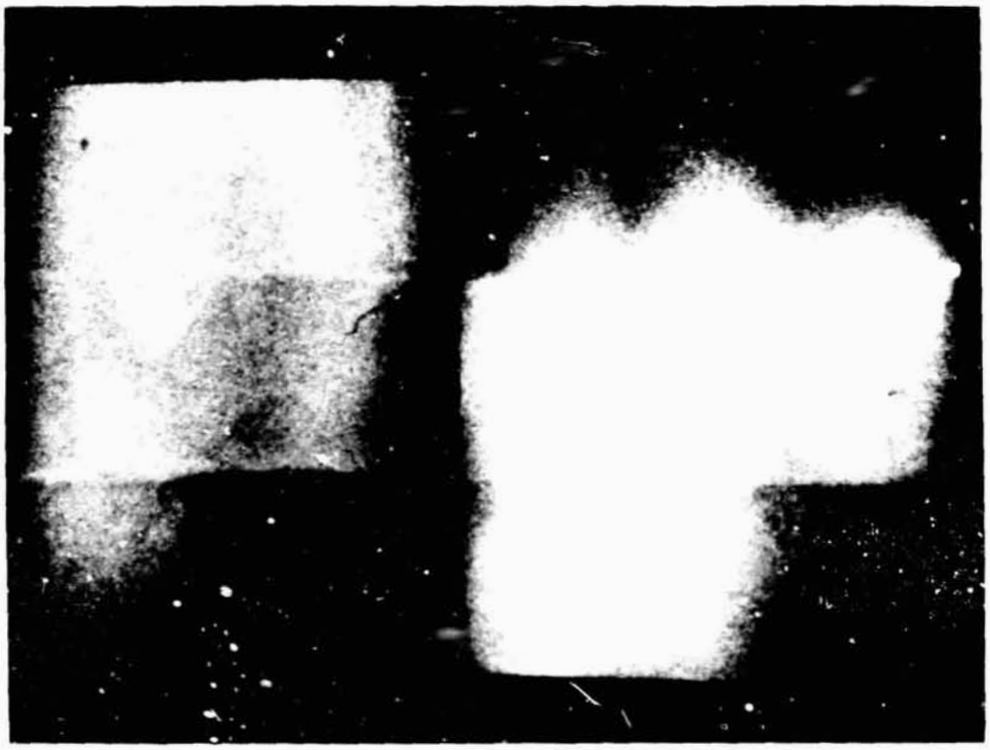

FIGURE B-5. INFRARED PHOTOGRAPH OF SPECIMEN DURING PLASMA-ARC EXPOSURE

A comparison of the specimen temperatures obtained from the infrared photographs with the calibrated film response curve (from Figure 14) is shown in Figure B-6. The data points were obtained from the temperatures indicated by the spring-loaded thermocouples (ordinate) and the film densitometer reading at the thermocouple location (abscissa). Thermocouple temperatures were determined at the times when the infrared photographs were taken. The location of the film calibration curve relative to the data points was established using a temperature from one of the spring-loaded

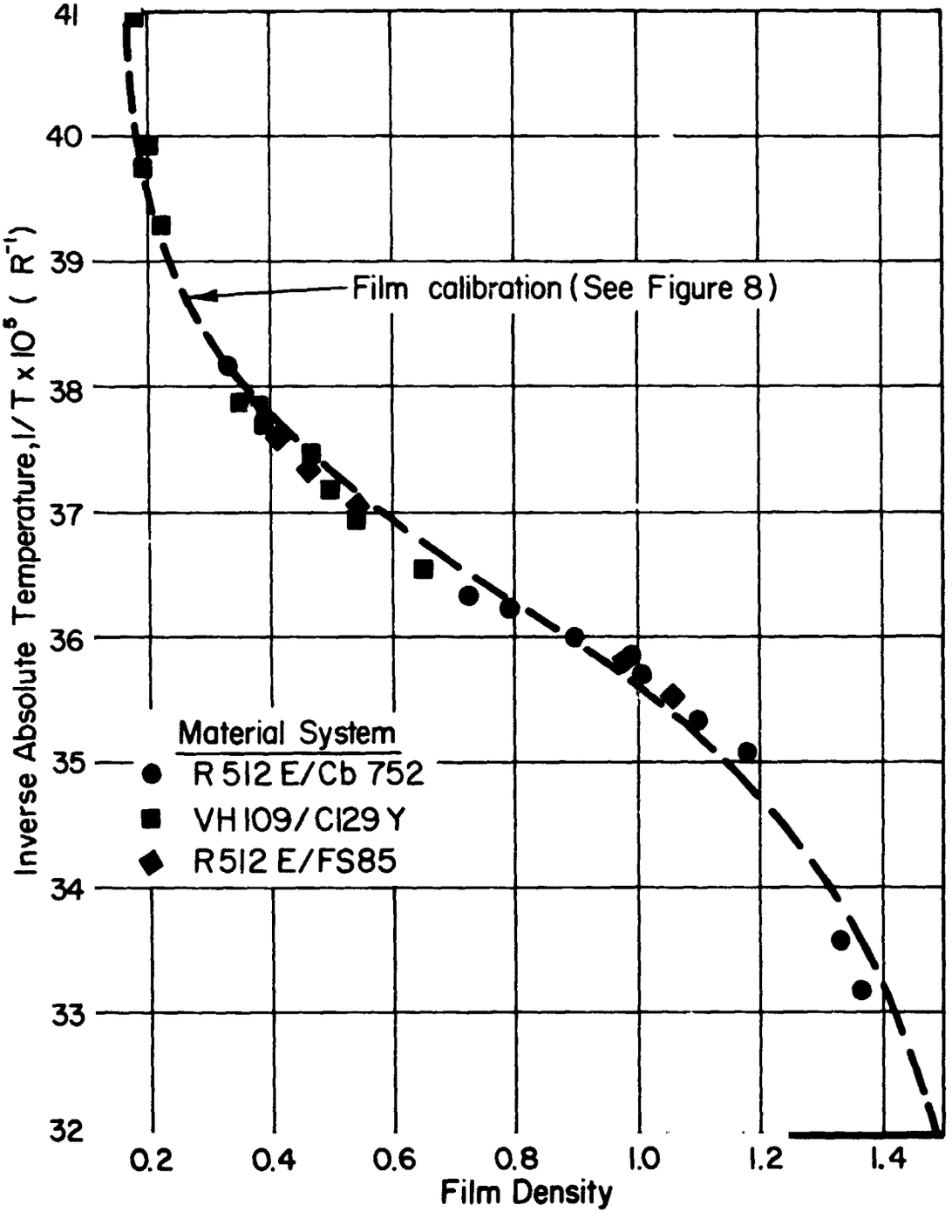


FIGURE B-6. COMPARISON OF CALIBRATED FILM RESPONSE CURVE WITH THERMOCOUPLE AND INFRARED-PHOTOGRAPHY DATA

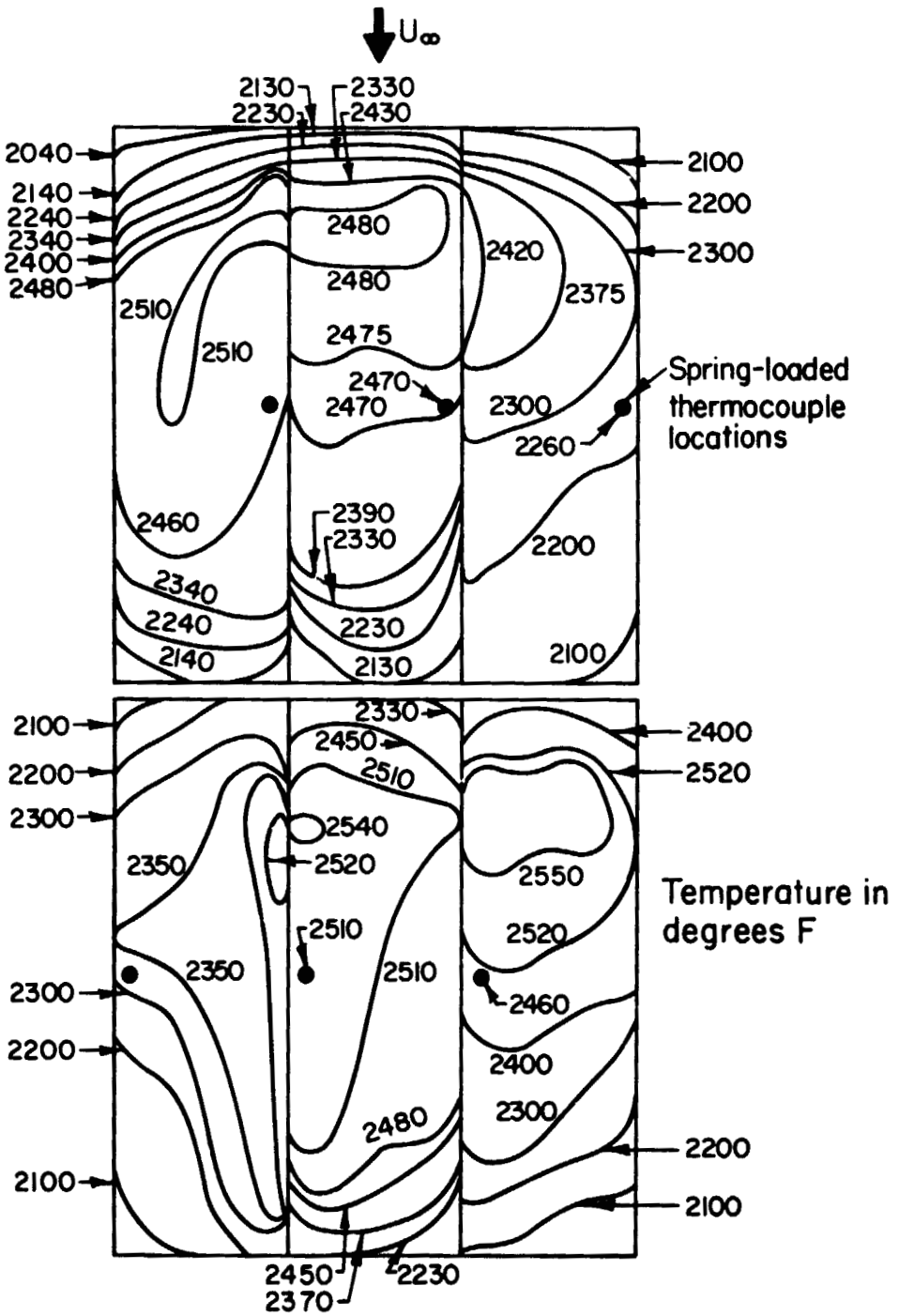


FIGURE B-7. SPECIMEN SURFACE TEMPERATURE CONTOURS OBTAINED FROM INFRARED PHOTOGRAPH

thermocouples. It can be seen that there is excellent agreement between the temperatures obtained from all the operating thermocouples and those obtained from the infrared photographs. From Figure B-6 the useful temperature range of the infrared photography can be determined for the particular exposure and developing conditions used in this program; this range is approximately 400 F.

Contours of the specimen surface temperature were generated using infrared positive transparencies and the temperature-density correlation of Figure B-6. A typical contour mapping is shown in Figure B-7 using the positive transparency from which the photograph of Figure B-5 was obtained. The locations of the spring-loaded thermocouples and the corresponding temperatures are also shown in Figure B-7. It can be seen that there is good agreement between the temperatures obtained from three of the thermocouples in addition to the one used for film calibration and temperatures obtained from the infrared photograph. At the time of film exposure, two thermocouples were behaving erratically and could not be used with good reliance. The surface temperatures can be determined with considerable accuracy by this infrared photographic mapping technique. A more detailed mapping of the surface-temperature contours can be obtained simply by reading the film densities in finer increments. The surface-temperature contours of Figure B-7 are useful in that an accurate surface-temperature distribution can be obtained in defect regions and in regions to be used for subsequent mechanical-property evaluations.

## Comparison of Temperature-Measuring Techniques

A comparison of all three methods used for determining the specimen surface temperatures is shown in Figure B-8. In this figure, the specimen surface temperature is plotted as a function of distance across the specimens. Also shown are the temperatures indicated by two of the spring-loaded thermocouples. This temperature distribution was taken across the center of the front row of specimens (see Figure B-7). In generating the curve representing the temperature distribution obtained from the pyrometer scan, it was necessary to adjust the level to account for differences in emissivities of the three columbium-alloy-system specimens. It can be seen that there is good agreement among the results obtained with the three temperature-measuring techniques, with a maximum difference of approximately 40 F occurring between temperatures obtained from the pyrometer and photographic techniques. This maximum difference is representative of those obtained from similar comparisons of other arc-jet runs.

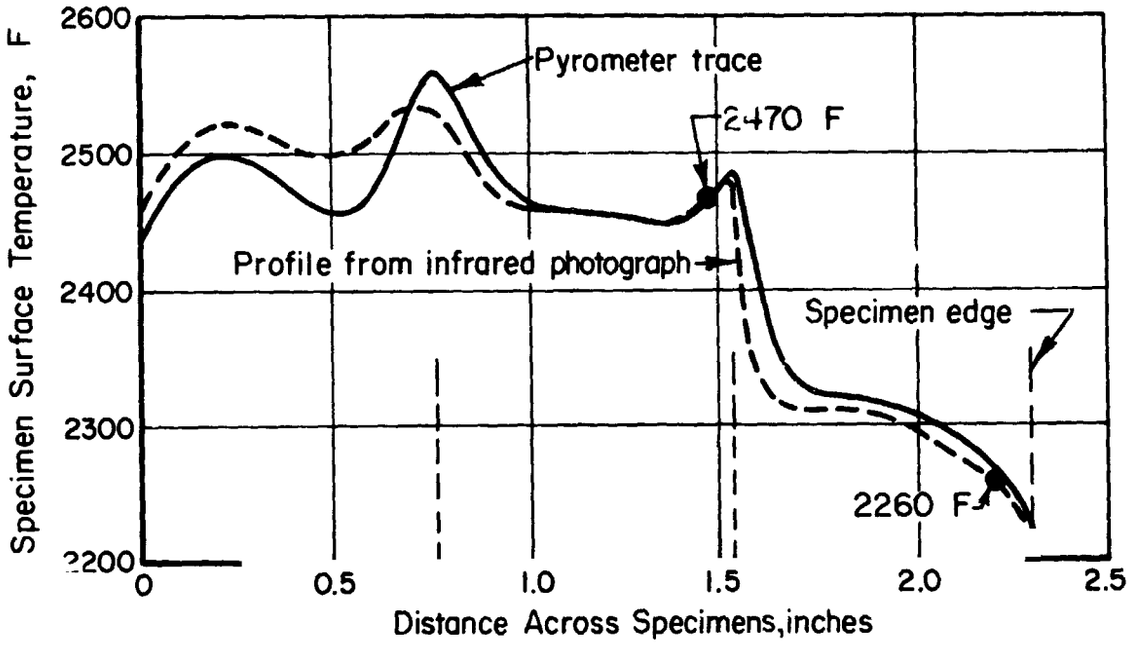


FIGURE B-8. COMPARISON OF PYROMETER AND INFRARED PHOTOGRAPHIC TEMPERATURE-DISTRIBUTION DATA

## References

(B-1) Lordi, J. A., et al., "Computer Program for the Numerical Solution of Nonequilibrium Expansions of Reacting Gas Mixtures", NASA CR-472 (1965), 120 pp.

(B-2) Cohen, C. B., and Reshotko, E., "The Compressible Laminar Boundary Layer With Heat Transfer and Arbitrary Pressure Gradient", NACA Report 1294 (1956), 16 pp.

(B-3) Harney, D. J., and Petrie, S. L., "Hypersonic Surface Pressure and Heat Transfer on Slender Bodies in Variable Composition and Nonequilibrium Atmospheres", AF FDL-TR-70-31 (April, 1970), 42 pp.

(B-4) Hankey, W. L., Jr., et al., "Design Procedures for Computing Aerodynamic Heating at Hypersonic Speeds", WADC-TR-59-610 (June, 1960), 157 pp.

# APPENDIX C

## PRELIMINARY STUDY OF A FAIL-SAFE SYSTEM

# APPENDIX C

## PRELIMINARY STUDY OF A FAIL-SAFE SYSTEM

Coated columbium offers excellent potential for providing the 100-mission life required for Shuttle TPS. Available failure-rate statistics, however, indicate that a low, but finite, probability for premature, random failures, rather than "wear-out life" per se, will be life limiting. These premature random failures are most often attributed to small coating cracks that permit oxygen to contaminate and oxidize the substrate. With an appropriate materials-system design, it is probable that coated columbium can be made far less sensitive to the consequences of early coating failure with a much closer approach to the attractive "wear-out life" capabilities as a result. This is the basic rationale at Battelle-Columbus for "fail-safe" coated columbium systems. The key to a fail-safe coated columbium system is a barrier layer to be positioned between the structural-columbium alloy substrate and the primary protective coating. This "barrier layer" would prevent substrate degradation for appreciable time after initial coating failure, and should have the following properties:

(1) Excellent metallurgical compatibility with the substrate

(2) Sufficient ductility to resist coating-fracture propagation

(3) Resistance to oxide scaling that is 1 to 2 orders of magnitude better than that of the substrate

(4) Capability to inhibit passage of oxygen to the substrate by either
   (a) Extremely low oxygen diffusivity in the barrier layer, or
   (b) High thermochemical affinity of the barrier layer for oxygen relative to that of the substrate (e.g., interstitial sink quality for the barrier).

(Of these, the latter is the more attractive for suitably thin barriers for Shuttle TPS application.)

Research studies conducted at Battelle-Columbus in 1963-64 offered encouragement to investigate this concept further. Accordingly, the supplementary task described in this appendix was undertaken by Battelle.

### Material and Exposure

The columbium alloy T166 (Cb-42Ti-4Cr-4Al) was selected as the barrier layer, as known alloy properties were nearly "ideal" in context with the requirements cited above. Strips of this alloy were placed over an FS85 core, vacuum encapsulated in steel, and hot roll clad, resulting in finished strip with total thickness of about 20 mils comprising 4 mils of cladding on each major surface of the FS85 core. From this strip, a plasma-exposure specimen was formed. This was then pack siliconized. Finally,

Type A, B, and C defects were introduced in the exposure surface as described in the body of this report. The Type B and C defects terminated just within the T166 layer, and did not penetrate to the FS85 core. This specimen was exposed for three dynamic cycles in Position D of Plasma Run 16 (Table 10 in this report). The reduced temperature data (backface thermocouple, IR pyrometer scan, and IR photography) indicated an average temperature of 2440 F for defect Types A and C and about 2400 F for defect Type B.

## Evaluation

Following exposure, the specimen was examined visually and sectioned through the center of each defect for metallographic observation and microhardness traverse.

Microscopic examination and measurements of the exposed flaw sites resulted in the following observations:

(1) None of the defects had grown perceptibly as a result of the dynamic, cyclic, simulated reentry exposure.

(2) Oxidation scaling of the T166 at the base of the 4-mil (Type C) defect was visibly no more severe than that observed on the surrounding protective silicide coating.

(3) At the base of the 40-mil (Type B) coating defect, a thin, blue, blistered-appearing oxide was noted. This was not at all characteristic of the voluminous fluffy, white oxide that forms on oxidation-prone columbium alloys. T166 obviously has attractive resistance to oxidation scaling under the cyclic exposure conditions involved.

(4) FS85 oxidation from exposed surfaces at the 40-mil (Type A) through defect was about as expected. In the absence of backup protection of the barrier layer, the white, fluffy FS85 oxide had grown inward from the sides of the defect.

(5) Oxidation product over the silicide coating grown on T166-clad surfaces was the thin, dense, tan oxide characteristic of titanium-modified $CbSi_2$. At edges where $CbSi_2$ not modified with titanium was grown by reaction with the FS85 substrate, the oxide was thicker and white, as is characteristic of a poorly modified $CbSi_2$ coating.

These observations were as expected.

Metallographic cross sections were prepared to show coating-cladding-substrate microstructural features at and around the centers of the three types of coating defects. Figures C-1, C-2, and C-3 illustrate the major findings, which are summarized below:

(1) At the smallest, 4-mil-diameter coating defect (Figure C-1), oxidation scaling of the T166 was indeed minor, as suggested by microscopic examination prior to sectioning. Although not metallographically apparent, the T166 layer in the vicinity of the flaw exhibited a DPH (Knoop hardness) of nearly 700, compared with a base value of about 280, indicating appreciable oxygen contamination hardening. A Knoop hardness traverse was made in the FS85 substrate. Khn (2-gram load) values ranged from 260 at 1 mil beneath the T166 under the defect to a base value of 190 at 4 mils from the barrier layer/FS85 interface. The 1-mil hardness value was also representative of widespread 1-mil-deep locations. Accordingly, shallow hardening observed is attributed to substitutional hardening from FS85-T166 interdiffusion rather than interstitial hardening by oxygen.

(2) At the 40-mil coating defect (Figure C-2), oxide scaling had not consumed much of the residual T166, indicating a fail-safe life well in excess of 3 cycles even in the presence of gross coating defects. The T166 was obviously severly contaminated. However, a hardness traverse in the underlying FS85 gave essentially the same result as in (1) above.

(3) At the 40-mil through defect (Figure C-3) where both T166 and FS85 were exposed, the expected range of oxygen contamination was observed. Surface hardness of FS85 at the oxide interface was Khn 650, and did not decrease to the base value (Khn 190) until a depth of 22 mils beneath the oxide metal interface was reached. Oxide scaling of the FS85 was minor in comparison with contamination.

The microhardness traverse data are plotted in Figure C-4. Data for similarly defected coatings (R512E, VH109) on Cb752 and C129Y alloys, i.e., where defects barely penetrated the silicide coating, but without the benefit of the intermediate layer are included for comparison.

This brief but demonstrative study allows the conclusion that severely degrading oxygen contamination of a structural-columbium-alloy substrate can be inhibited for substantially more than three reentry cycles even in the presence of quite severe coating defects by the inclusion in the materials system of an interlayer of a semi-oxidation-resistant, reactive-metal-containing alloy.

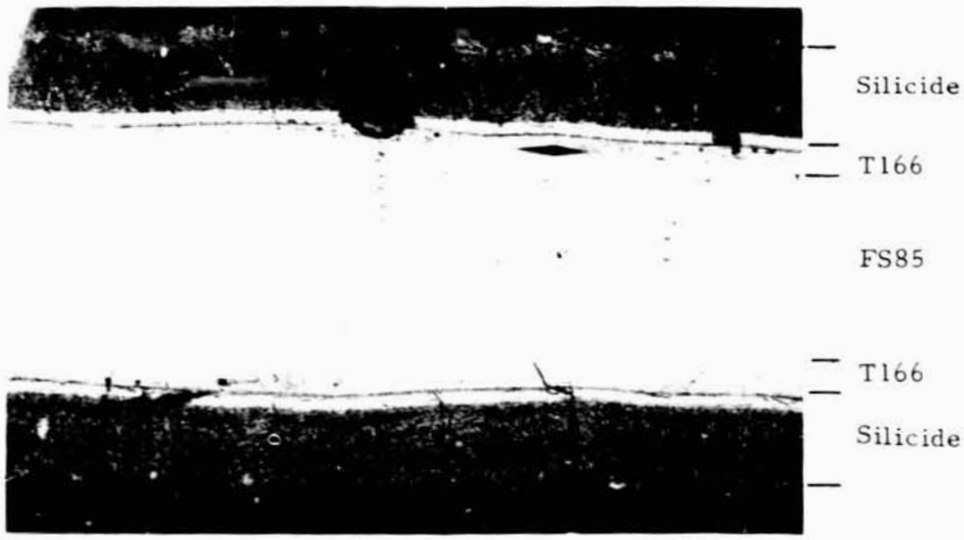


100X 6F090

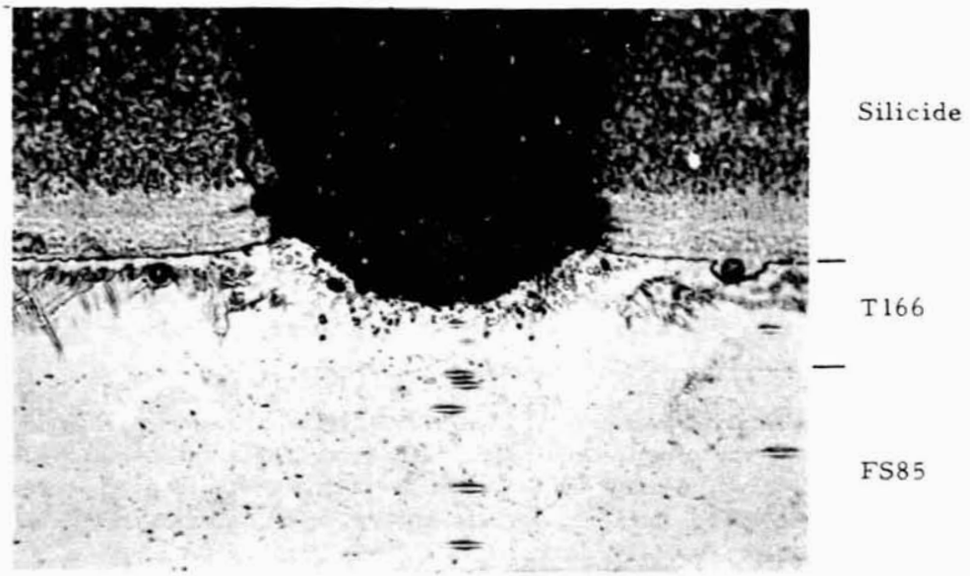


500X 6F091

FIGURE C-1. OXIDATION AND CONTAMINATION OF T166 LAYER EXPOSED TO THREE SIMULATED REENTRY CYCLES BY THE PRESENCE OF A 4-MIL -DIAMETER DEFECT IN THE SILICIDE COATING

Note the 3-layer oxide structure and relatively low level of T166 contamination. FS85 substrate is completely protecied.


FIGURE C-2. OXIDATION AND CONTAMINATION OF T166 LAYER EXPOSED TO THREE SIMULATED REENTRY CYCLES BY THE PRESENCE OF A 40-MIL-DIAMETER DEFECT IN THE SILICIDE COATING

Note the thin, blistered T166 oxide and visibly severe contamination of the T166. Despite severe contamination, nearly the full thickness of T166 remains. FS85 substrate is completely protected.

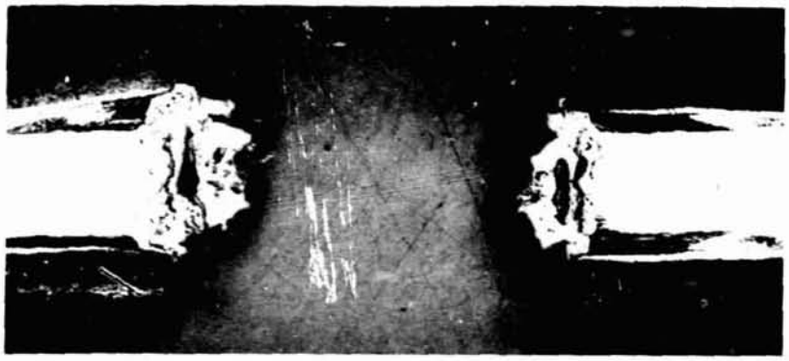

50X 6F088

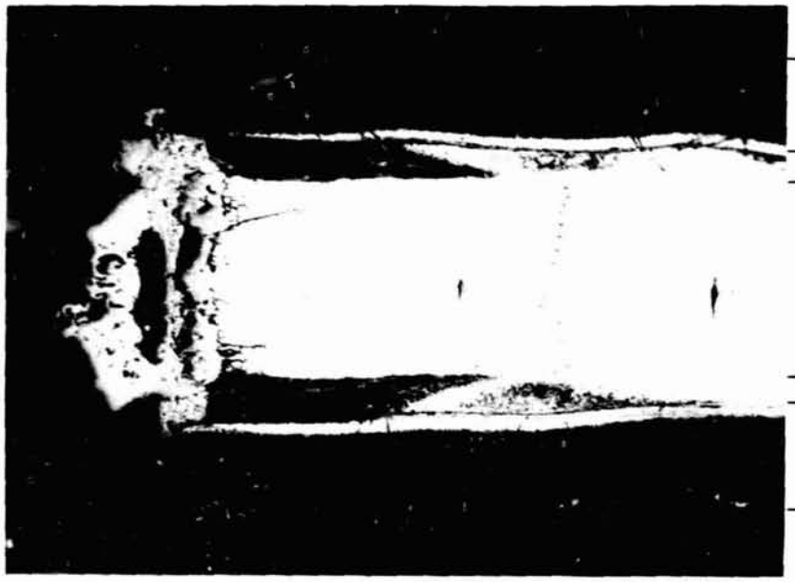


100X 6F087

FIGURE C-3. OXIDATION AND CONTAMINATION AT THE 40-MIL-DIAMETER THROUGH FLAW AFTER THREE SIMULATED REENTRY EXPOSURES

Note voluminous, nonprotective FS85 oxide and visibly severe contamination of T166. Surface recession of FS85 is 3 to 5 mils. Depth of contamination of FS85 is to a point about midway between larger hardness indentations – about 25 mils from original surface.

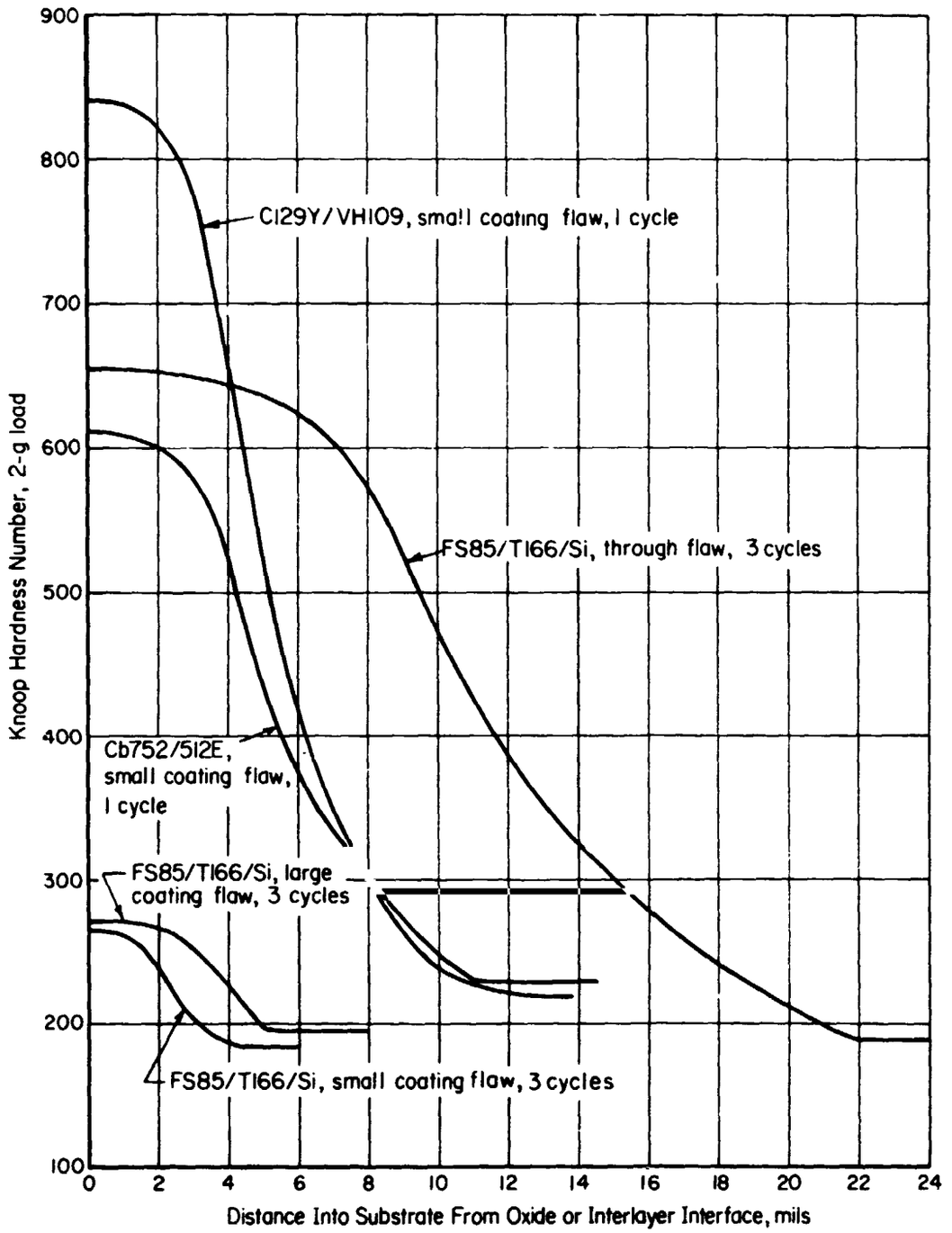


FIGURE C-4. HARDNESS TRAVERSE PROFILES UNDER INTENTIONAL DEFECTS IN COATED COLUMBIUM EXPOSED TO SIMULATED REENTRY CYCLING